# Soil Characterization in Centrifuge Models through Measurement of S- and P-wave Velocities Using an Enhanced Bender Elements System

By

Waleed El-Metwally El-Sekelly

A Thesis Submitted to the Graduate

Faculty of Rensselaer Polytechnic Institute

in Partial Fulfillment of the

Requirements for the Degree of

MASTER OF SCIENCE

Major Subject: Civil Engineering

Approved by the
Examining Committee:

_____
Tarek Abdoun
Thesis Adviser

_____
Ricardo Dobry, Member

_____
Mourad Zeghal, Member

Rensselaer Polytechnic Institute
Troy, New York

April 2011
(For Graduation May 2011)

**CONTENTS**

## LIST OF TABLES

## LIST OF FIGURES

## ACKNOWLEDGMENT

I would like to start by thanking my advisor, Professor Tarek Abdoun for his continuous support, advice and belief in my abilities throughout the course of this research. I would also like to thank my committee members, Professor Ricardo Dobry and Professor Mourad Zeghal for their help and support. I am grateful to Professor Ricardo Dobry for his excellent teaching of the Soil Dynamics course. I am also thankful to him for his recommendations regarding my research work and the writing process.

I am particularly grateful to my parents and brother for their continuous love and support throughout my life. They never stopped supporting, guiding and believing in me. No words can ever describe their great impact on my life.

I would also like to thank all my friends and officemates for their friendship and for their continuous supply of information.

I am grateful to the staff of NEES@RPI for their help and support. Anthony Tessari and Eric Johannesen have been extremely helpful and supportive throughout the course of the research.

Also, I would like to thank my professors at both RPI and Mansoura University, Egypt. Professor Salah El-Metwally, Professor Ahmed El-Nimr and Professor Mahmoud El-Meligy have always believed in my abilities never stopped supporting me.

To my family

## ABSTRACT

The determination of the dynamic properties of the soil is a critical issue in geotechnical Engineering. It is of a particular importance in problems involving dynamic excitation of soil systems, such as earthquakes. This research focus on measuring the velocity of seismic waves, particularly shear waves, in dry and saturated soil models in the centrifuge. The high noise during the centrifuge operation and the need of using a number of bender elements in the same model make the use of bender elements in the centrifuge more challenging. The research starts with improving the current bender elements system at RPI Geotechnical Centrifuge. This involves solving the electric and electromagnetic problems in the system and reducing noise and ghosting effects. The improved bender elements system is then used to determine the shear (S) and dilatational (P) wave velocities of dry and saturated Ottawa sand at different void ratios and different overconsolidation ratios in the centrifuge. The research also involves the determination of the effect of preshaking on the dynamic properties of soil. Moreover, the shear wave velocity measurements are also used to estimate the effect of overconsolidation on the coefficient of lateral earth pressure at rest ($K_0$). A comparison of the results of this study is done with those published in the literature.

# 1. INTRODUCTION

## 1.1 Importance of shear wave velocity

Shear wave velocity ($V_s$) is an important parameter for geotechnical works design, particularly in seismically active areas. The $V_s$ value reflects geotechnical properties such as shear stiffness and density of the soil. It is also very important parameter for design and site response purposes.

The shear wave velocity ($V_s$) is also applicable to evaluate the stiffness of foundation, site response during earthquakes, liquefaction potential, soil density, site classification, soil stratigraphy and settlement of foundations (Richart et al., 1970; Seed and Idriss, 1970; Schnabel et al., 1972; Sykora and Stokoe, 1983; Burland, 1989; Sasitharan et al., 1994; Shibuya et al., 1995; Kramer, 1996; Andrus and Stokoe, 1997; Wills and Silva, 1998; Mayne et al., 1999; Dobry et al., 2000; Lehane and Fahey, 2002; Seed et al., 2003; Stewart et al., 2003; McGillivray and Mayne, 2004; Holzer et al., 2005; McGillivray, 2007).

## 1.2 Centrifuge modeling

Modeling using geotechnical centrifuge is a powerful technique that can be used for testing soil and soil structure interaction under static or dynamic loading. Many geotechnical research centers have become interested in using geotechnical centrifuge modeling since 1980. A number of these centers have obtained these capabilities. The geotechnical centrifuge offers the ability to simulate full-scale stress states with uniform

and measurable soil properties. Centrifuge modeling is considered a cost-effective method for modeling and predicting the properties and behavior of soil deposits (Ubilla, 2007).

Centrifuge modeling is useful for measuring parameters in which the earth's gravity is present and has a dominant effect in determining material properties. Generally, the properties of the soil are dependent on the gravitational stresses, and hence modeling using geotechnical centrifuge can very useful for that kind of systems (Ubilla, 2007).

The main principle in centrifuge modeling is that the model scaled by a factor of 1/N and subject to a gravitational acceleration of Ng is subjected at equivalent points in the soil mass to the same stresses as the prototype, where g is the acceleration of gravity as shown in Figure 1.1 (Ubilla, 2007). Using the same soil in both the model and the prototype, the stress-strain relation at equivalent points in model and prototype would be preserved (Arulandan et al., 1988)). A complete set of scaling relationships governing different geotechnical problems is available based on dimensional analysis or the physics of the problem. A list of centrifuge scaling relations is presented in Table 1.1 (Whitman and Arulanandan, 1985).

### 1.3 Introduction to piezoelectricity and Piezo transducers

A Transducer can be defined as a device that converts one form of energy to another. In Piezo actuators electrical energy is converted to mechanical energy. They are referred to as "motors" (often linear motors). In Piezo sensors mechanical energy is converted into electrical energy. They are referred to as "generators". Usually, the same

element can be used to perform either task. However, different configuration can be used to be more efficient (PIEZO SYSTEMS, INC.).

The 2-layer elements shown in Figure 1.2 are the most adaptable configuration of all. They may be used like single sheets (made up of 2 layers), they can be used to bend, or they can be used to extend (PIEZO SYSTEMS, INC.).

### 1.4 Research Purpose

The purpose of this research is to efficiently use piezoelectric sensors (bender elements) in dry and saturated centrifuge soil models, in order to measure the value of shear wave velocity ($V_s$) in the soil at different g-levels. The results are then used to characterize the soil. A secondary objective of the research is to measure the value of the dilatational wave velocity ($V_D$).

### 1.5 Thesis Organization

The thesis consists of six chapters including this introduction. The shear wave velocity, the factors affecting its value and ways of measurements is presented in the literature review in Chapter 2. The description of the centrifuge facility and the instruments used are described in Chapter 3. The work done as part of this research to improve the bender elements system is presented in Chapter 4. Details of the experiments and data analysis are presented in Chapter 5. Conclusion and recommendations are presented in Chapter 6.

Table 3.1: Centrifuge Scaling Relations (Whitman and Arulanandan, 1985).

| Quantity | Prototype scale | Centrifuge Model at Ng |
|---|---|---|
| | | |
| Length | 1 | 1/N |
| Area | 1 | $1/N^2$ |
| Volume | 1 | $1/N^3$ |
| Acceleration | 1 | N |
| Dynamic Frequency | 1 | N |
| Force | 1 | $1/N^2$ |
| Stress | 1 | 1 |
| Strain | 1 | 1 |
| Dynamic Time | 1 | 1/N |
| Diffusion Time | 1 | $1/N^2$ |

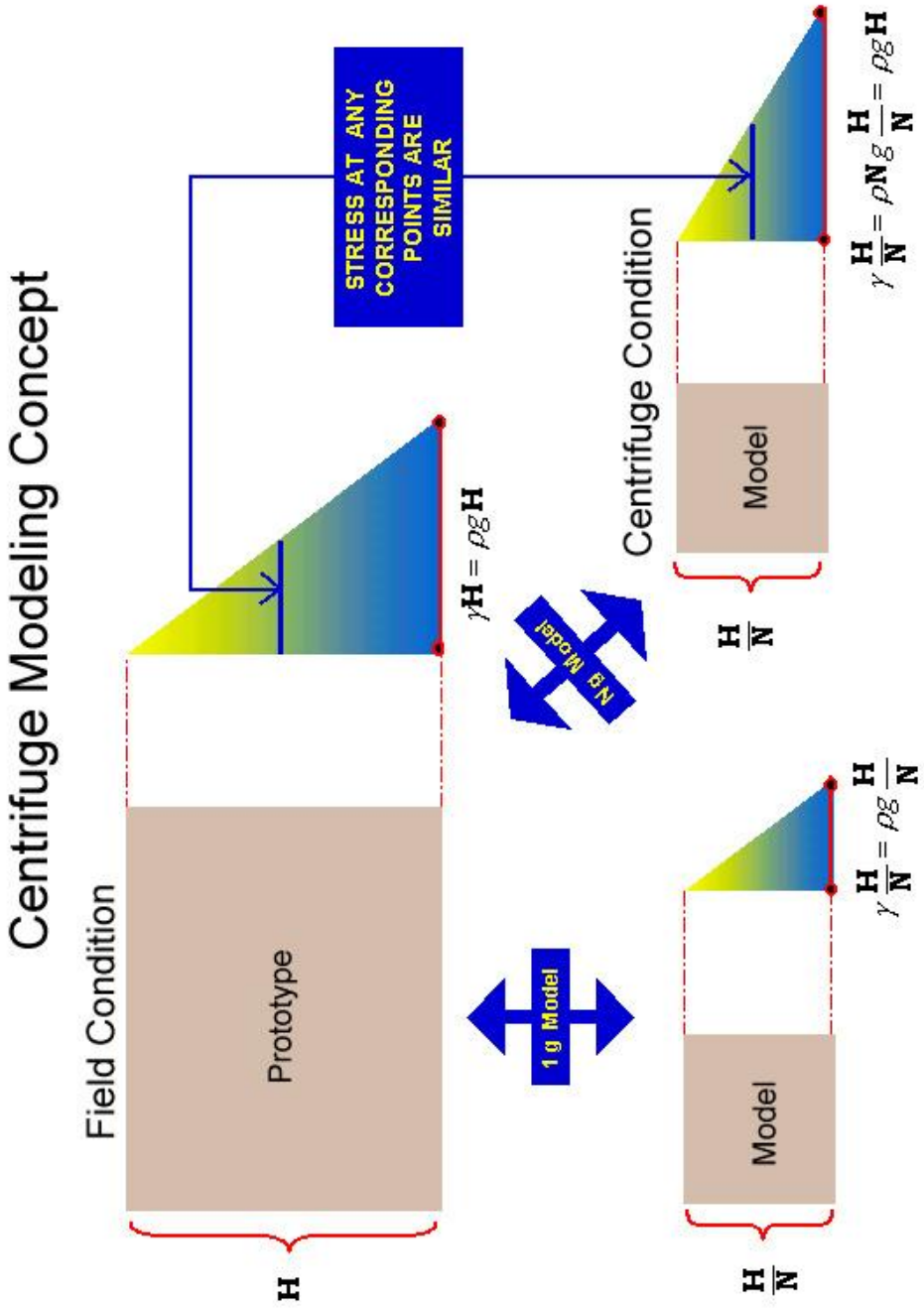


Figure 1.1: Centrifuge modeling concept (NEES@RPI)

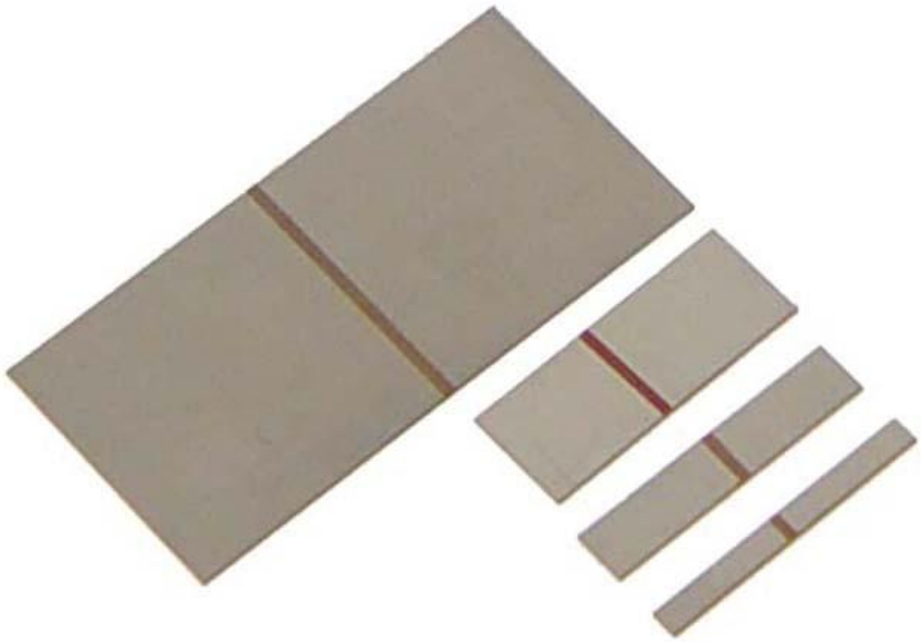

Figure 1.2: Different sizes of Bender Elements (PIEZO SYSTEMS, INC.).

# 2. LITERATURE REVIEW

## 2.1 Different methods of measuring shear wave velocity

### 2.1.1 Laboratory

#### 2.1.1.1 Resonant column

A non destructive method (within strain amplitude of $10^{-4}$ rad) is used to evaluate the low strain, maximum shear modulus ($G_{max}$) and the shear damping for a cylindrical soil specimen under undisturbed and remolded states. A triaxial chamber can be used to enclose the vibrator and the soil specimen to apply all-around pressure and axial load, as shown in Figure 2.1.

#### 2.1.1.2 Bender elements

Bender elements are piezoelectric transducers that can be used generate and receive mechanical waves in a soil. Primary and secondary wave velocities can be obtained using the system. This is accomplished by measuring the time difference between generation and receiving of a wave. Bender elements have been previously used in small specimens by attaching them to the cell of the triaxial or the resonant column machines.

### 2.1.2 Field

The measurement of soil shear wave velocity by field tests is commonly used in practice. Low strain field tests including seismic reflection, seismic refraction, suspension

logging, spectral analysis of surface waves, seismic crosshole, downhole-uphole tests and seismic cone tests are used to obtain dynamic soil properties including shear wave velocity ($V_s$) and maximum shear modulus ($G_{max}$). Several of these methods are also used to measure the dilatational wave velocity ($V_D$) in the field. Standard penetration, cone penetration, dilatometer and pressuremeter tests correspond to high strain test levels. Bang and Kim (2007) newly introduced a combination of low- and high-strain tests. This test is a modified form of the seismic uphole method. This method uses the impact energy of the split spoon sampler of SPT test as a source, as shown in Figure 2.2. This is called the SPT-based uphole method (Kim et al., 2004; Bang and Kim, 2007). The impact energy generated by the SPT test can be used as a source for the uphole method. The aim of this method is to record the shear waves during the SPT test without any additional explosives or mechanical sources (Akin et al., 2010).

### 2.1.3 Measuring Shear wave velocity in Centrifuge

#### 2.1.3.1 System identification

The system identification technique has successfully been used to calculate shear wave velocity in either the field or the centrifuge. The soil needs to be equipped with accelerometers in order to use this technique. The idea is based on calculating the shear stress at various elevations using the accelerometers readings. The Strain is also calculated from displacement measurements. These values are then used to draw the stress-strain loops and estimate the small strain shear modulus ($G_{max}$) (Zeghal et al., 1996). $G_{max}$ is then used to calculate the shear wave velocity using the relation:

$$G_{max}=\rho V_s \quad (2.1)$$

#### 2.1.3.2 Bender Elements

As described before, Bender elements are piezoelectric transducers that can generate and detect mechanical waves in a soil medium. Both primary and secondary wave velocities can be obtained using the system. Measuring S-wave ($V_s$) and P-Wave ($V_D$) velocities is of great importance in the analysis of the experimental data. However, using the bender elements in the centrifuge to measure wave velocities might be challenging. This is due to the very noisy environment associated with spinning (Lee & Santamarina, 2005). Other reason is the interference between channels when using more than one sender and one receiver in the same model. Also, controlling the wave so that it travels through the soil and not directly through the metal container might be challenging. The scope of the first part of the thesis is to modify the previous bender element system used in RPI centrifuge in order to solve these challenges.

## 2.2 Wave Velocity in Cohesionless Soil

In dry cohesionless soils, waves are transmitted via the contacting particles. The soil can be modeled in the first approximation as an isotropic elastic material defined by two constants; $G_{max}$ and the Poisson's ratio ($\mu$). The value of $G_{max}$ can generally be estimated using the value of shear wave velocity ($V_s$) using equation (2.1)

### 2.2.1 Main Factors Affecting Wave Velocity

#### 2.2.1.1 Confining pressure

Figure 2.3 shows the effect of confining pressure on dry sand on both shear wave velocity $V_s$ and dilatational wave velocity $V_D$. These data were taken from experiments done at the University of Texas (Stokoe et al., 1985). The loading condition was essentially isotropic. It was found that the Velocity increase with the increase in the pressure.

$$V_s = C1 * \sigma_0^{\ n} \tag{2.2}$$

$$V_D = C2 * \sigma_0^{\ n} \tag{2.3}$$

Where n is a constant ranging between 0.2 and 0.25 which can be as low as 0.17 and as high as 0.35, as mentioned in the literature.

#### 2.2.1.2 Void Ratio

The effect of void ratio on shear wave velocity was examined by Hardin and Richard (1963). Resonant Column tests were conducted for this purpose. The results are shown in Figure 2.4. It was found that $V_s$ decreases as the void ratio gets larger following the relation (for clean rounded sand).

$$V_s = 51 * (2.17 - e) * \sigma_0^{\ 0.25} \tag{2.4}$$

Where:

$V_s$ = Shear wave velocity (m/s)

$\sigma_0$ = Confining Pressure (KPa)

#### 2.2.1.3 Cementation

Wave velocity and modulus increase by Cementation. This is due to the increase in the stiffness of the interparticle contacts (Sponseller and Stokoe, 1995).

#### 2.2.1.4 Anisotropy

For the anisotropic case, due to the stress being different in different directions, the shear wave velocity is dependent on both the direction of polarization and propagation. The influence of both directions was found to be the same. The relation between the shear wave velocity and the stresses in the direction of propagation and polarization is as follows (Stokoe et al., 1985):

$$V_s = C * \sigma_a^{\,n/2} * \sigma_b^{\,n/2} \qquad (2.1)$$

Where:

C = constant depends on the soil type and the voids ratio

n ranges from 0.2 to 0.25

a is the direction of polarization

b is the direction of propagation

This effect of anisotropy on shear wave velocity is important for centrifuge modeling. The loading in the centrifuge experiments is typically anisotropic, due to the different values of vertical and horizontal stress, thus simulating the field conditions.

## 2.3 Piezoelectric Transducers

### 2.3.1 Two-Layer Motors (Benders & Extenders)

2 -layer elements can be made to elongate, bend, or twist depending on the polarization and wiring configuration of the layers. A center shim laminated between the two piezo layers adds mechanical strength and stiffness, but reduces the motion. "2-layer" refers to the number of piezo layers. A "2-layer" element actually has nine layers, consisting of:

a) four electrode layers,
b) two piezoceramic layers,
c) two adhesive layers, and
d) a center shim.

The two layers offer the opportunity to reduce drive voltage by half when configured for parallel operation (PIEZO SYSTEMS, INC.).

#### 2.3.1.1 Bending Motors

A 2-layer element bends when one layer expands and the other layer contracts. They are referred to as benders, or flexural elements. Bender moves on the order of

hundreds to thousands of microns, and bender force is typically about tens to hundreds of gram force. Figure 2.5 shows the common bending motor configurations. The variety of mounting and motion options make benders a popular choice of design engineers (PIEZO SYSTEMS, INC.).

### 2.3.2 Two-Layer Generator (Benders & Extenders)

Applying a mechanical stress to a laminated two layer element results in electrical generation. The electric signal depends on the direction of the force, the direction of polarization, and the wiring of the individual layers (PIEZO SYSTEMS, INC.).

#### 2.3.2.1 Bending Generators:

When a mechanical force causes a suitably polarized 2-layer element to bend, one layer is compressed and the other is stretched. Charge develops across each layer in an effort to counteract the imposed strains. This charge may be collected and converted into digital signal in computer. Figure 2.6 shows the bender generator configuration (PIEZO SYSTEMS, INC.).

Making a 2-layer piezo element either bend or extend is determined by how it is polarized and wired (PIEZO SYSTEMS, INC.).

### 2.3.3 Series and Parallel Operation

#### 2.3.3.1 Series Operation:

Series operation refers to the case where supply voltage is applied across all piezo layers at once. The voltage on any individual layer is the supply voltage divided by the total number of layers. A 2-layer device wired for series operation uses only two wires (one attached to each outside electrode), as shown in Figure 2.7 (PIEZO SYSTEMS, INC.).

#### 2.3.3.2 Parallel Operation:

Parallel operation refers to the case where the supply voltage is applied to each layer individually. This means accessing and attaching wires to each layer. A 2-layer bending element wired for parallel operation requires three wires (one attached to each outside electrode and one attached to the center shim), as shown in Figure 2.8. For the same motion, a 2-layer element poled for parallel operation needs only half the voltage required for series operation. This is why it’s usually used as senders requiring only half voltage than that of the series (PIEZO SYSTEMS, INC.).

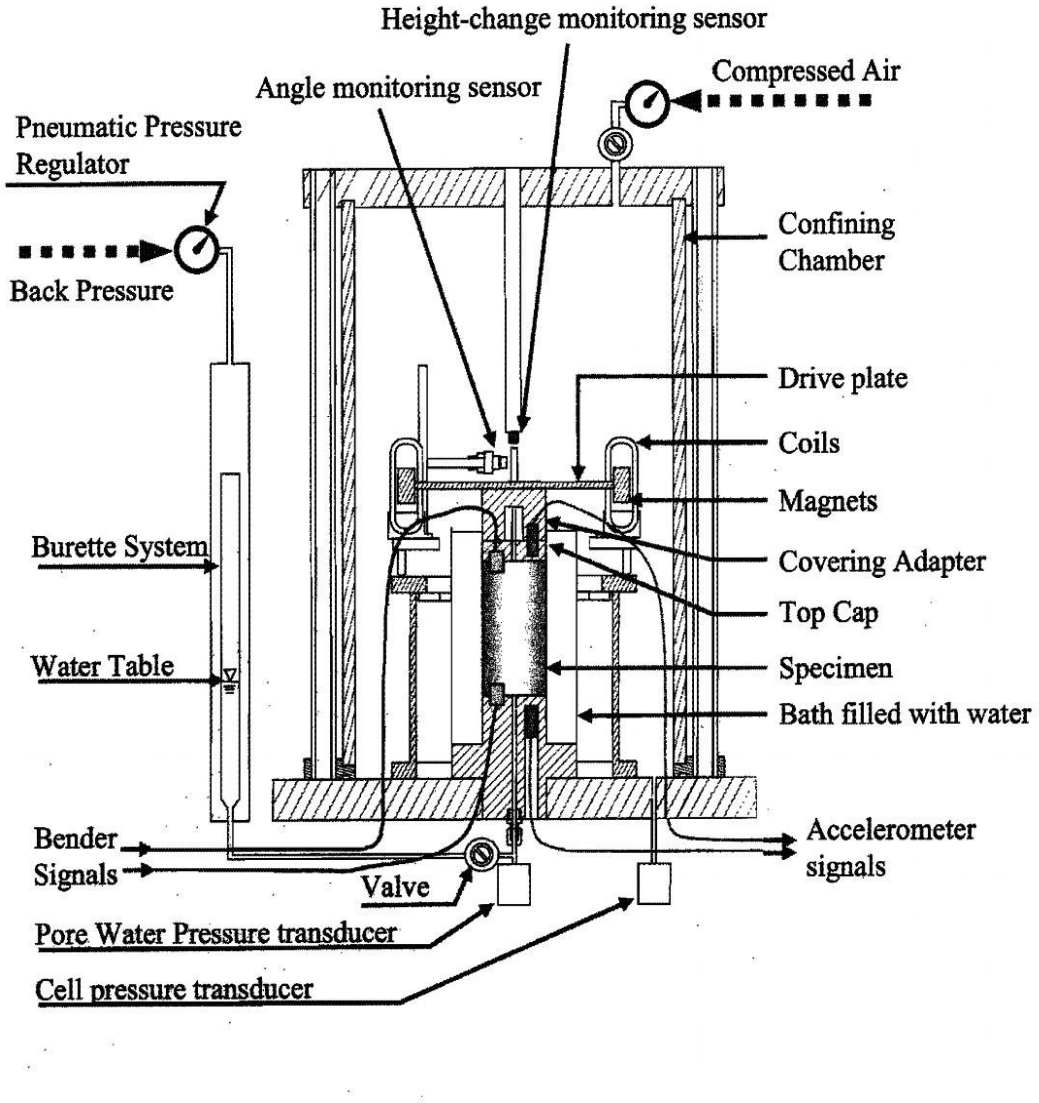


Figure 2.1: Resonant Column (Kim et al., 2006)

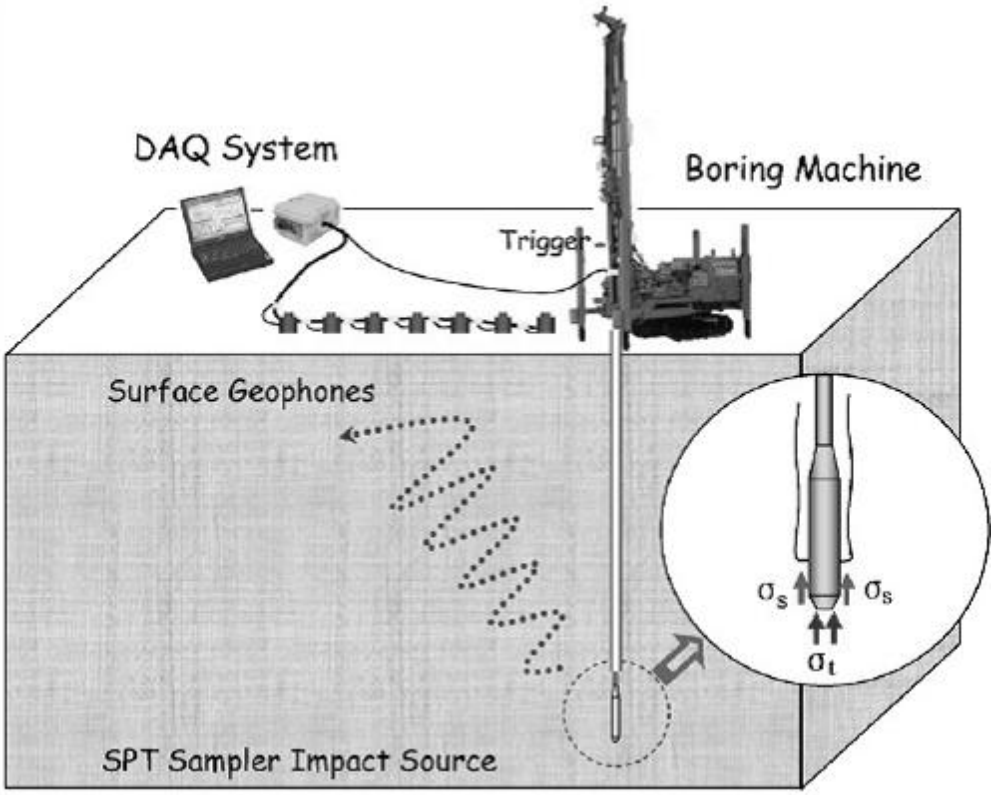


Figure 2.2: A schematic diagram of the SPT-based uphole method (After Bang and Kim, 2007)

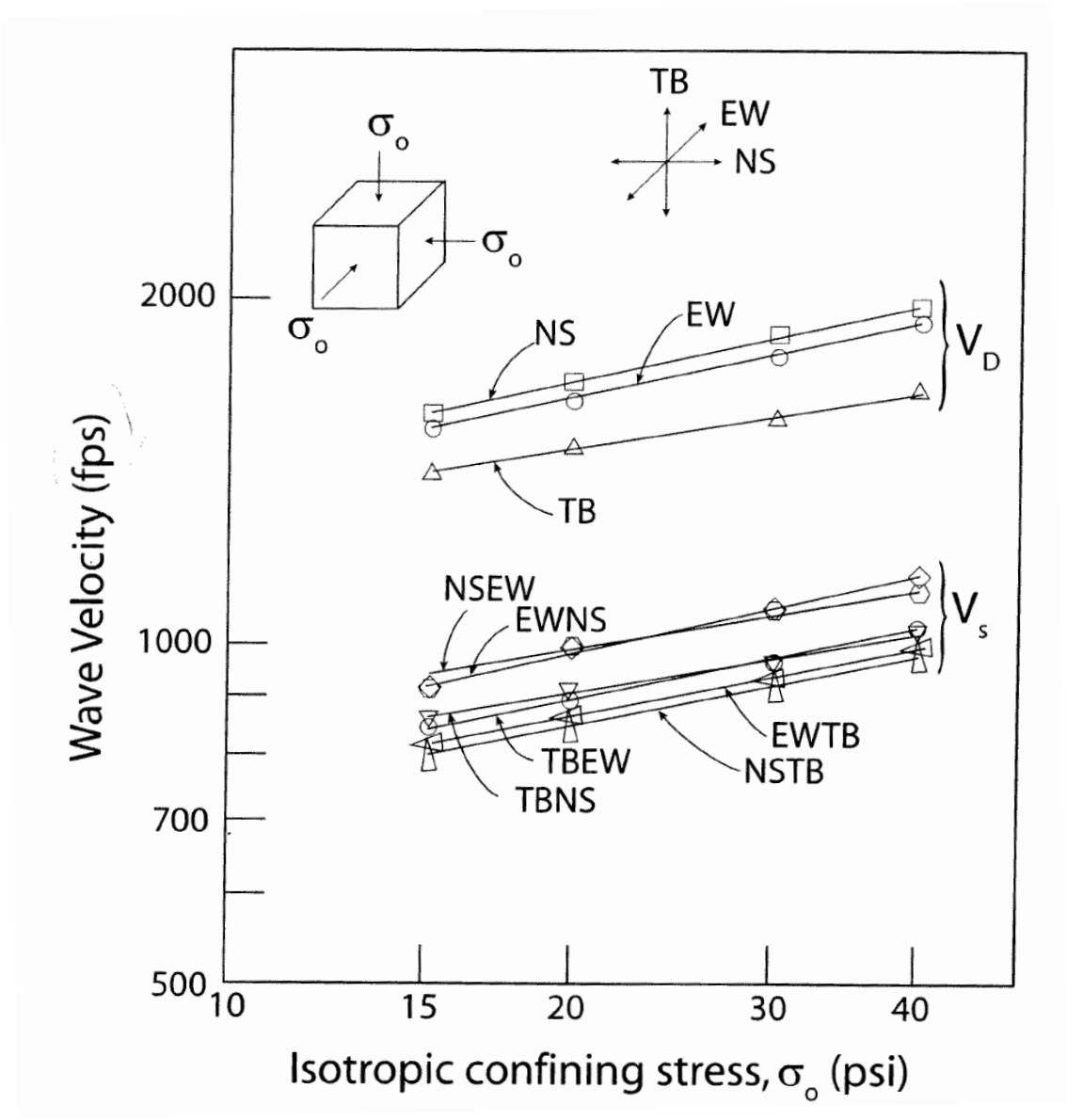


Figure 2.3: Log-log variation of $V_s$ and $V_D$ with isotropic confining stress $\sigma_0$ in dry sand (after Stokoe et al., 1985)

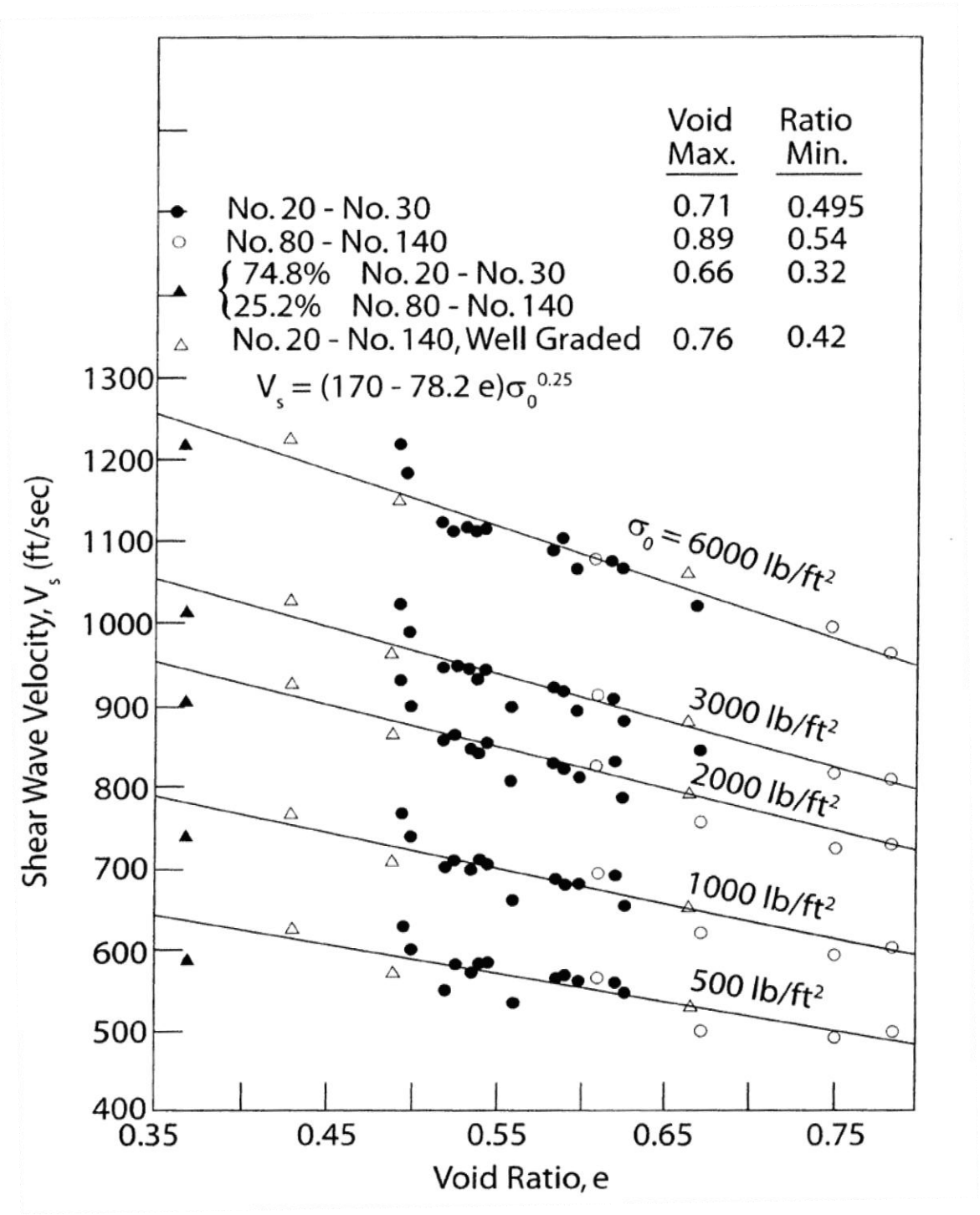


Figure 2.4: Variation of shear wave velocity with confining pressure and void ratio in dry clean sand with rounded particles (after Hardin and Richard, 1963; reproduced by Richard et al., 1970)

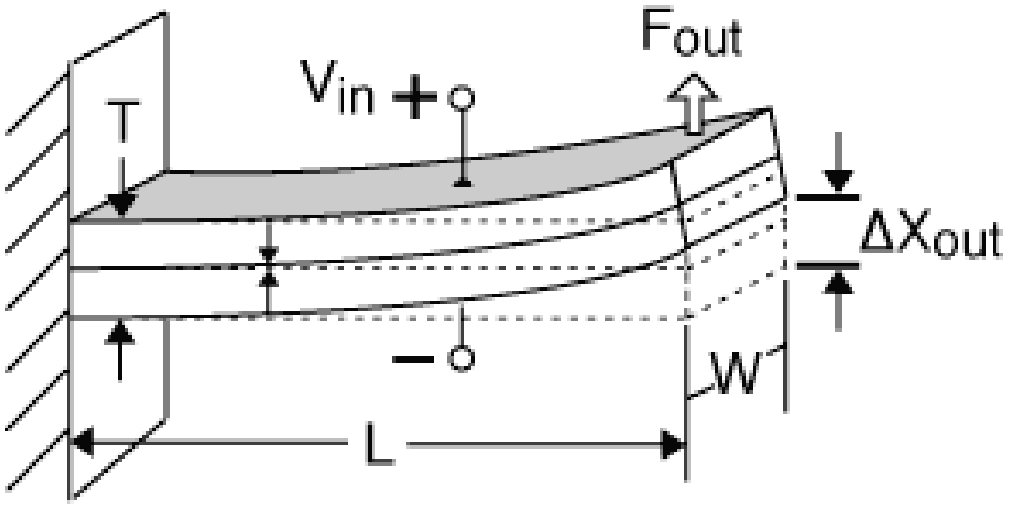


Figure 2.5: 2-Layer Bending Motor Mounted as a Cantilever (PIEZO SYSTEMS, INC.)

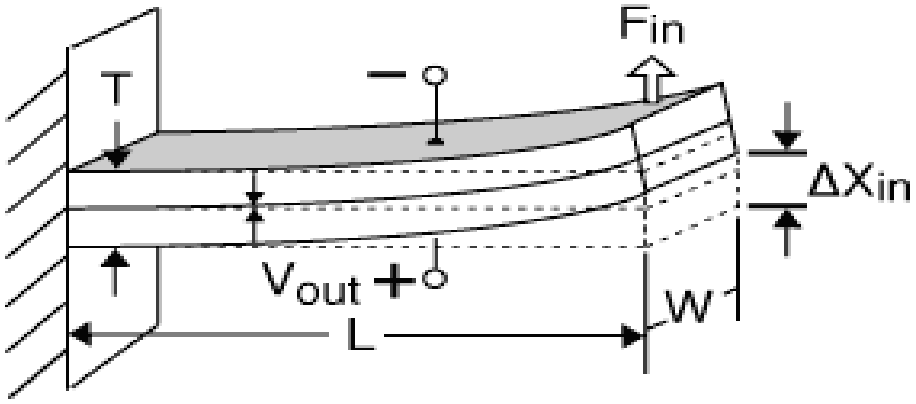


Figure 2.6: Bending Generator Cantilever Mount (PIEZO SYSTEMS, INC.)

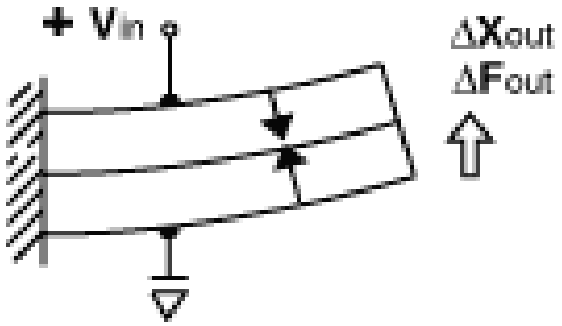


Figure 2.7: 2-Layer Bending Element Poled for Series Operation (2-wire) (PIEZO SYSTEMS, INC.)

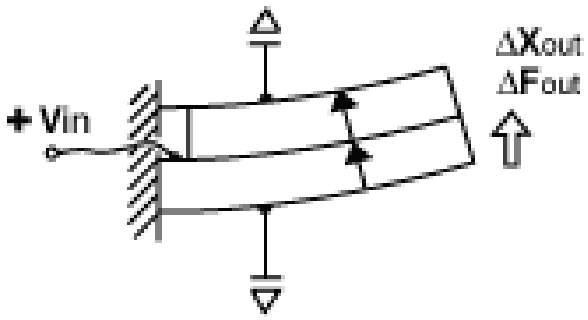


Figure 2.8: 2-Layer Bending Element Poled for Parallel Operation (3-wire) (PIEZO SYSTEMS, INC.)

# 3. INSTRUMENTATION

## 3.1 The RPI Centrifuge Facility

Experiments mentioned in this research were conducted using The Rensselaer Polytechnic Institute 150g-ton Geotechnical Centrifuge shown in Figure 3.1. This centrifuge is 3m in radius. It is one of fifteen state-of-the-art facilities in the US being part of the Network for Earthquake Engineering Simulation, NEES.

The original 100 g-ton RPI centrifuge was manufactured by Acutronic, France. It belonged to a line of Acutronic Machines all of which have the same basic mechanical structure. After the NEES upgrade to 150 g-ton by Actidyn Systemes in 2003, the current RPI centrifuge machine comprises (Ubilla, 2007)

- Swinging basket

- Centrifuge boom

- Balancing counterweight

- Hydraulic rotary joint and electrical slip-rings assembly

- Drive system

- Aerodynamic enclosure

- In-flight imbalance measurement and automatic balancing systems including automatic shutdown if excessive imbalance is detected.

This Centrifuge is located in the basement of the Jonsson Engineering Center (JEC) of the RPI campus in Troy, NY. The JEC also contains the offices of essentially all personnel, offices of graduate students conducting centrifuge and associated analytical research, and offices available for visiting users. The layout of the facility is shown in Figure 3.2. Main spaces shown in blue include the centrifuge itself and surrounding circular enclosure, as well as the connecting tunnel housing the variable speed motor controller and power electronics cabinets. Other main spaces of the centrifuge facility shown in blue in the image below are (Ubilla, 2007)):

(i) two model preparation rooms;

(ii) state-of-the-art control and teleparticipation room with four plasma screens and capacity for 6+ on-site operators/visitors;

(iii) robot room;

(iv) electronic development room;

(v) state-of-the-art teleconference room;

(vi) two rooms containing respectively the data acquisition (DAQ) and LAN servers; and

(vii) geotechnical computer laboratory.

More information about this state of the art geotechnical research center can be found at the website of NEES @ RPI.

### 3.2 Instrumentation, Hardware and Data Acquisition.

The bender element system includes hardware that was built in the centrifuge facility and devices from external manufacturers. Custom built hardware are the voltage follower and the bender element assembly system. The function of each hardware device is explained in the following sections (Tessari, 2007). Figure 3.3 illustrates the relation between hardware components in this system and how they interact with each others.

#### 3.2.1 Unity Gain Buffer (Voltage Follower) with a DAQ Device

Transducers, such as bender elements, convert physical phenomena into electrical signals that can be acquired by a data acquisition (DAQ) device. Bender elements convert mechanical waves into electrical signal, as discussed earlier. Considering the input and output range of the transducer is of great importance when selecting a transducer for use with a DAQ device. To acquire a signal from the sensor or to take full advantage of the resolution of the DAQ device, the sensor and DAQ device require signal conditioning to the system. One of the most important considerations that should be taken care of when building a DAQ system is the transducer's output impedance (National Instruments Corporation) & (Tessari, 2007).

Impedance can be defined as combination of resistance, inductance, and capacitance across the input or output terminals of a circuit. The input impendence of the DAQ device has to be much higher relative to the output impedance of the selected transducer (bender elements in this case). Generally, the lower the input impedance of the DAQ device the higher the measured signal will be disturbed by the DAQ device. It is

also important to make some reconditioning to the transducer to have as low output impedance as possible to accurately achieve analog input (AI) readings by the DAQ device. This reconditioning is done by adding the voltage follower to the system (National Instruments Corporation) & (Tessari, 2007). Part of this research includes using a different design for the voltage follower than the one previously used to decrease the output impedance of a sensor which would result in a clearer signal with less noise. The design was taken from NATIONAL INSTRUMENTS web site (National Instruments Corporation). Figure 3.4 shows the voltage follower that was used in the research and was partially manufactured at RPI Centrifuge sensors lab by the lab electrical engineer.

### 3.2.2 Linear Amplifier

A linear amplifier is an electronic device that can be used to increases an input voltage by a defined multiple and sends the modified signal to the desired output terminal. The necessity of the usage of a linear amplifier in the system is due to the fact that the data acquisition hardware can provide a maximum output of ± 10V. The strength of the mechanical wave generated by a sender bender element is related to the input voltage to the bender element. This range of 10V was found to be not high enough to produce a mechanical wave that can detected by a receiver bender element in the other side. It was found that a reasonable voltage necessary for the sender bender element system is in the range of 40 to 80 volts (Tessari, 2007). This voltage range was found to be enough for producing a mechanical wave that can be detected by the receiver. The device used in this experiment is a Piezo Systems EPS-104 Linear Amplifier shown in Figure 3.5. The input voltage can be increased to maximum of ± 200V and the multiplier

range is from 0 to 20. The time delay added is in the range of nanoseconds (PIEZO SYSTEMS, INC.). In most cases, this time delay can be considered negligible, as the time scale for this sensor system is on the order of milliseconds (Tessari, 2007).

### 3.2.3 PXI Computer

PXI stands for **P**CI e**x**tensions for **I**nstrumentation. This is the computer that interfaces with their data acquisition cards. They are provided by National Instruments Company. The computer is installed in a chassis placed in the cabinet of the Centrifuge. Multiple cards can be installed in the computer allowing for communication with local software programs. Windows remote desktop software is used to access the PXI. The centrifuge and the cabinet spin together. This allows for cabled connections to be established between the PXI and the transducers in the centrifuge basket as shown in Figure 3.6.

### 3.2.4 Data Acquisition Card

The card used in this system is a PXI-6259 DAQ shown in Figure 3.7. The National Instruments PXI-6259 is a high-speed multifunction M Series data acquisition (DAQ) board optimized for high accuracy at fast sampling rates. The fast sampling rate is of great importance in bender elements data acquisition. The card has two connector ports which allowing for a total of 32 analog input channels, and 4 analog output channels. The sampling rate of the card is 1.25 MS/s. The high sampling rate is important in the bender elements system due to the high frequency of the waves used. Also, the relatively high number of input channel is of great importance allowing for using multiple bender

elements in the same soil model. One purpose of this research is making use of the large number of channels provided by the card to help reduce interference between channels as will be discussed in chapter 4.

### 3.2.5 SCB-68

The SCB-68 is the link between the Voltage Follower and the DAQ card Figure 3.8. It is Noise Rejecting, Shielded I/O Connector Block with 68-Pin Connectors.

### 3.2.6 Signal Switch

Due to the relatively large size of the centrifuge model and the need to measure both S-waves and P-waves, multiple transmitting bender elements has to be used. This can be achieved by using a National Instruments 2565 General Purpose Relay (switch). This switcher is located in the PXI Chassis

The output signal from the linear amplifier is split between multiple channel and communication ports on the switch. This split is done using a wire that has one input coming from the amplifier and multiple outputs split between the switch channels as shown in Figure 3.9. The software instructs the switch to either open or close a port depending on which transmitter is selected (Tessari, 2007). Using this configuration, the switch can handle up to eight benders.

### 3.3 Data Acquisition Software

BEDAQ is the software used for data Acquisition. BEDAQ was developed at RPI as part of the research done by A. Tessari (2007). The software was developed using labVEIW. LabVIEW is a graphical programming environment used to develop control systems using graphical icons and wires that resemble a flowchart. labView is product of National Instruments company which is the same company providing the PXI and the DAQ card. This makes both the software and the hardware very compatible with each other allowing for maximum efficiency.

### 3.4 Laminar Container

A rectangular laminar container was built at RPI in 2002. Laminar containers reduce the boundary effect created by rigid containers in case of earthquake simulations. This box was designed to handle a wide range of cyclic lateral deformations occurring in the soil model in the free field. Laminar containers can be used to simulate the free field shear beam conditions in the soil during vertical shear wave propagation simulating earthquake waves (Whitman and Lambe, 1986). Such a container must be relatively light in weight, very flexible in the longitudinal direction of the wave polarization, rigid in the transversal direction, must dissipate minimal energy, and should have enough strength in the confining walls to provide the necessary complementary shear stresses. A horizontal cross section should also be maintained during the test to prevent undesirable horizontal straining of the soil. In order to increase flexibility, thin rings are used. This also accommodates possible shear strain concentrations. The main use of the laminar box at

RPI is modeling liquefaction and lateral spreading in the free field, so it was designed to allow relatively large lateral displacements (Ubilla, 2007).

The 1-D large laminar box used in this research, showed in Figure 3.10, consists of a stack of up to 38 rectangular rings separated by roller bearings These rings are arranged to permit relative motion between rings longitudinally only with reduced friction. Bearing cages are used between each two adjacent rings to properly align and space the rollers. The box is made of high strength aluminum alloy. Its weight is about 80 kg and has internal dimensions of 14" in width, 28" in length. The height of the box is adjusted according to the height of the model. The laminar box can be divided in two chambers: the inner chamber and the outer chamber. The inner chamber is the space inside the rectangular rings where the model is constructed, a flexible membrane is installed on the boundaries of this space to prevent water and sand grains to leak to the rings and the outer chamber. The outer chamber is the space between the outer walls of the laminar box and the membrane. Using pumps it is possible to create vacuum inside each of these chambers independently; this is very important for purpose of saturation (Ubilla, 2007).

### 3.5 Inflight 1-D Shaking table

The RPI In-flight 1-D shaker is of the type ES-18. This shaker generates an Earthquake-like shaking on a model in flight on the Centrifuge. It has the ability to work under high centrifugal force and provide high frequency output. This requirement arises from the centrifuge scaling law at a high g-level.

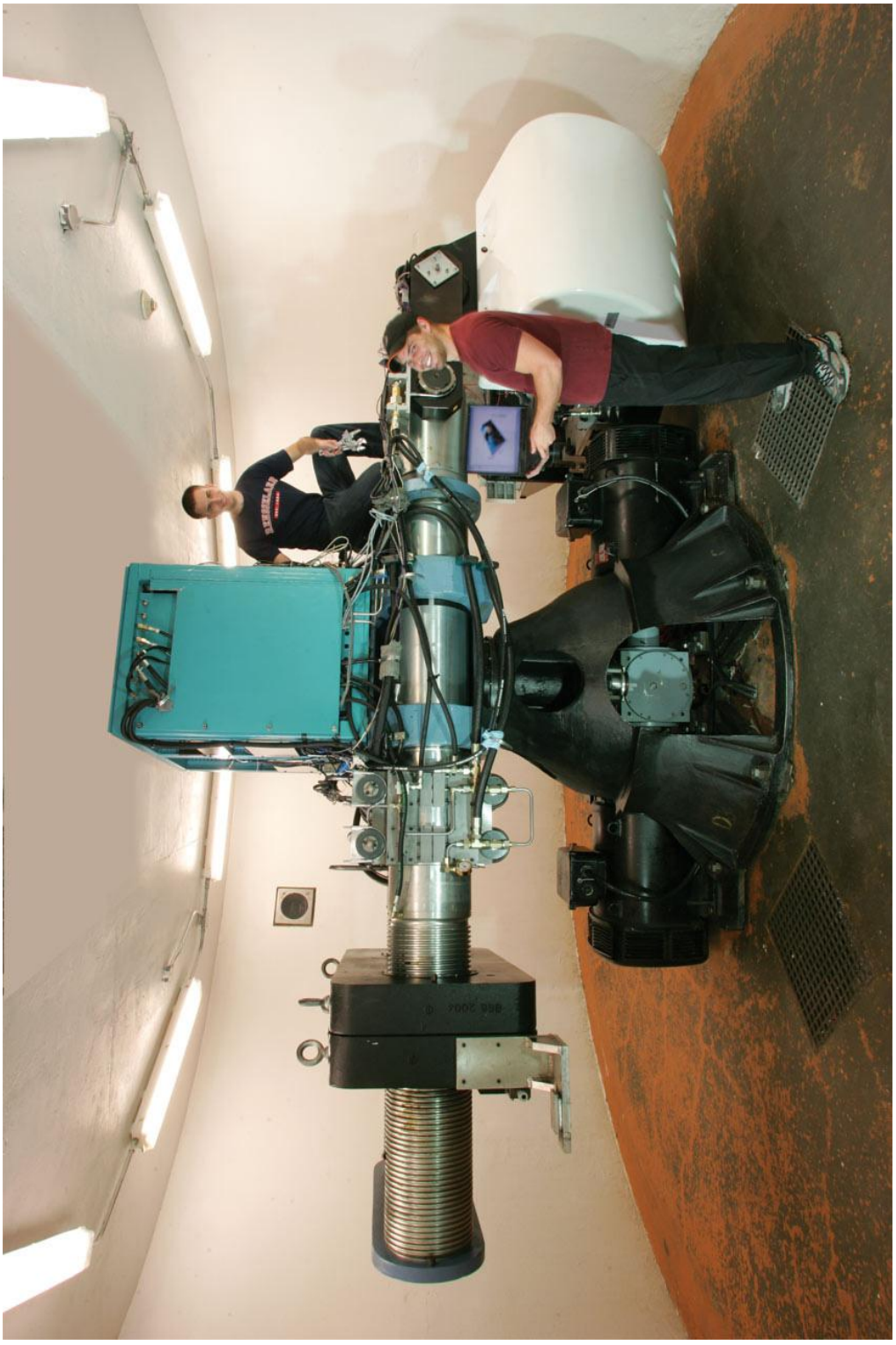

Figure 3.1: RPI geotechnical centrifuge (NEES@RPI)

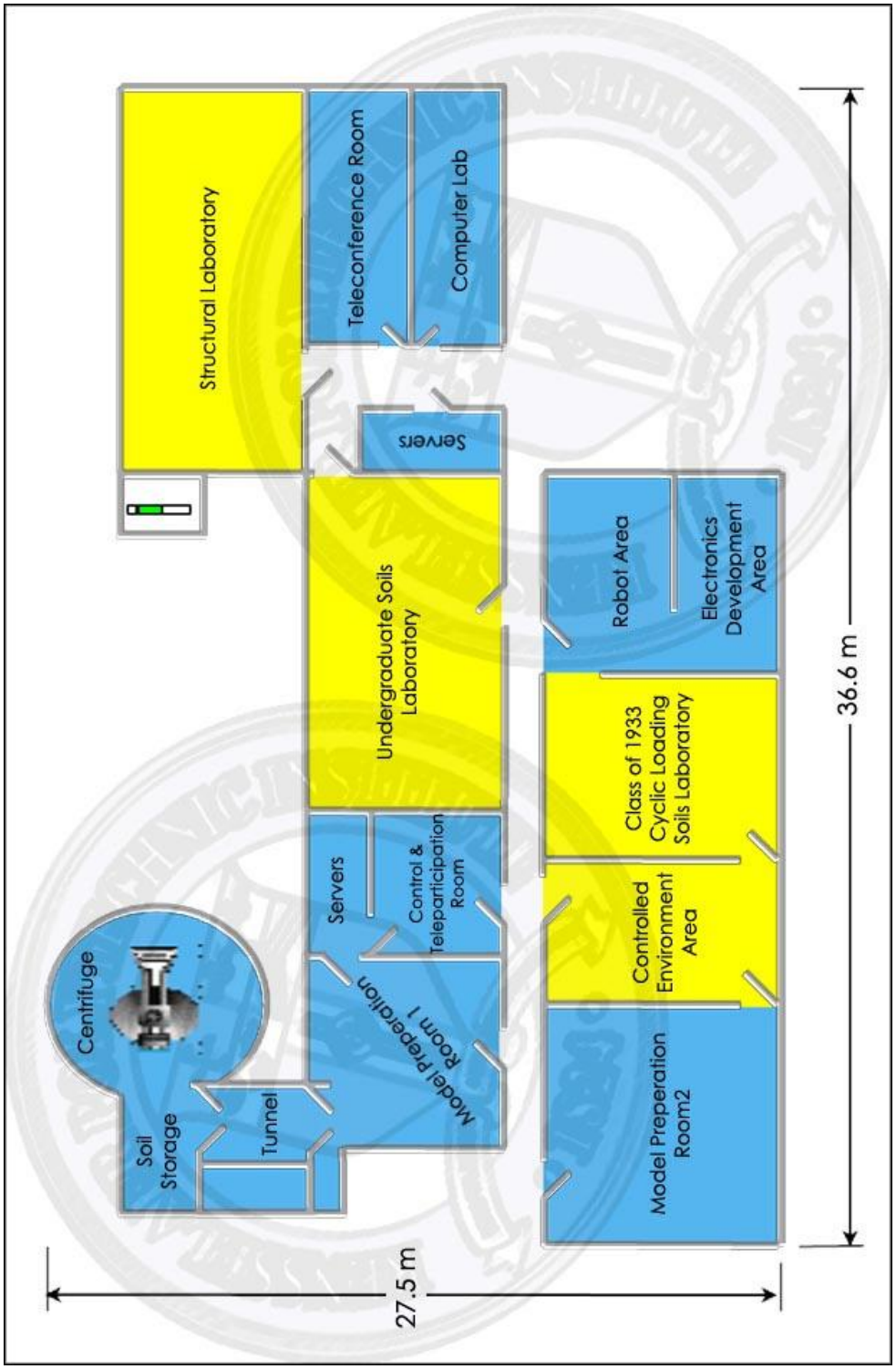


Figure 3.2: Layout of the centrifuge facility at RPI (NEES@RPI)

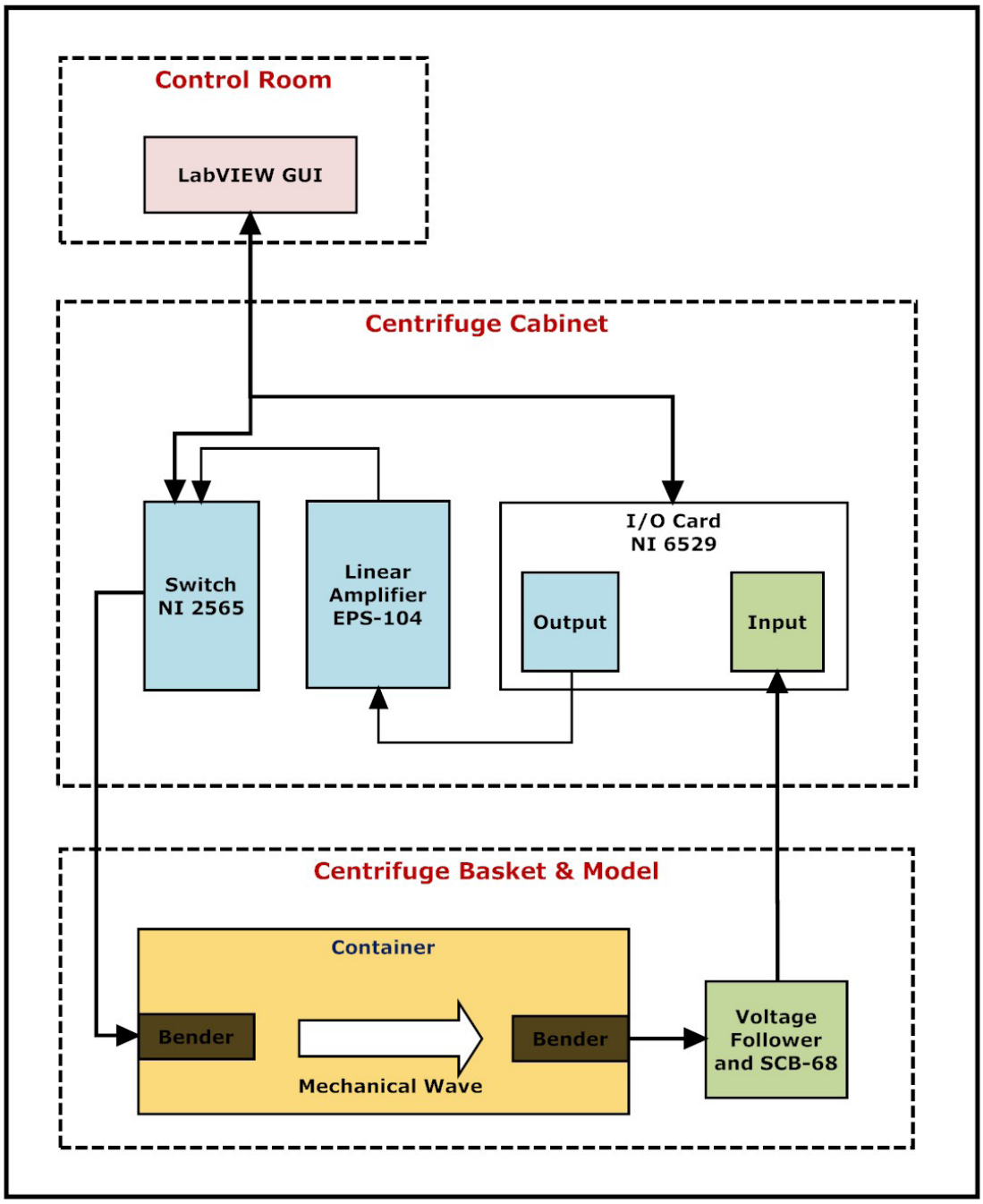


Figure 3.3: Layout of bender element system at RPI (Tessari, 2007)

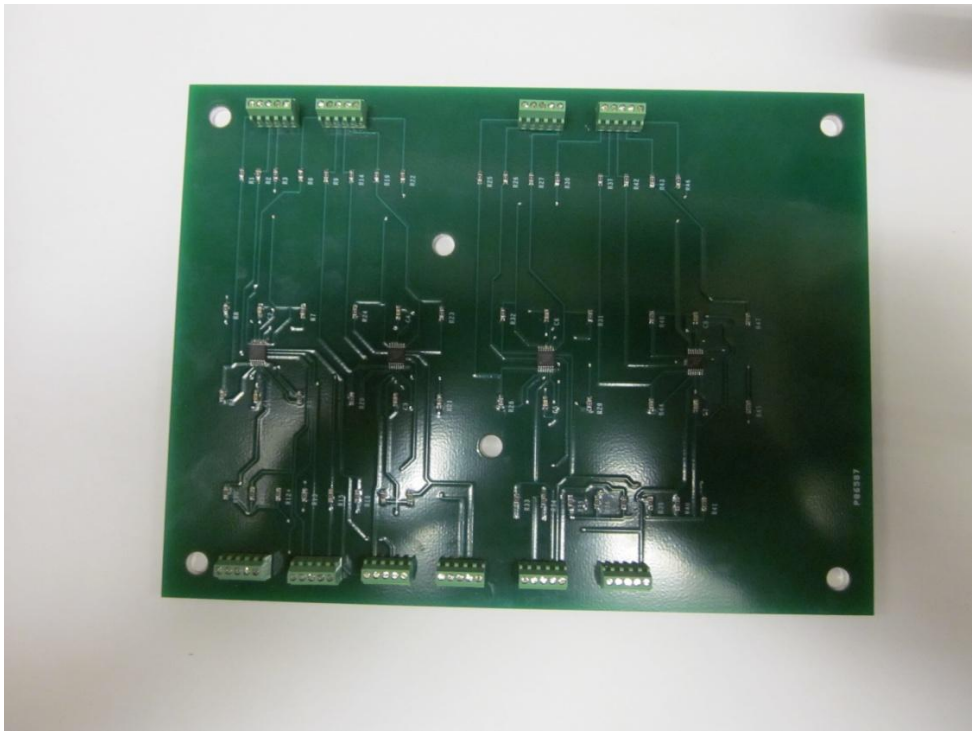

Figure 3.4: Voltage follower


Figure 3.5: Linear Amplifier (PIEZO SYSTEMS, INC.)

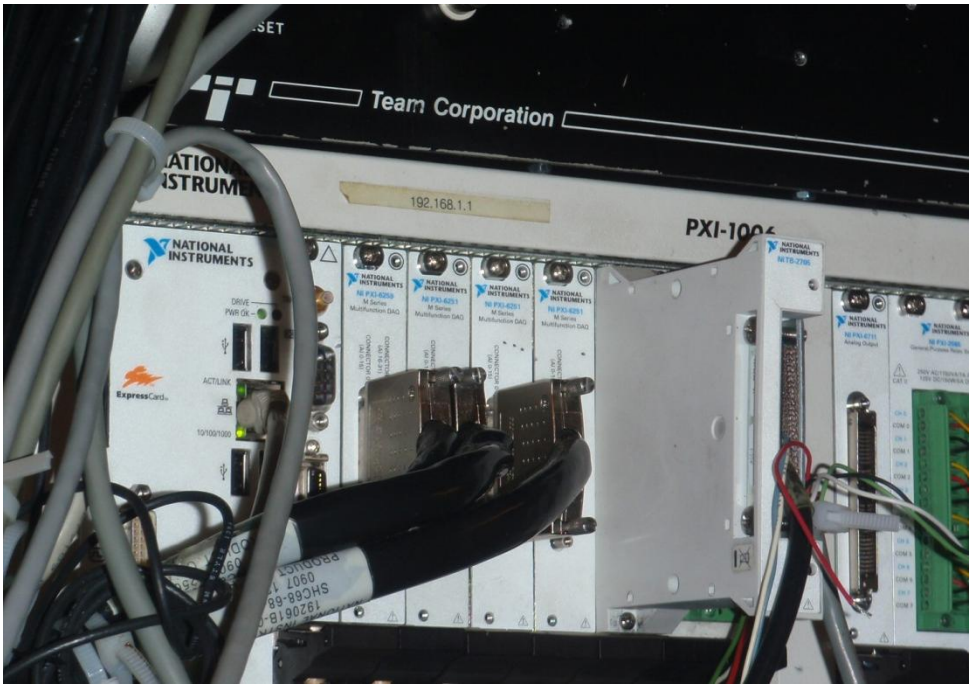


Figure 3.6: PXI Computer


Figure 3.7: NI-6259 DAQ Card (NI)

Figure 3.8: SCB-68 (NI)

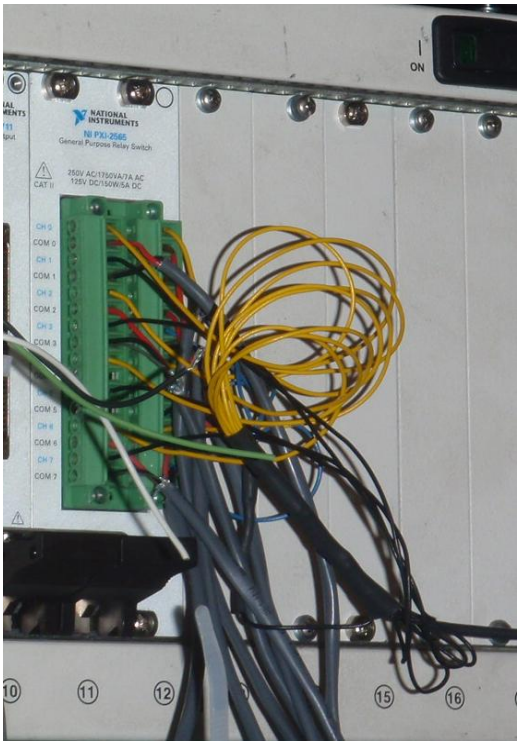


Figure 3.9: Signal Switch


Figure 3.10: Laminar Container (NEES@RPI)

# 4. ENHANCEMENT OF THE BENDER ELEMENT SYSTEM

The first part of this research includes troubleshooting of the previous configuration of the bender elements system and solving the existing problems. Figures 4.1 & 4.2 show the software output of the received signal before and after solving the problems of the system, respectively.

## 4.1 Challenges with the Previous System

After making several trials using the previous configuration of the bender elements, it was found that there was interference between channels of both the voltage follower and the SCB-68. This was found by isolating each part of the system and testing it separately. A function generator was used to produce a simulated wave to that expected to be produced by the receiver bender element. Figure 4.3 shows the function generator used. A scopemeter was used to read the output of the voltage follower and the SCB-68. Figure 4.4 shows the scopemeter used.

The major problems found in the previous bender element configuration can be summarized as follows:

- It was found in the previous configuration that there was a wave in the received signal occurring at zero time from the sent wave. This wave was found to be due to electromagnetic interference between sender and receiver bender elements.
- It was also found that there were some strange spikes in the received wave. These spikes lead to unclear received waves. Also, these spikes were found to be misleading when determining the peak of the received waves.

- It was found that the received waves did not have the same references. For instance, they did not average around the same average voltage.
- The use of one Aluminum rod to hold the bender elements was found to increase the noise and the interference.
- Interference between channels (Crosstalk & Ghosting)

### 4.2 Possible Solution to the problems

According to the National Instruments (NI) website, Ghosting is related to sampling rate. It is related to: 1) settling time, and 2) source impedance. When the impedance is high, more ghosting will affect the measurement. On the other hand, if the source impedance is kept below about 1 kOhm, any ghosting that occurs will be within the accuracy limits. This is the point behind using a Voltage follower. The voltage follower decreases the input impedance to the DAQ device. Figure 4.5 shows an example of the effect of ghosting on the scanned channels.

After searching for different reasons for ghosting on the internet, particularly the NI website, it was found to be due to one or more of the following reasons:

- Improper Grounding

  The measured signal should be in reference to the same ground plane as the DAQ device, else there will be a potential for ground loops. Ground loops can cause offsets and error in measurements.

- Unconnected or Open Channels

If unconnected channels are included in your scan list, you may see voltages from one scanned channel reflected on another scanned channel.

- High Source Impedance

  If the input to the multiplexed systems has high source impedance, you may see a behavior similar to the unconnected or open channel.

- Noise

  The surrounding environment may have the effect of noise or unwanted signals on the measured signals. This noise may be from other signals measured by the same DAQ device or from the surrounding working machines, the centrifuge for instance. It can be also due to the electric current.

- Damaged DAQ card

  If the card is damaged, it's more likely to receive readings that are not accurate.

- Bent or broken pins on DAQ card

  If a pin is broken or bent, it's more likely that the card reading is not accurate.

- Improper settings of the software

  This happens when the software settings is incompatible to the DAQ device.

The procedures done in order to solve the ghosting and other problems in the system are as follows:

- ✓ The DAQ card was examined to make sure that it was not damaged and does not have any broken pins.

- ✓ To prevent crosstalk between channels, a grounded channel was scanned between each scanned channels. This was meant to discharge the capacitance. To achieve that, each other channel in the SCB-68 was grounded and not connected to any input source as shown in Figure 4.6.

- ✓ Also, the grounding of unused channel was checked. This is important to prevent voltages from one scanned channel reflected on another scanned channel.

- ✓ In order to minimize the effect of noise from the surrounding environment, proper shielding had to be implemented. To achieve this purpose, the end of the cable shielding, from the bender element side, had to collect any undesired electric signals surrounding the bender elements. These signals may be due to any surrounding magnetic field. To achieve this purpose, a Faraday's Cage was made as a final layer of the finished bender elements. This was achieved by drawing a continuous strip of silver paint (a conductive material) rotating around the bender element, as shown in Figure 4.7. The shielding of the cable was then fixed to the silver strip. The Faraday's Cage prevents the production of any electric field

within the enclosure of the bender elements and helps in removing any undesired charges. These procedures were found to be extremely helpful in reducing ghosting and crosstalk in the system. Moreover, it helped in eliminating the undesired signal occurring at zero time. This undesired signal is thought to have been an electromagnetic leakage from the sender to the receiver bender elements. Shielding both the sender and the receiver bender elements using the procedures discussed earlier helps eliminating this signal from the results (Deniz, 2008).

- ✓ The shielding in the other end of the cable was then attached to the common ground of the system. The ground of the PXI was connected to the ground of both the SCB-68 and the voltage follower. The shielding of the receiver bender elements was connected to the ground of the system through the ground of the voltage follower. The shielding of the sender bender elements was directly connected to the ground of the PXI.

- ✓ The aluminum rod, shown in Figure 4.8, was used in the old configuration. To maintain its stability, it had to be attached to the base of the container. While the shear wave velocity in soil is in the order of hundreds m/sec, the shear wave velocity in Aluminum is in the order of thousands m/sec. This leads to a faster mechanical wave traveling directly through the Aluminum from the rod to the container. This wave was sometimes mistaken to be the wave passing through the soil with misleading results. Also, the exposed Aluminum rod is thought to be acting like an antenna collecting noise and undesired electric waves. To solve this

problem, each bender element was put inside a Jam screw which was then fitted in a small Aluminum angle, as shown in Figure 4.9. The purpose of the Aluminum angle was to easily fix the orientation of the bender elements in the soil model. The use of the Aluminum angle not only helps reducing noise, but also allows for more flexibility in placing the bender elements in the soil in different elevations and with different orientation. This allows for measuring both S-wave and P-wave velocities. Moreover, it helps to reduce the undesired effect of the rod in enforcing the soil during the horizontal shaking in seismic analysis testing using the laminar container.

- ✓ In the previous system, the SCB-68 was used as power supply to the voltage follower. After several trials and testing the stability of the SCB-68 power source, it was found that it did not have a stable voltage. Moreover, the voltage was found to have some spikes. The instability of the power source was found to lead to unstable results. The dry battery cells were found to be a good and stable alternative power source, and were used in the system in the early stages. Later on, an independent power source fixed in the centrifuge cabinet was used.

- ✓ The coaxial cable, shown in Figure 4.10, was used in the old configuration. The coaxial cable did not allow for complete isolation between the negative pole of the bender elements and shielding of the cable, due to the absence of a negative pole in the cable. To solve this problem, a dual core cable was used. This dual core cable has a positive pole, a negative pole and a shielding as shown in Figure

4.11. The dual core allows for complete separation between the ground and the negative pole resulting in a more stable signal.

- ✓ In order to make sure that the software is working properly and sending the required wave with no time delay in the system, a system check was done. This was done by connecting the output signal (sine wave) of the software to one of the input channels to the system. The software displayed the exact sine wave at a time delay in the order of nanoseconds. The time expected in the bender elements system is in the order of milliseconds. So, the time delay in the system is expected to have a very negligible effect on the results.

### 4.3 Bender Elements Fabrication Process

Bender Elements can easily be fabricated in laboratory. The manufacturing process can take up to two hours for a group of eight benders. However, the bender element cannot be used before one week, because of the need to cure the polyurethane which acts as a sealant to protect the bender elements. In this research, two configurations are used. These are the series configuration and the parallel configuration. The series configuration is used for the receiver bender elements, while the parallel configuration is used for the sender bender elements. Both configurations can work as senders or receivers. However, for the same motion, a 2-layer element poled for parallel operation needs only half the voltage required for series operation. This is why the parallel configuration is used in the case of sender bender elements (NEES @ RPI), (Tessari, 2007) & (Deniz, 2008). In this research, a total of eight sender and eight receiver bender

element sensors were manufactured. The manufactured bender elements were used to conduct experiments discussed in Chapter 5. Also, they were later used by other researchers in the centrifuge lab at RPI to measure wave velocities in the centrifuge soil models.

### 4.3.1 Tools and supplies required for the manufacturing process:

- cable
- piezoelectric chip (dimensions:12.7 mm x 8 mm x 0.6 mm)
- flux
- solder
- jam screw
- polyurethane
- epoxy
- silver paint
- oil
- wax
- soldering iron
- Rotating-tip hand tool
- wire strippers

### 4.3.2 Preparing the cables

The first step in the manufacturing process is preparing the cable. Although this sounds like an easy process, it has to be made precisely to fit exactly in place.

The preparation procedures are as follows.

1. Remove about 3.0 cm of the outer plastic cover of the wire.

2. Separate the red and black conducting wires, shield wire, and foil from each other and cut the outer foil.

3. Cut off about 1.0 cm from the tip of the red and black wires to make the shield wire longer than them.

4. Remove about 0.4 cm of the plastic cover of both red and black wires.

5. For the parallel configuration wire, split the strands of the black wire into two groups. Each group stick to one side of the bender element ship as will be discussed later.

6. Tin the black and the red wires.

7. Make the shield wire as flat as possible to easily fix it with the silver paint.

After the preparation of the wires, the bender elements should be ready for the manufacturing process.

The manufacturing process for the parallel configuration is slightly harder than the series configuration, as will be discussed in the following section.

### 4.3.3 Manufacturing process

#### 4.3.3.1 Parallel Configuration

The manufacturing procedures for the parallel configuration are as follows:

- The outer ceramic layer must be removed in a small area (2 mm X 2 mm) of either sides of the parallel chip as shown in Figure 4.12. This should be done very carefully using a rotary tool with abrasive tip until the middle electrode material is exposed. Make sure you don't cut the middle electrode material or else the whole chip has to be disposed.

- The chip should then be washed with water to remove extra powder.
- In order for the solder to stick, flux has to be applied to the exposed electrode.
- Solder the red wire to the previously exposed middle electrode making the positive pole of the bender.
- Carefully apply flux to both sides of the chip in the place where the split black wire is fixed.
- Solder the split black wire to each surface of the chip, where you applied the flux, making the negative pole of the input signal as shown in Figure 4.13.
- Wipe the chip with water to remove extra flux and dirt.

- Dry the chip using air. Make sure that the wires and the chip are totally dry before moving to the next step. The reason is that water, if left behind, might act as a conductor between the two poles of the bender elements, and thus destroying the results.
- Separate the shield wire from the chip. After that, apply the first coat of polyurethane using a brush. Let the bender elements vertically stand for 20 minutes for the coating to dry. Apply four more layers of polyurethane waiting 20 minutes between each layer. After applying the five layers of polyurethane, let the bender elements vertically stand for 7 days for the polyurethane to cure.
- The next step is to fix the chip inside of the screw. Usually, half of the chip is left outside the screw free to move and the other half is fixed in the screw using epoxy. First, tape the exposed part of the chip and shield wire to protect it from the epoxy. Then, protect the threads of the screw from the epoxy using a tape or Teflon sheet. After that, apply the epoxy to the front of the chip, following the instructions on the back of the epoxy tube. Make sure to have enough epoxy that it can drip through the screw.
- Remove the tape, and then apply silver paint as a continuous strip around the bender chip. Stick the flattened shield to the silver paint before it dries. Add another layer of silver paint to ensure connection between the silver and the shield.
- Let the silver paint to totally dry. You can also coat the screw in oil to protect from rusting.

- The screw is then fitted into the aluminum angle to maintain the desired orientation of the bender elements in the soil model as discussed earlier.
- It is also recommended to cover the exposed parts of the screw with wax to protect it from rusting.

Figure 4.14 shows a finished bender element after applying all the previously mentioned procedures.

#### 4.3.3.1 Series Configuration

The manufacturing procedures for the series configuration are as follows:

1. Rinse the chip with water and then let dry.

2. Apply flux to the ends of the piezo chip where the wire should be place.

3. Solder the red wire to one side, and the black wire to the other side making the two poles of the bender elements.

4. Follow the same steps from 6 to 10 of the parallel configuration manufacturing process.

### 4.4 Placing the Bender Elements in the soil model

After finishing of the fabrication process, the bender elements are ready to be placed in the soil model. Placement and orientation of the bender elements depend on the type of wave velocity required to be measured. For measuring S-wave velocity, the bender

elements are placed so that the tip of the receiver bender element is facing the tip of the sender. For measuring P-wave velocity, the bender elements are placed such that the wide side of the receiver bender element is facing the wide side of the sender as shown in Figure 4.15.

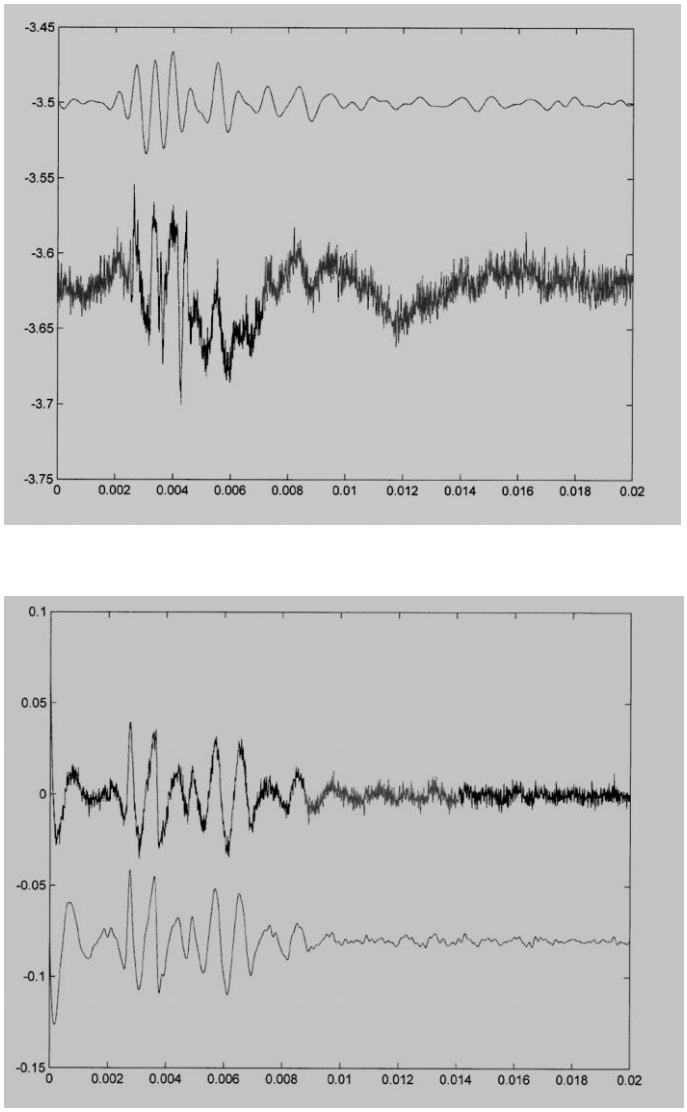


Figure 4.1: Samples of results from the previous system at high g-level filtered and unfiltered

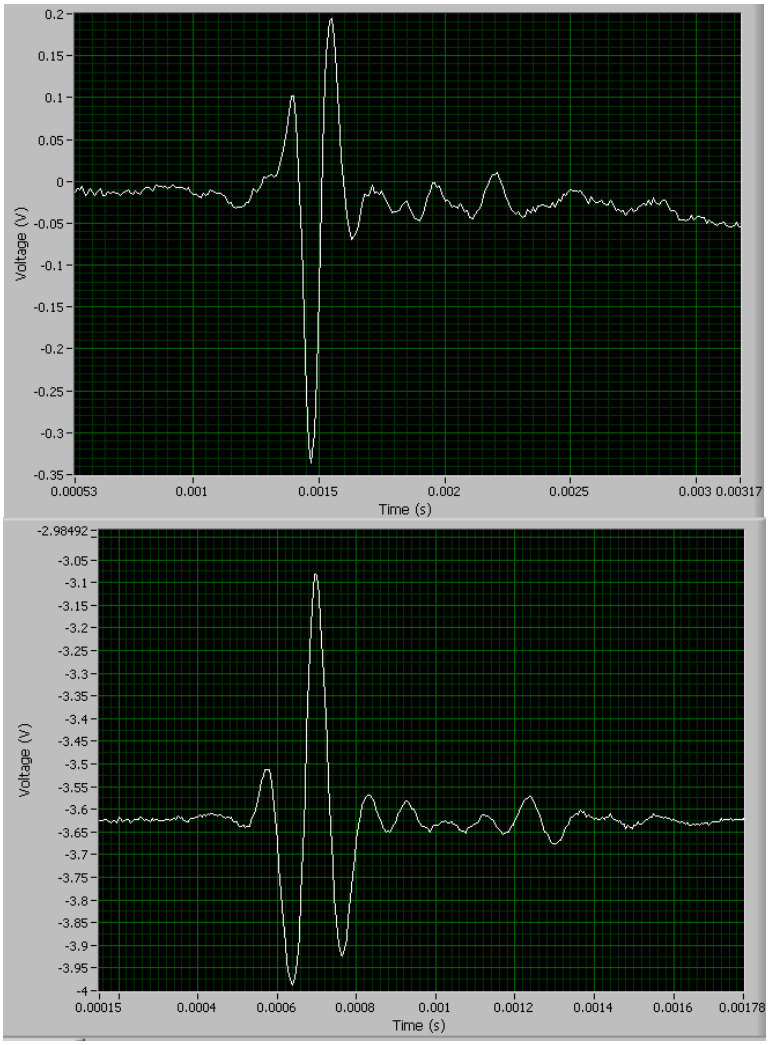


Figure 4.2: Samples of results at high g-level after Enhancement of the system (No filter is applied)


Figure 4.3: The function generator used in the research (Agilant 33220A)


Figure 4.4: The Scopemeter used in the research (Fluke 192B)

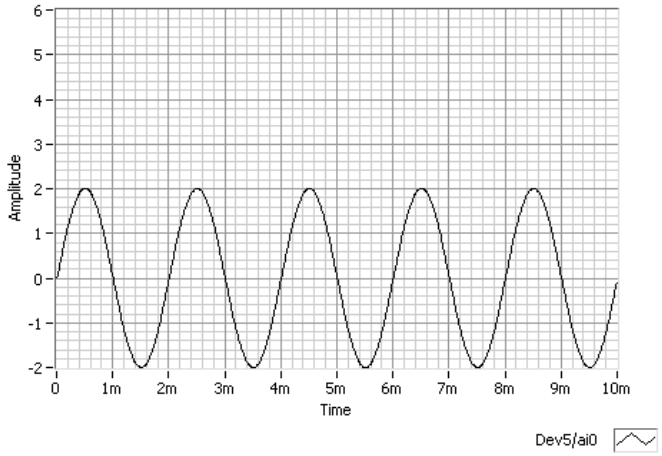
Amplitude
Time
Dev5/ai0
Dev5/ai1

(a)

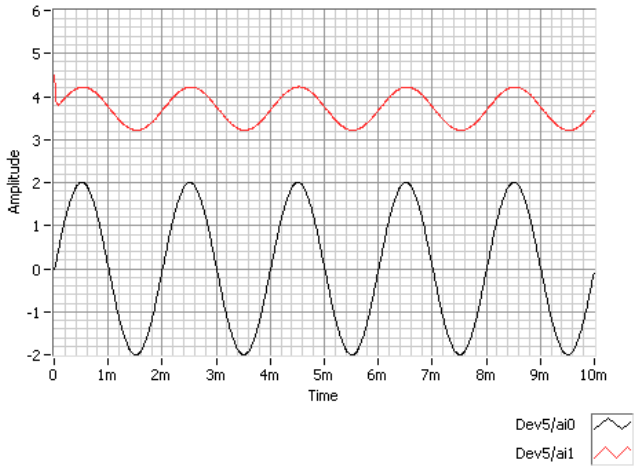
Amplitude
Time
Dev5/ai0
Dev5/ai1

(b)

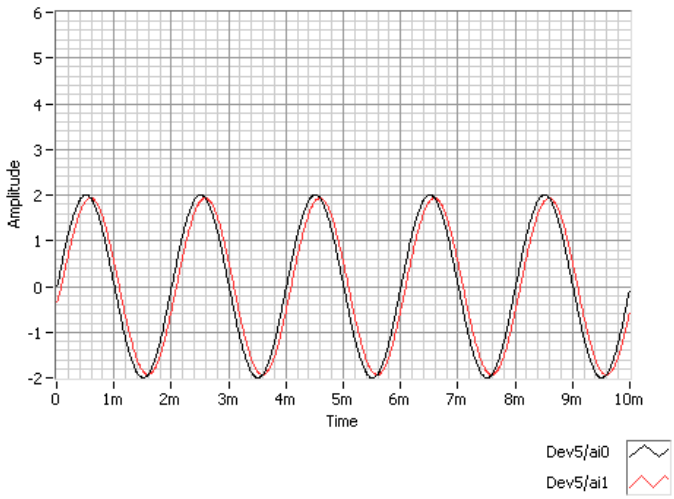


(c)

Figure 4.5: Explaining ghosting. Sine wave of amplitude 2 volts source is connected to ai0, constant 5 volts to ai1 a) scanning each signal individually (no ghoasting) b) both channels are scanned (reflected sine wave into channel 1) c) constant 5 volts is completely disconnected, ai0 &ai1 are scanned. Reflected sine wave into ai1 of the same amplitude of the original wave.

(adapted from National Instruments Corporation)

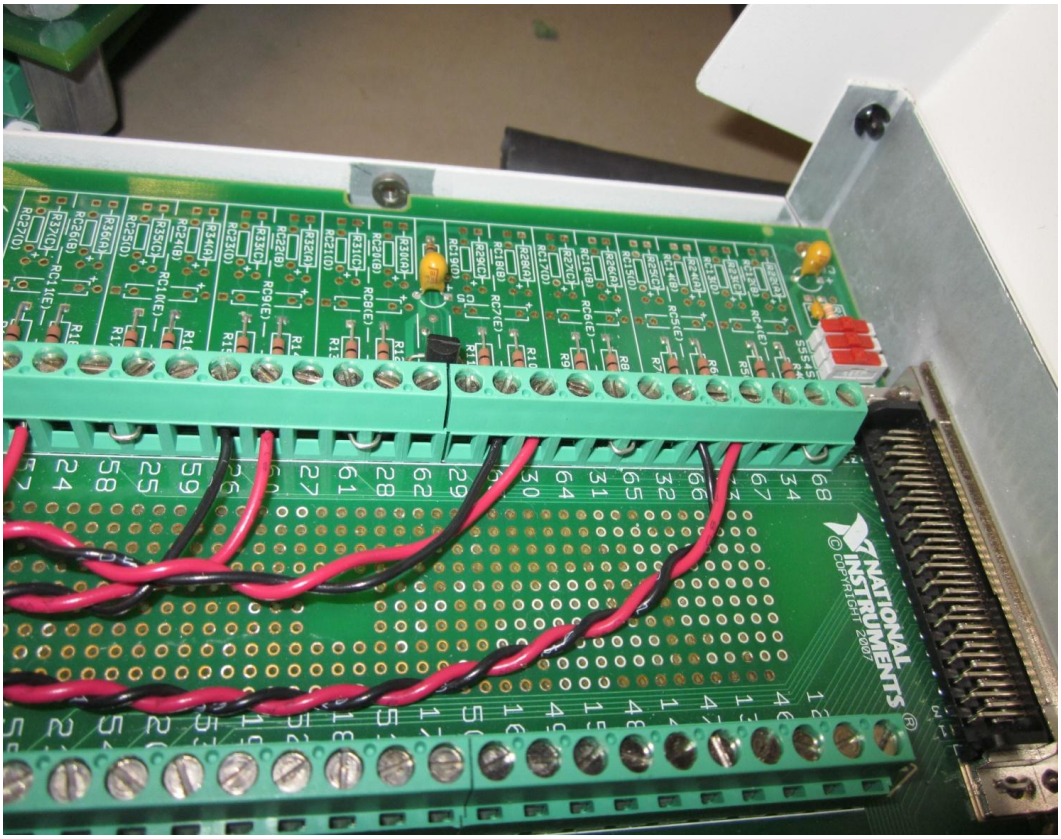


Figure 4.6: Grounding a channel between each scanned channel in the SCB-68

Figure 4.7: Finished bender element in the screw before putting in the mounting angle

Figure 4.8: Channel used to mount the bender elements in the previous system

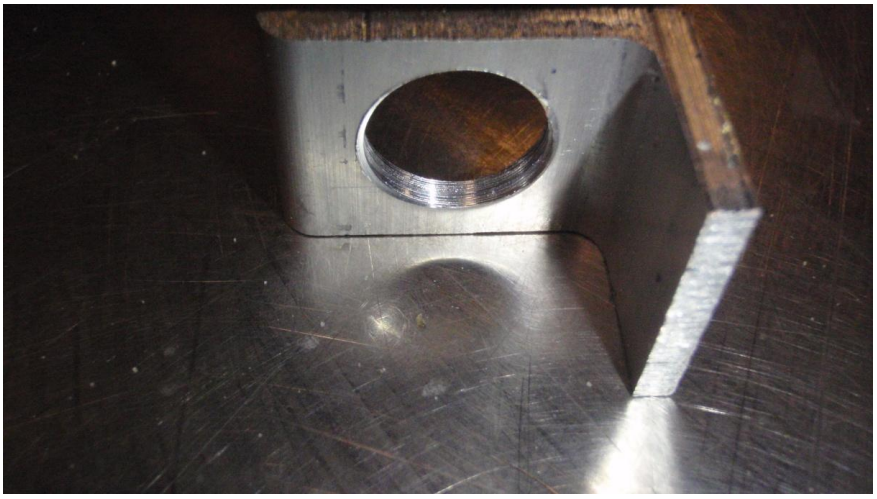

Figure 4.9: The angle used to support the bender elements in soil in the enhanced system

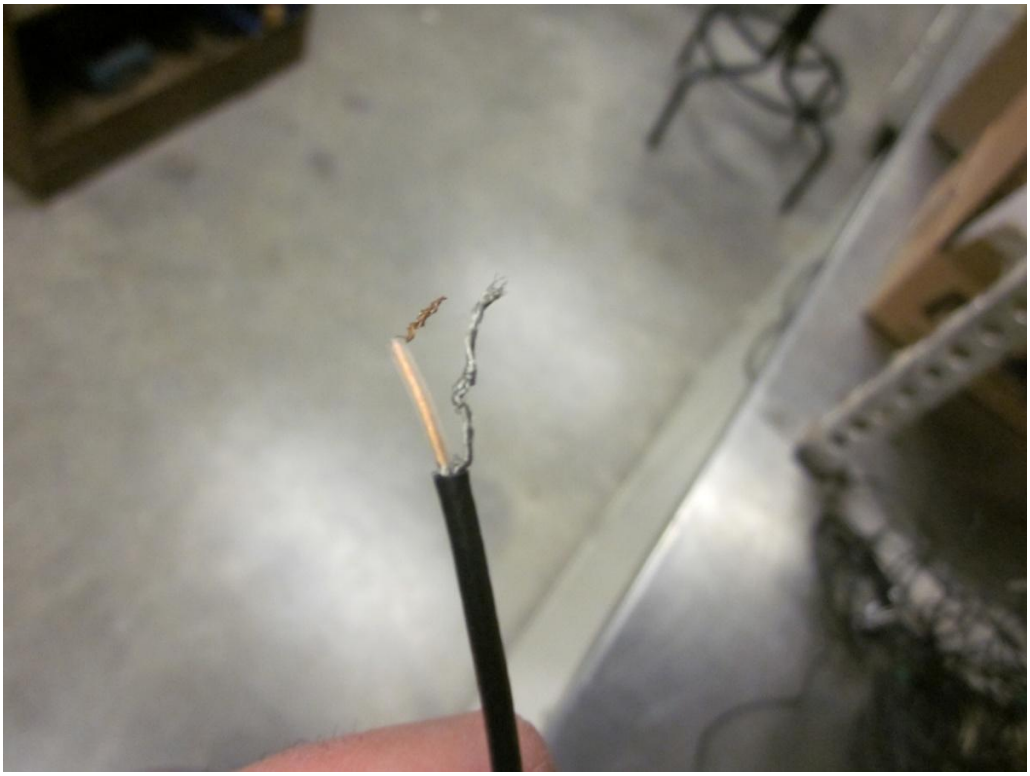

Figure 4.10: Coaxial Cable used in the previous system

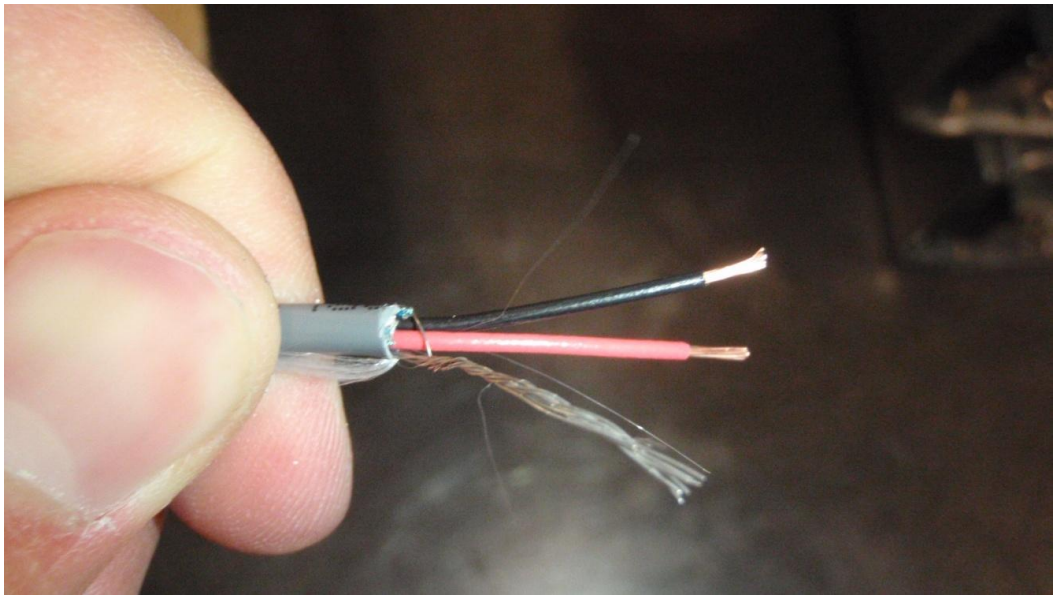

Figure 4.11: Shielded dual core wire used in the enhanced system

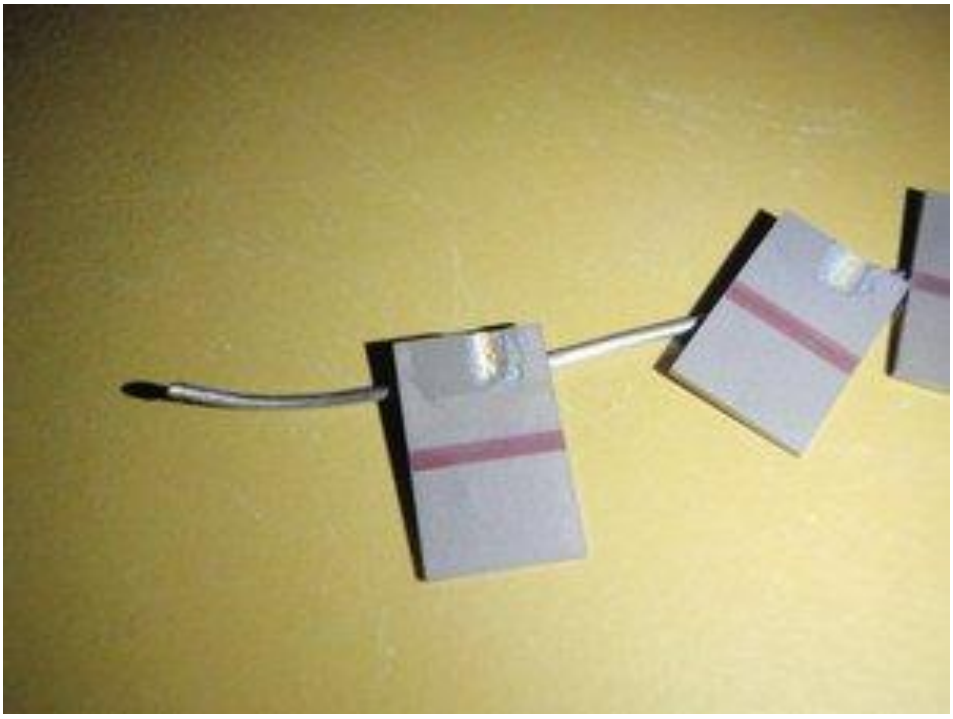

Figure 4.12: Parallel type bender element with removed ceramic layer for wires soldering

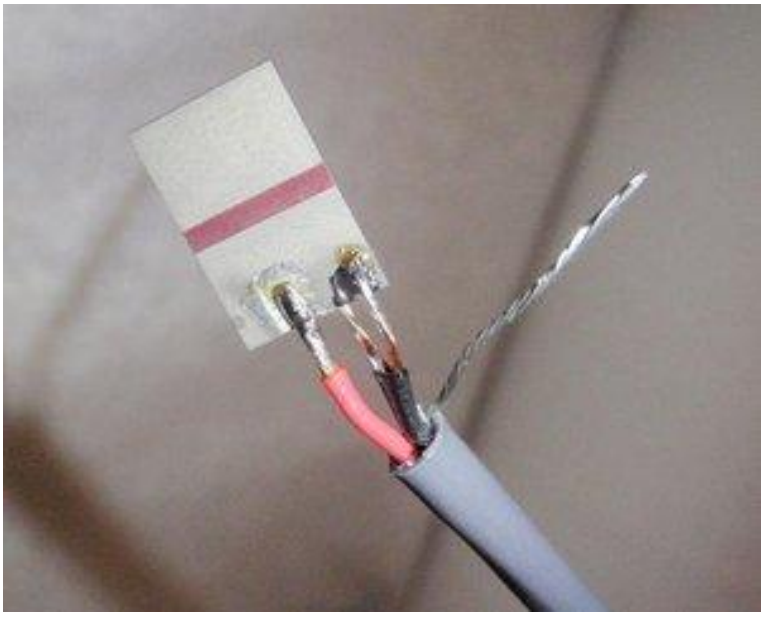

Figure 4.13: Sender bender element with wires in place

Figure 4.14: Finished and mounted Bender Element

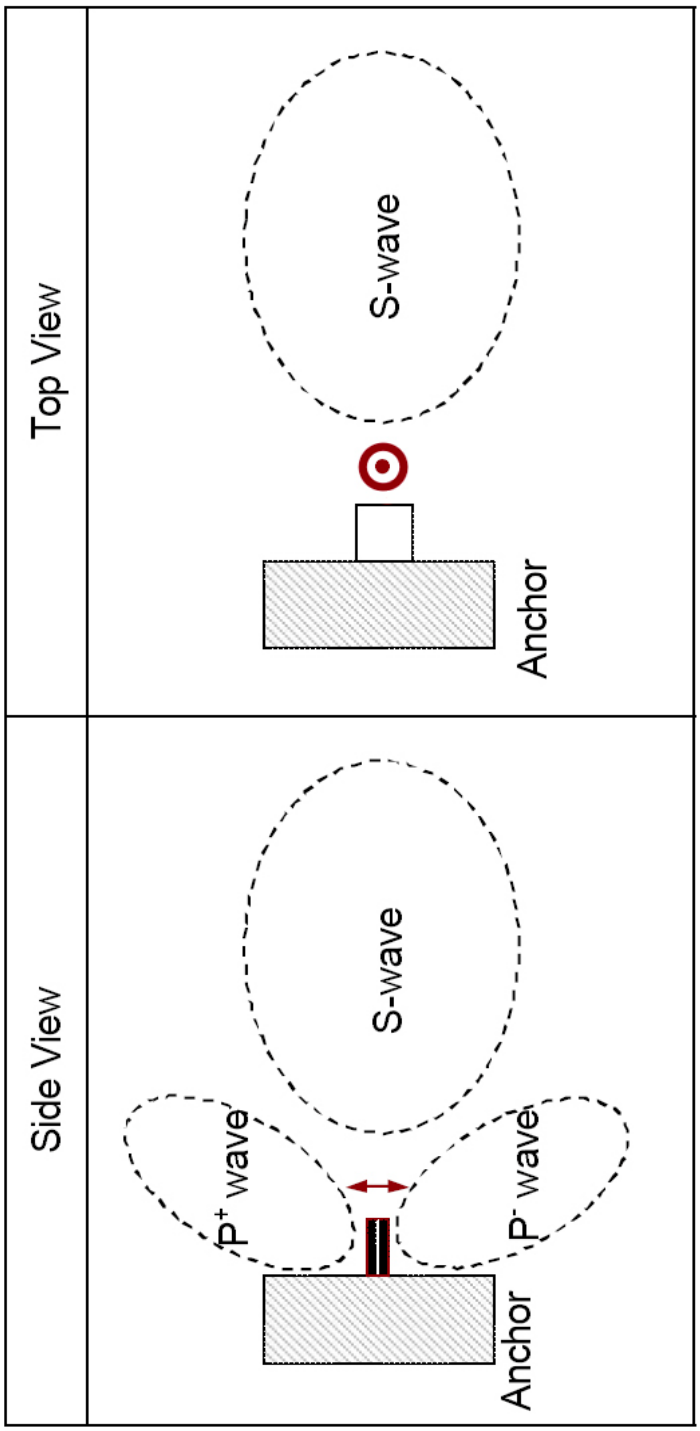


Figure 4.15: Orientation of bender elements (after Lee and Santamarina, 2005)

# 5. CENTRIFUGE EXPERIMENTS AND DATA ANALYSIS

## 5.1 Centrifuge Experimental Setup

A number of centrifuge experiments were conducted as part of this research. Early experiments were utilized to develop and validate the bender elements system. Data from these experiments are not presented in the thesis. Data presented in this chapter correspond to four centrifuge experiments. These experiments were conducted in the laminar container described in Chapter 3. Tests 1 and 2 were conducted on dry Ottawa sand while Tests 3 and 4 were conducted on saturated Ottawa sand. The height of the soil model in all four experiments was 9.5 inches. Properties of the soil used Tests 1 to 4 are presented in Tables 5.1 to 5.4, respectively.

The method used in building the models is the dry pluviation method. It was used for both the dry and the saturated experiments. In this method, the sand is placed in layers, typically 0.5 inch thick, using a pluviator. The pluviation process was interrupted at pre-defined elevations for placement of the bender elements as shown in Figures 5.1-5.8. The S and P symbols used in labeling the bender elements indicate Series and Parallel operations for the receiver and sender bender elements respectively. Some bender elements in the model were used as redundant to confirm results. The container is then placed over the 1-D shaker in the centrifuge basket as shown in Figure 5.9. For saturated experiments, the saturation was then done using de-aired water.

## 5.2 Data Acquisition technique

During the spinning of the centrifuge, predefined mechanical waves (S and P waves) were sent from the sender bender elements to the receiver bender elements. In all the cases, the sender bender elements were excited with one cycle of sine wave having a frequency of 7000Hz and amplitude of 80V shown on Figure 5.10. The wave is then received by the receiver bender elements. The first arrival time of the waves were defined. The outputs of the program showing the received waves along with arrows indicating the first arrival points are shown in Figures 5.11 - 5.18. The wave velocity was then calculated using the relation:

$$V = \frac{d}{t} \tag{5.1}$$

Where:

V: velocity of the shear or dilatational waves

d: distance between sender and receiver

t: time between sending and receiving the body waves

Alternative signal processing procedures includes cross-correlation and frequency domain analyses. However, such techniques must relate signals of the "same nature" in addition to being more difficult to process (Lee & Santamarina, 2005).

An example showing the calculation of shear wave velocity and the corresponding vertical stress is as follows:

For Test 1 conducted on dry Ottawa sand having void ratio 0.723 and unit weight 15.46 KN/m³, it is required to calculate the shear wave velocity measured from [BE-P-7] to [BE-S-5] and the corresponding vertical stress at 50g. The sender and receiver bender elements are both located at elevation 2.5 inches from the base. The height of the soil model is 9.5 inches.

$$\sigma_v = \rho * g * N * h \tag{5.2}$$

$$\sigma_v = g * N * (9.5-2.5) * \frac{2.54}{100} \tag{5.3}$$

$$\sigma_v = 15.46 * 50 * (9.5-2.5) * \frac{2.54}{100} = 137.4 \text{ KPa} \tag{5.4}$$

The wave was detected by the receiver bender element after time t=0.00085 sec from sending. The distance (d) between the sender and the receiver is equal to 20 cm.

$$V_s = \frac{d}{t} = \frac{0.2}{0.00085} = 235.3 \text{ m/sec} \tag{5.5}$$

The arrival of S-waves is sometimes masked by the near field effect. The near field effect is a phenomenon related to the frequency and the velocity of the wave. It can result in a masking wave just before the arrival of the S-wave. In order to reduce any error in the reading that may result from the near field effect, two precautions were adopted. First, the sender and the receiver bender elements were kept as far apart as possible. Second, the frequency of the waves was taken as high as possible. Increasing

the frequency resulted in decreasing the wave length (λ), thus increasing the ratio $\frac{d}{\lambda}$. The ratio $\frac{d}{\lambda}$ was kept more than 4 in all the cases.

Different wave shapes and frequencies were examined during the experiments. The clearest results were found to be in the case of a sine wave with frequency 7000 Hz and amplitude 80V. Thus the sender bender elements, in all the cases, were excited with one cycle of a sine wave having a frequency of 7000 Hz and amplitude 80V.

### 5.3 Experiments on Dry Sand

Tests 1 and 2 were conducted on dry Ottawa sand. Figures 5.19 shows the setup and the instrumentation of centrifuge model test conducted on dry Ottawa sand for both Test 1 and 2. The void ratios of the soil used in Tests 1 & 2 were 0.723 and 0.595 respectively.

#### 5.3.1 Shear Wave Velocity measurements in the Horizontal Direction with Vertical Polarization

The orientation of some of the bender elements in Tests 1 and 2 was designed such that the direction of polarization is vertical and the direction of propagation is horizontal, as in the case of the wave from [BE-P-7] to [BE-S-5].

##### 5.3.1.1 Normally Consolidated

For Tests 1 and 2, the test started at 1g and reached a g-level of 100g with data from bender elements were collected at different g-levels. The sand in this phase is

considered to be normally consolidated. Figures 5.20 & 5.21 show the value of the shear wave velocity ($V_s$) versus vertical stress for dry Ottawa sand having void ratio equal to 0.723 and 0.595 respectively. The blue points indicate the normally consolidated data points. Figures 5.22 & 5.23 show the value of the small strain Shear Modulus ($G_{max}$) versus vertical stress for dry Ottawa sand having void ratio equal to 0.723 and 0.595 respectively. The blue points indicate the normally consolidated data points.

#### 5.3.1.2 Overconsolidated

For Tests 1 and 2, after reaching 100 g, and on the way back to 1 g, data were again collected at the same g-levels considered in the normally consolidated phase. The sand in this phase is considered to be overconsolidated. Figures 5.20 & 5.21 show the value of the shear wave velocity versus vertical stress for dry Ottawa sand having void ratios equal to 0.723 and 0.595 respectively. The red points indicate the overconsolidated data points. Figures 5.22 & 5.23 show the value of the small strain Shear Modulus ($G_{max}$) versus vertical stress for dry Ottawa sand having void ratio equal to 0.723 and 0.595 respectively. The red points indicate the overconsolidated data points.

#### 5.3.1.3 Effect of OCR on $V_s$ and $K_o$

The shear wave velocity ($V_s$) was used to calculate the ratio between $K_o$ of the overconsolidated soil to $K_o$ of the normally consolidated soil for different values of OCR. The technique used is based on the fact that the loading in the Centrifuge experiments is anisotropic, simulating the field conditions. For the anisotropic case, the shear wave velocity is dependent on both the direction of polarization and propagation. The

directions of polarization and propagation were assumed to be equally effective on the value of shear wave velocity (Stokoe et al.,1985), (Stokoe et al.,1995) & (Knox et al., 1982). The relation between the shear wave velocity and the stresses in the direction of polarization and propagation is as follows (after Stokoe):

$$V_s = C * \sigma_a^{\,n/2} * \sigma_b^{\,n/2} \tag{5.6}$$

Where:

C: constant depends on the soil type and the voids ratio

n: constant having average value of 0.25

a: the direction of polarization

b: the direction of propagation

In the cases where the direction of polarization is vertical and the direction of propagation is horizontal, as in the case of the wave from [BE-P-7] to [BE-S-5], this relation can be written as

$$V_s = C * \sigma_v^{\,0.125} * \sigma_h^{\,0.125} \tag{5.7}$$

$$V_s = C * \sigma_v^{\,0.125} * (K_0\sigma_v)^{\,0.125} \tag{5.8}$$

$$V_s = C * K_0^{\,0.125} * \sigma_v^{\,0.25} \tag{5.9}$$

Let $V_{s_{NC}}$ and $K_{0NC}$ are the shear wave velocity and the coefficient of earth pressure at rest for a given vertical stress $\sigma_v$ during the normally consolidated loading phase.

$$V_{s_{NC}}=\text{C} * K_{0NC}{}^{0.125} * \sigma_v{}^{0.25} \tag{5.10}$$

Let $V_{s_{OC}}$ and $K_{0OC}$ are the shear wave velocity and the coefficient of earth pressure at rest for a given vertical stress vertical stress $\sigma_v$ during the overconsolidated loading phase.

$$V_{s_{OC}}=\text{C} * K_{0OC}{}^{0.125} * \sigma_v{}^{0.25} \tag{5.11}$$

$$\frac{V_{s_{NC}}}{V_{s_{OC}}} = \left(\frac{K_{0NC}}{K_{0OC}}\right)^{0.125} \tag{5.12}$$

$$\frac{K_{0NC}}{K_{0OC}} = \left(\frac{V_{s_{NC}}}{V_{s_{OC}}}\right)^{8} \tag{5.13}$$

Figures 5.24 & 5.25 show the value of $K_0$oc/$K_0$nc versus OCR for void ratios equal to 0.723 and 0.595 respectively.

### 5.3.2 Shear Wave Velocity measurements in the Horizontal Direction with Horizontal Polarization

The orientation of some of the bender elements in Test 1 and 2 was designed such that the direction of polarization is horizontal and the direction of propagation is also horizontal, as in the case of the wave from [BE-P-6] to [BE-S-7].

Data were also collected in the normally consolidated and overconsolidated phases, as in the previous case.

Figures 5.26 & 5.27 show the value of the shear wave velocity versus vertical stress in the case of normally and overconsolidated dry Ottawa sand having void ratios equal to 0.723 and 0.595 respectively. The blue points indicate the normally consolidated phase while the red points indicate overconsolidated phase.

The shear wave velocity ($V_s$) was used to calculate the ratio between $K_0$ of the overconsolidated soil to $K_0$ of the normally consolidated soil for different values of OCR. as follows:

$$V_s = C * \sigma_h^{0.125} * \sigma_h^{0.125} \quad (5.14)$$

$$V_s = C * (K_0\sigma_v)^{0.125} * (K_0\sigma_v)^{0.125} \quad (5.15)$$

$$V_s = C * K_0^{0.25} * \sigma_v^{0.25} \quad (5.16)$$

Let $V_{s_{NC}}$ and $K_{0NC}$ are the shear wave velocity and the coefficient of earth pressure at rest for a given vertical stress $\sigma_v$ during the normally consolidated loading phase.

$$V_{s_{NC}} = C * K_{0NC}^{0.25} * \sigma_v^{0.25} \quad (5.17)$$

Let $V_{s_{OC}}$ and $K_{0OC}$ are the shear wave velocity and the coefficient of earth pressure at rest for a given vertical stress $\sigma_v$ during the overconsolidated loading phase.

$$V_{s_{OC}} = C * K_{0OC}^{0.25} * \sigma_v^{0.25} \quad (5.18)$$

$$\frac{V_{sNC}}{V_{sOC}} = \left(\frac{K_{0NC}}{K_{0OC}}\right)^{0.25} \quad (5.19)$$

$$\frac{K_{0NC}}{K_{0OC}} = \left(\frac{V_{sNC}}{V_{sOC}}\right)^{4} \quad (5.20)$$

Figures 5.28 & 5.29 show the value of $K_0$oc/$K_0$nc vs. OCR for soil models having voids ratio equal to 0.723 and 0.595 respectively (The wave is horizontally propagating & horizontally polarized).

### 5.3.3 Shear Wave Velocity measurements in the Vertical Direction with Horizontal Polarization

In addition to the measurement of the waves propagating in the horizontal direction, measurements of the shear wave velocities were also taken in the vertical direction as in the case of the wave from [BE-P-4] to [BE-S-3]. Although the effective confining pressure for the vertical measurement is not clearly defined, the measurements were used to calculate $K_0$oc/$K_0$nc as an average value over depth. This was done based on the fact that the effective confining pressure, even though not exactly determined, is dependent on the g-level. For example, the effective confining pressure at 50g during the spin up is the same during the spin down. However, the first case is normally consolidated while the second case is overconsolidated. Figures 5.30 & 5.31 show the value of the average shear wave velocity versus g-level in the case of normally and overconsolidated dry Ottawa sand having voids ratio equal to 0.723 and 0.595 respectively.

The shear wave velocity ($V_s$) was used to calculate the ratio between $K_0$ of the overconsolidated soil to $K_0$ of the normally consolidated soil for different values of OCR. as follows:

$$V_s = C * \sigma_v^{0.125} * \sigma_h^{0.125} \quad (5.21)$$

$$V_s = C * \sigma_v^{0.125} * (K_0\sigma_v)^{0.125} \quad (5.22)$$

$$V_s = C * K_0^{0.125} * \sigma_v^{0.25} \quad (5.23)$$

Let $V_{s_{NC}}$ and $K_{0NC}$ are the shear wave velocity and the coefficient of earth pressure at rest for a given vertical stress $\sigma_v$ during the normally consolidated loading phase.

$$V_{s_{NC}} = C * K_{0NC}^{0.125} * \sigma_v^{0.25} \quad (5.24)$$

Let $V_{s_{OC}}$ and $K_{0OC}$ are the shear wave velocity and the coefficient of earth pressure at rest for a given vertical stress $\sigma_v$ during the overconsolidated loading phase.

$$V_{s_{OC}} = C * K_{0OC}^{0.125} * \sigma_v^{0.25} \quad (5.25)$$

$$\frac{V_{s_{NC}}}{V_{s_{OC}}} = \left(\frac{K_{0NC}}{K_{0OC}}\right)^{0.125} \quad (5.26)$$

$$\frac{K_{0NC}}{K_{0OC}} = \left(\frac{V_{s_{NC}}}{V_{s_{OC}}}\right)^{8} \quad (5.27)$$

Figures 5.32 & 5.33 show the value of $K_0$oc/$K_0$nc vs. OCR for soil models having voids ratio equal to 0.723 and 0.595 respectively (The wave is vertically propagating & horizontally polarized).

### 5.3.4 Discussion of the ratio of $K_0$oc/$K_0$nc obtained in this research

A comparison is done between the measured increase in $K_0$ with overconsolidation and the values reported by Hendron (1963). Hendron used four different sand types in his research, however only Minnesota sand tend to have the same particle characteristics of Ottawa sand used in this research. Both sand types have rounded shapes. Also, they have relatively uniform particle sizes. However, Minnesota sand tends to have larger particles size. The comparison is shown in Figure 5.34.

### 5.3.5 Comparison between vertically and horizontally propagating $V_s$

An integration technique was used to predict the values of $V_s$ vertically propagating & horizontally polarized versus g-level from the measured $V_s$ horizontally propagating & vertically polarized. This was done assuming the effect of the direction of propagation and polarization is the same on the value of shear wave velocity. The comparison is shown in Figures 5.35 & 5.36 for voids ratio 0.723 & 0.595 respectively.

### 5.3.6 P-Wave Velocity measurements

The orientations of some of the bender elements in the centrifuge models were utilized to measure the P-wave velocity. However, the P-waves tend to attenuate much faster than the S-waves leading to faded received signal. Hence, P-wave velocity

measurements proved to be difficult to achieve using the current bender elements system. However, the P-wave velocity measured vertically in the dry soil model having voids ratio of 0.723 was successful. Figure 5.37 shows the change of P-wave velocity with g-level. These values were used, along with the shear wave velocity, to calculate the average Poisson's ratio over depth at different g-levels, as shown in Figure 5.38, using the following relation:

$$\mu = \frac{(V_D/V_S)^2 - 2}{2*[(V_D/V_S)^2 - 1]} \tag{5.28}$$

## 5.4 Experiments on Saturated Sand

### 5.4.1 Shear Wave Velocity measurements in the horizontal direction with vertical polarization

Tests 3 and 4 were conducted on saturated Ottawa sand. Figures 5.39 & 5.40 show the setup and instrumentation of centrifuge model Tests 3 & 4 respectively. The void ratios of the soil used in Tests 3 and 4 were 0.723 and 0.625 respectively. For the two experiments, the test started from 1g and reached a g-level of 27g. Data from bender elements were collected at different g-levels. Figures 5.41 & 5.42 show the profile of shear wave velocity versus vertical effective stresses for void ratios 0.723 and 0.625 respectively. Figures 5.43 & 5.44 show the profile of small strain shear modulus ($G_{max}$) versus effective vertical stresses for voids ratios 0.723 and 0.625 respectively.

### 5.4.2 Effect of shaking on $V_s$ measurement after excess pore pressure has dissipated

Tests 3 and 4 were conducted as part of liquefaction assessment project. The models were shaken at 25g by the base acceleration shown in Figures 5.45 & 5.46 (El-Ganainy, 2011). The results in Figures 5.47 & 5.48 show the effect of shaking on the shear wave velocity. The red points indicate the value of shear wave velocity after shaking.

## 5.5 Discussion of the results

### 5.5.1 Dry Ottawa Sand

- The value of n in the relation $V_s$=C * $\sigma_v{}^n$ was found to range from 0.19 to 0.27. This range is consistent with what was measured by Hardin, Stokoe and others using different techniques in measuring the shear wave velocity.
- The change in the shear wave velocity due to overconsolidation appears to be very small. This appears to be the case for the vertically polarized horizontally propagating shear waves and the horizontally polarized vertically propagating shear waves. This emphasizes the fact that shear wave velocity may be considered independent of the stress history.
- The effect of overconsolidation on the shear wave velocity seems to be larger in the case of horizontally propagating horizontally polarized shear waves. This is expected, due to the higher contribution of the horizontal stress to the value of shear wave velocity. The horizontal stress is dependent on the value of $K_0$ which increases with overconsolidation.

- The value of the shear wave velocity horizontally propagating horizontally polarized was found to be higher than expected. It was expected to have lower values than that of horizontally propagating and vertically polarized, due to the contribution of horizontal stresses in both the propagation and polarization. This was thought to be as a result of elongated rectangular shape of the box. This kind of elongation might lead to the long side of the box deforming laterally outside and the short side of the box deforming laterally inside maintaining the rigid connection at the corners. This was expected to have made the effect of passive earth pressure increasing the horizontal stresses in the long direction of the box.
- A comparison is done between the measured increase in $K_0$ with overconsolidation and the values reported by Hendron (1963). The comparison is shown in Figure 5.34. The measured values tend to follow the trend of the range reported by Hendron for Minnesota sand in most of the cases.
- The comparison between measured vertically propagating $V_s$ and that predicted from horizontally propagating shows some discrepancy. The discrepancy is consistent with what reported by Roesler (1979). He reported that the influence of the direction of propagation and polarization on shear wave velocity is not identical, giving more weight to the direction of propagation. Also, Bellotti (1996) reported that the inherent anisotropy of the test sand leads to increasing the velocity of horizontally polarized body waves on average by 10% to those of vertically polarized body waves. Similar results were also reported by Knox et al. (1982), kopperman et al. (1982), chu et al. (1984), lee & Stokoe (1986), Stokoe et al. (1991). Also, Cai et al

(2011) reported different values for vertically propagating and horizontally propagating shear wave velocity based on field measurements.

- The calculated values of Poisson's ratio tend to be lower than expected for this type of sand, especially for relatively higher g-levels. This is probably attributed to the lateral deformation of the box.
- The results obtained from experiments on dry sand are compared to the values from Hardin's equation after modifying it to take into account the effect of anisotropy (after Stokoe).

$$V_s = 51*(2.17 - e) * \sigma_v^{\,0.125} * (K_0\sigma_v)^{\,0.125} \qquad (5.29)$$

$\sigma_v$ is chosen to be 45 KPa for both measured and calculated $V_s$. This corresponds to g-level about 15g.

El-Ganainy (2011) measured, using the tactile sensors, the value of the coefficient of earth pressure ($K_0$) for dry Nevada sand in the laminar container. The reported results are shown in Figure 5.49. It was found that $K_0$ reaches a value of 0.5 at 10 g. The value of $K_0$ then starts to decrease at 20 g. For the purpose of comparison, the value of $K_0$ was assumed to be 0.5 at 15g.

The result of the comparison is shown in Figure 5.50. The measured $V_s$ at voids ratio of 0.723 compare very well. However, the measured $V_s$ tend to be slightly higher than that predicted by Hardin equation for voids ratio of 0.595.

### 5.5.2 Saturated Ottawa Sand

- The value of n in the relation $V_s$=C * $\tilde{\sigma}_v{}^n$ was found to range from 0.24 to 0.29. This range is consistent with what was measured by Hardin, Stokoe and others.
- The effect of preshaking of the models by the accelerations shown in Figures 5.45 & 5.46 is recorded. The shear wave velocity appears to increase by about 20% due to preshaking. This is indicated by the red points in Figures 5.47 & 5.48. The results emphasize the effect of preshaking in increasing the shear stiffness of the soil due to rearrangement of soil particles.
- The results obtained from the experiments on saturated sand were compared to the values from Hardin's equation after modifying it to take into account the effect of anisotropy (after Stokoe).The comparison in the case of saturated soil is not straight forward. In order to calculate $V_s$, $G_{max}$ has to be calculated first.

$$G_{max}=6900*\frac{(2.17-e)^2}{1+e}*\tilde{\sigma}_v{}^{0.125}*(K_0\tilde{\sigma}_v)^{0.125} \quad (5.30)$$

$$V_s=\sqrt{\frac{G_{max}}{\rho_{sat}}} \quad (5.31)$$

$\sigma_v$ is choosen to be 45 KPa for both measured and calculated $V_s$. This corresponds to g-level about 25 g

El-Ganainy (2011) measured, using the tactile sensors, the value of the coefficient of earth pressure ($K_0$) for saturated Ottawa sand in the laminar container at 25 g. The reported results are shown in Figure 5.51. It was found that $K_0$ averages between 0.4

and 0.3 for loose and dense saturated Ottawa sand. For purpose of comparison, the value of $K_0$ was assumed to be 0.35 at 25g.

The result of the comparison is shown in Figure 5.52. The comparison shows perfect match between measured and predicted $V_s$ at different voids ratios.

- Note that the variation in the value of estimated $K_0$ in the case of dry and saturated sand is believed to be as a result of lateral deformation of the box. The effective stress considered in the comparison is the same for both dry and saturated soil. However, in the case of saturated soil, there exists water pressure acting in all directions. The water pressure is believed to have resulted in more lateral deformation in the box reducing the coefficient of earth pressure in the case of saturated Tests.

- A comparison is done between the measured $V_s$ for the saturated soil models and the values predicted from the dry soil experiments, both having $\tilde{\sigma}_v = 45$ kpa. The prediction was done assuming $G_{max}$ is the same for dry and saturated sand for the same effective stress.

$$G_{max} = \rho_{dry} * V_{s(dry)}^{\ 2} \tag{5.32}$$

$$V_{s(sat)} = \sqrt{\frac{G_{max}}{\rho_{sat}}} \tag{5.33}$$

The comparison, shown in Figure 5.53, indicates that the results are not perfectly matching. As discussed before, the value of $K_0$ in the case of dry sand at $\tilde{\sigma}_v = 45$ kpa is expected be around 0.5. However, for the case of saturated sand, $K_0$ is expected to be around 0.35. The difference in $K_0$ was thought to result in the two lines not perfectly matching.

- A Comparison is done between $V_s$ obtained by bender elements measurements in saturated sand having e=0.723 & e=0.625 and $V_s$ estimated by system identification technique (Abdoun et al., 2010; Mercado, 2011). The comparison shows very good agreement between the results as shown in Figures 5.54 & 5.55.

  - A summary of the comparisons between measured and calculated shear wave velocities in dry and saturated sand is shown in Figure 5.56.

**5.6 Parametric Study**

As discussed earlier in the chapter, the arrival of S-waves is sometimes masked by the near field effect. In order to estimate the percentage of the expected error in case of wrong estimation of the point of first arrival of the shear wave due to near field effect, a parametric study was done. This study is based on the assumption that the received wave and the masking wave (due to near field effect) have almost the same frequency of the sent wave. The results of the study are shown in Figures 5.57 & 5.58 for frequencies equal to 7000 Hz & 2000 Hz respectively. The results show the benefit of using large frequency and large distance between the sender and receiver bender elements, not only

in fading of the masking wave, but also in reducing the error in case it was mistakenly considered as part of the received shear wave.

Table 5.1: Soil Properties in Test (1)

| **Test 1** | |
|---|---|
| **Condition** | Dry |
| **ρ (kg/m³)** | 1560 |
| **γ (KN/m³)** | 15.46 |
| **Sand type** | Ottawa |
| **e** | 0.723 |

Table 5.2: Soil Properties in Test (2)

| **Test 2** | |
|---|---|
| **Condition** | Dry |
| **ρ (kg/m³)** | 1700 |
| **γ (KN/m³)** | 16.7 |
| **Sand type** | Ottawa |
| **e** | 0.595 |

Table 5.3: Soil Properties in Test (3)

| **Test 3** | |
|---|---|
| **Condition** | Saturated |
| **ρ (sat.) (kg/m³)** | 1957 |
| **γ (sat.) (KN/m³)** | 19.2 |
| **Sand type** | Ottawa |
| **e** | 0.723 |

Table 5.4: Soil Properties in Test (4)

| **Test 4** | |
|---|---|
| **Condition** | Saturated |
| **ρ (sat.) (kg/m³)** | 2020 |
| **γ (sat.) (KN/m³)** | 19.8 |
| **Sand type** | Ottawa |
| **e** | 0.625 |

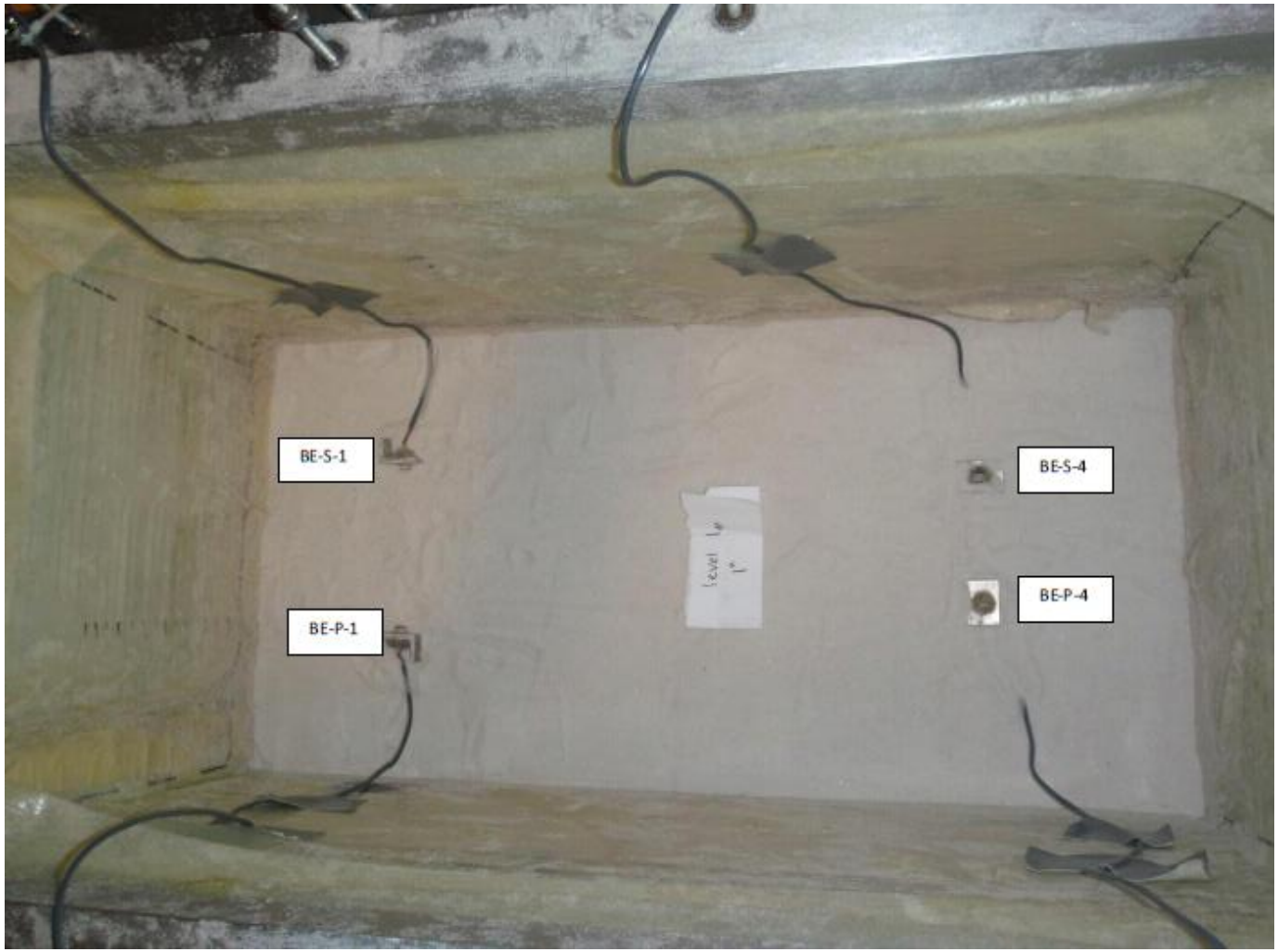


Figure 5.1: Position and orientation of the bender elements at elevation 1” from the base for dry Ottawa sand e=0.723 (Test 1)

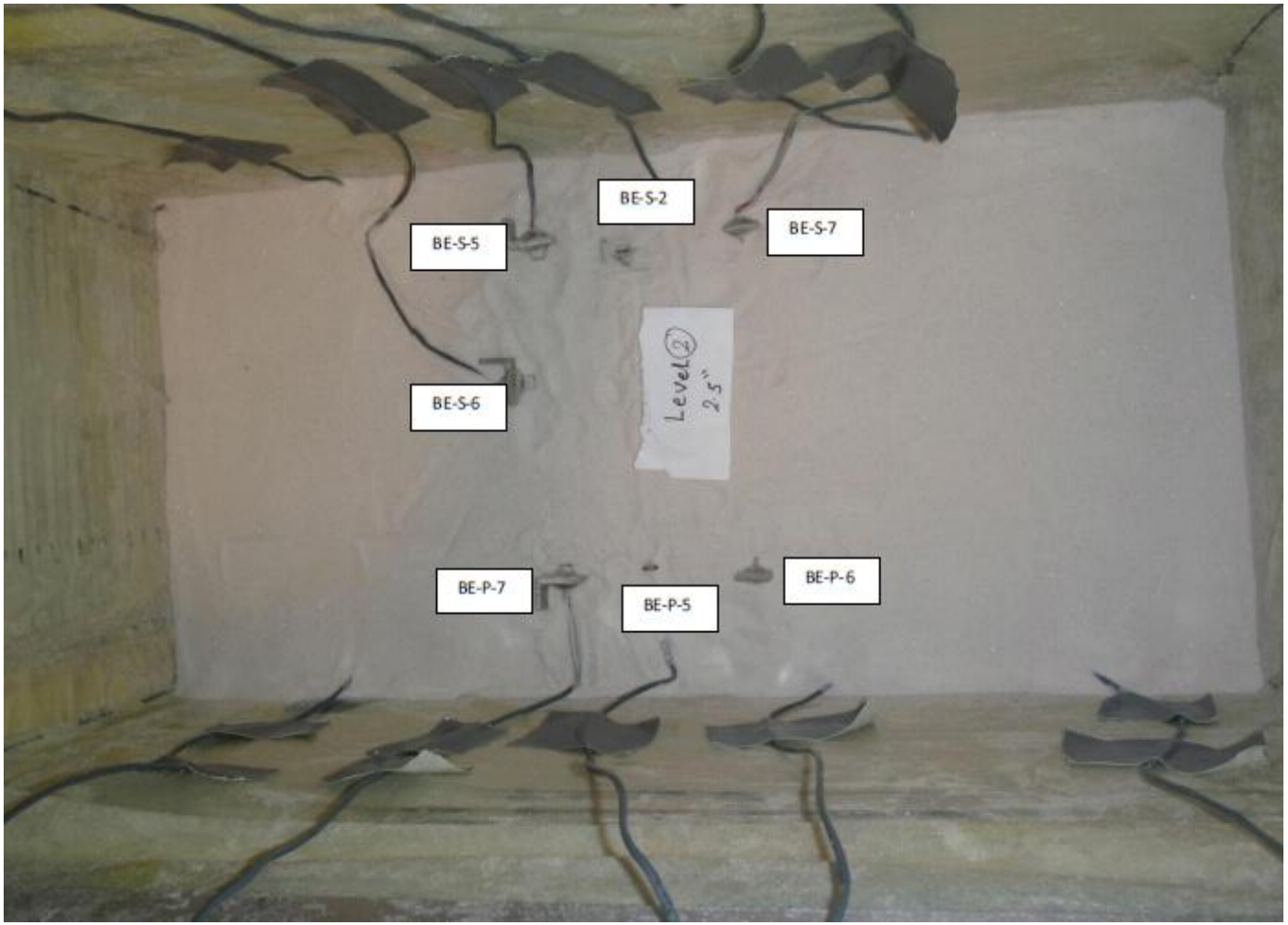


Figure 5.2: Position and orientation of the bender elements at elevation 2.5” from the base for dry Ottawa sand e=0.723 (Test 1)

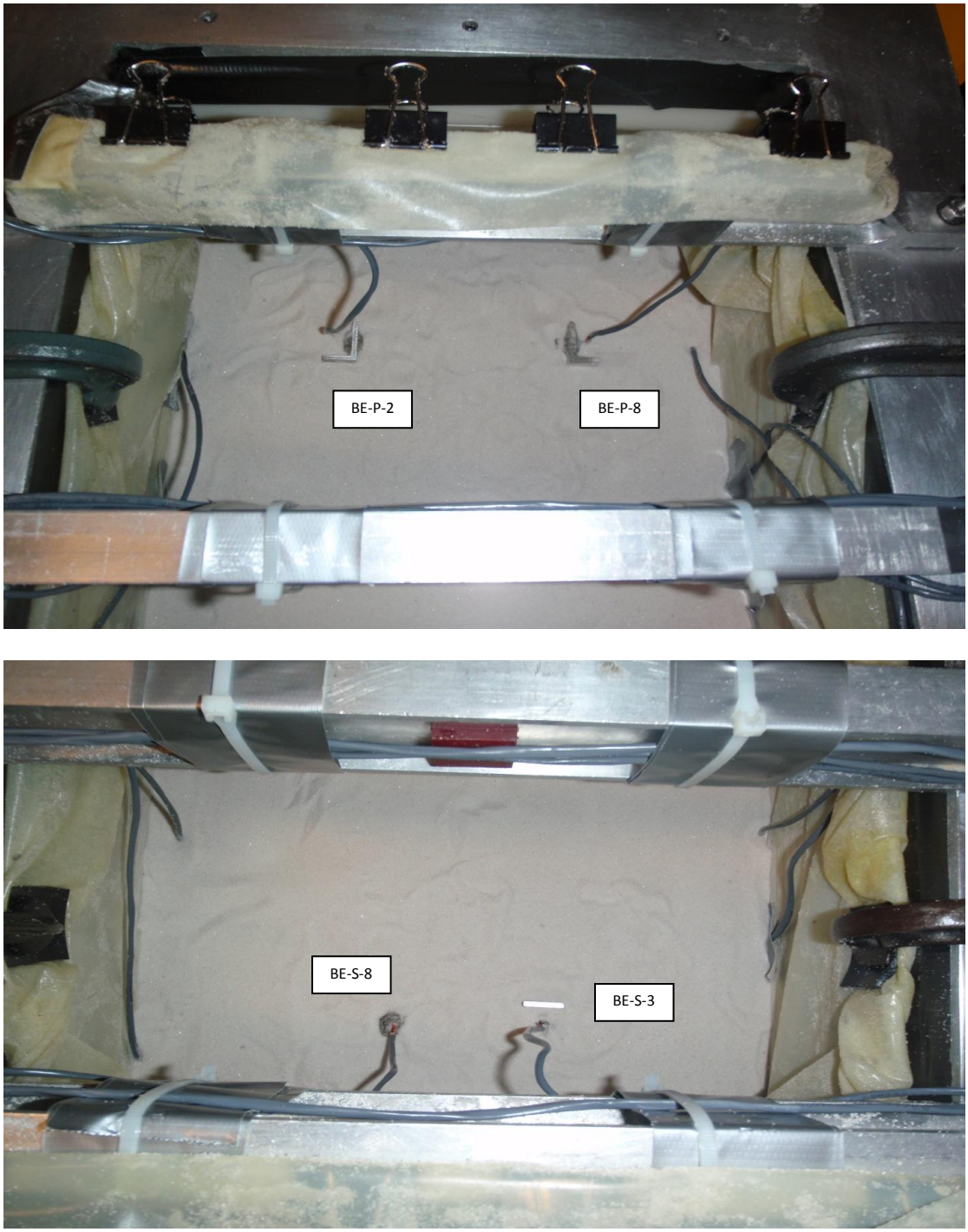


Figure 5.3: Position and orientation of the bender elements at the surface for dry Ottawa sand e=0.723 (Test 1)

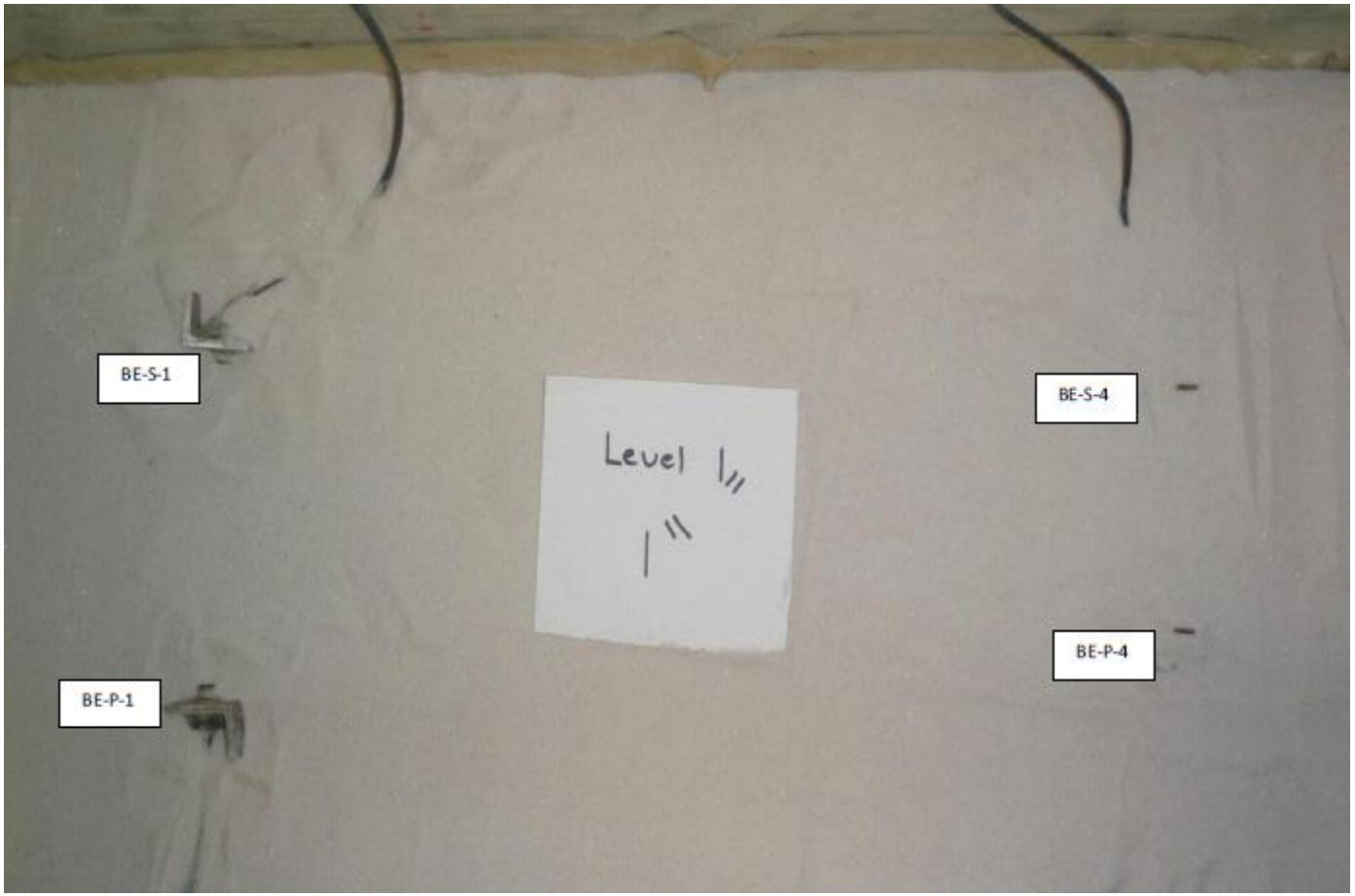


Figure 5.4: Position and orientation of the bender elements at elevation 1” from the base for dry Ottawa sand e=0.595 (Test 2)

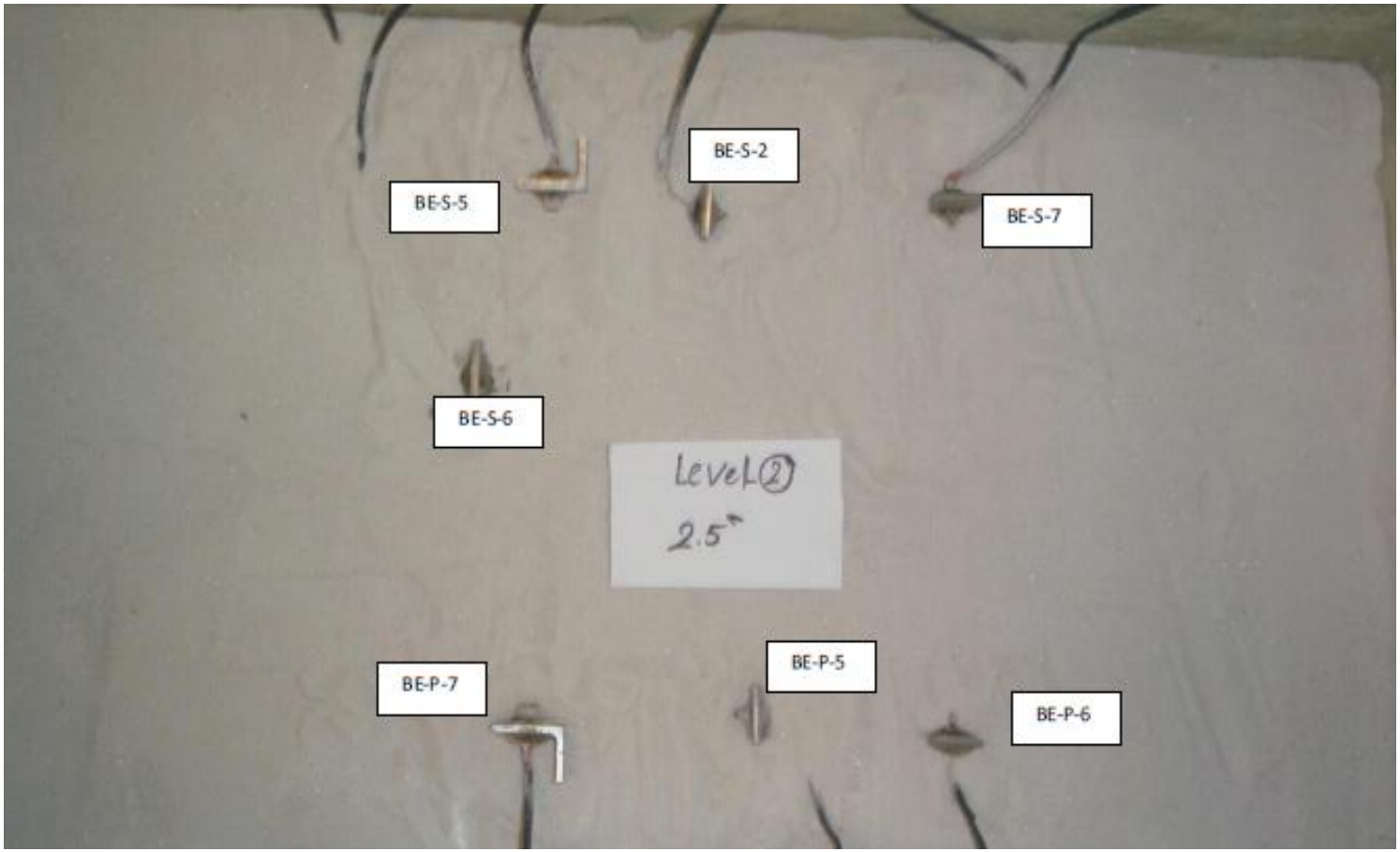


Figure 5.5: Position and orientation of the bender elements at elevation 2.5" from the base for dry Ottawa sand e=0.595 (Test 2)

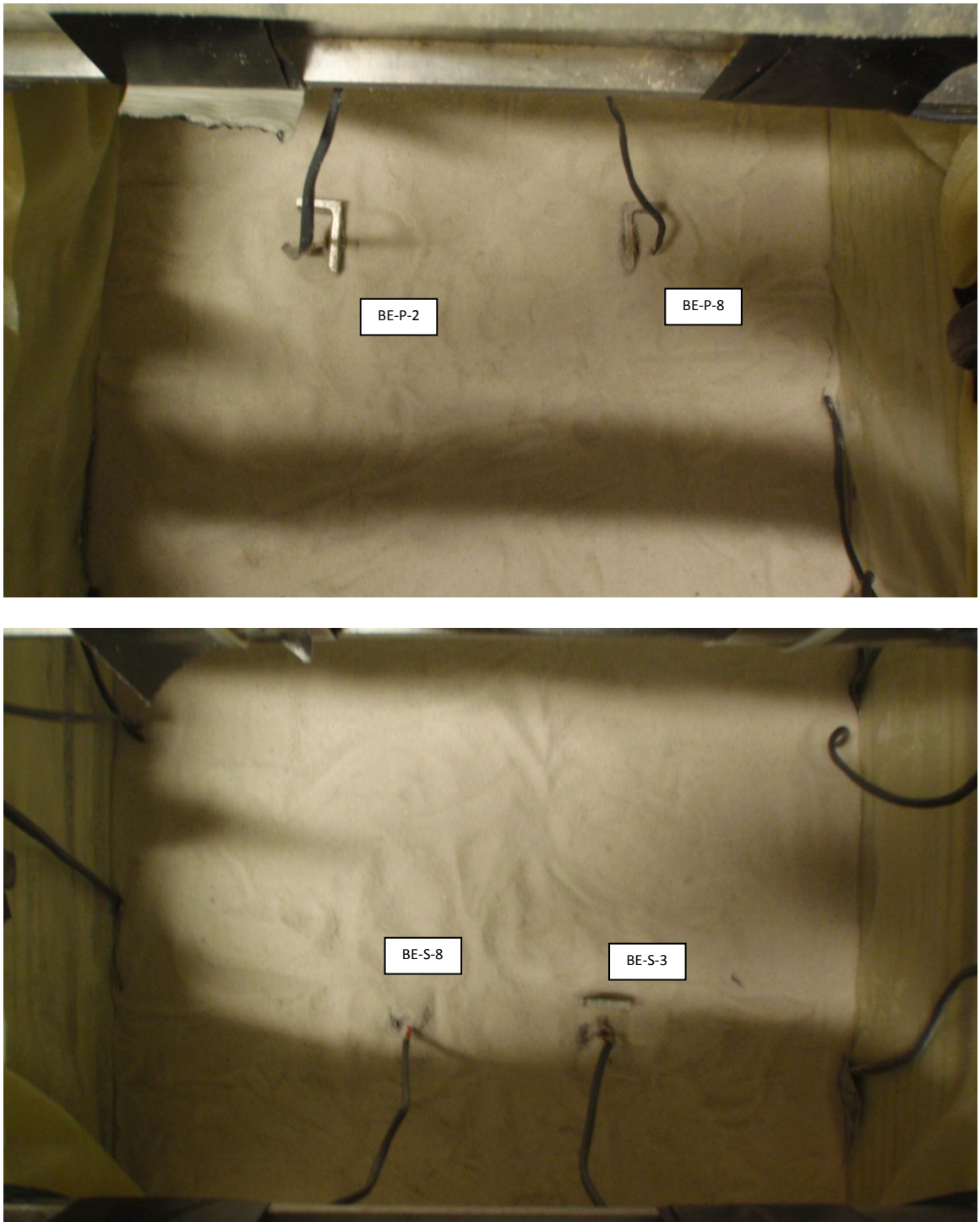


Figure 5.6: Position and orientation of the bender elements at the surface for dry Ottawa sand e=0.595 (Test 2)

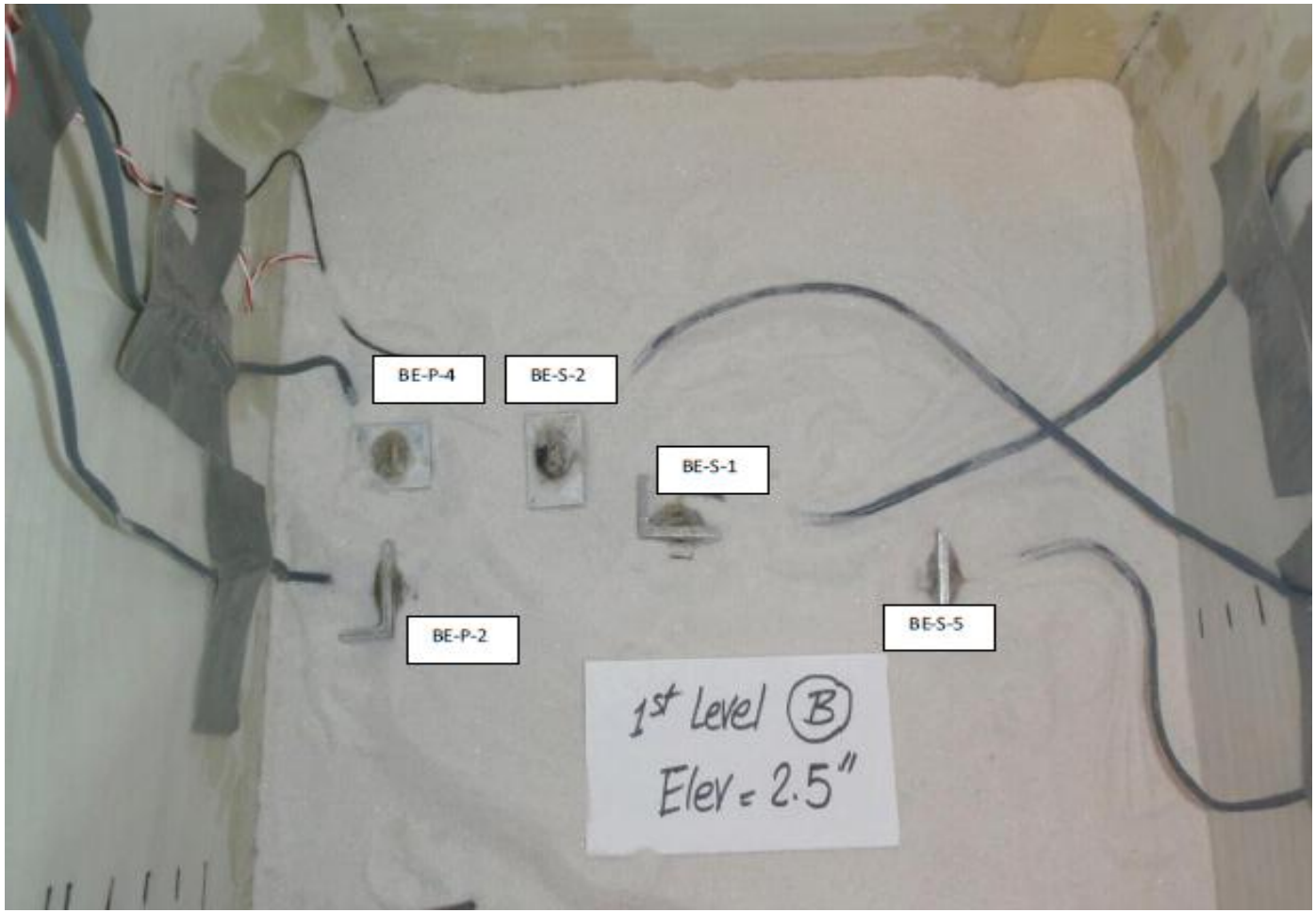


Figure 5.7: Position and orientation of the bender elements at elevation 2.5” from the base for saturated Ottawa sand e=0.723 (Test 3)

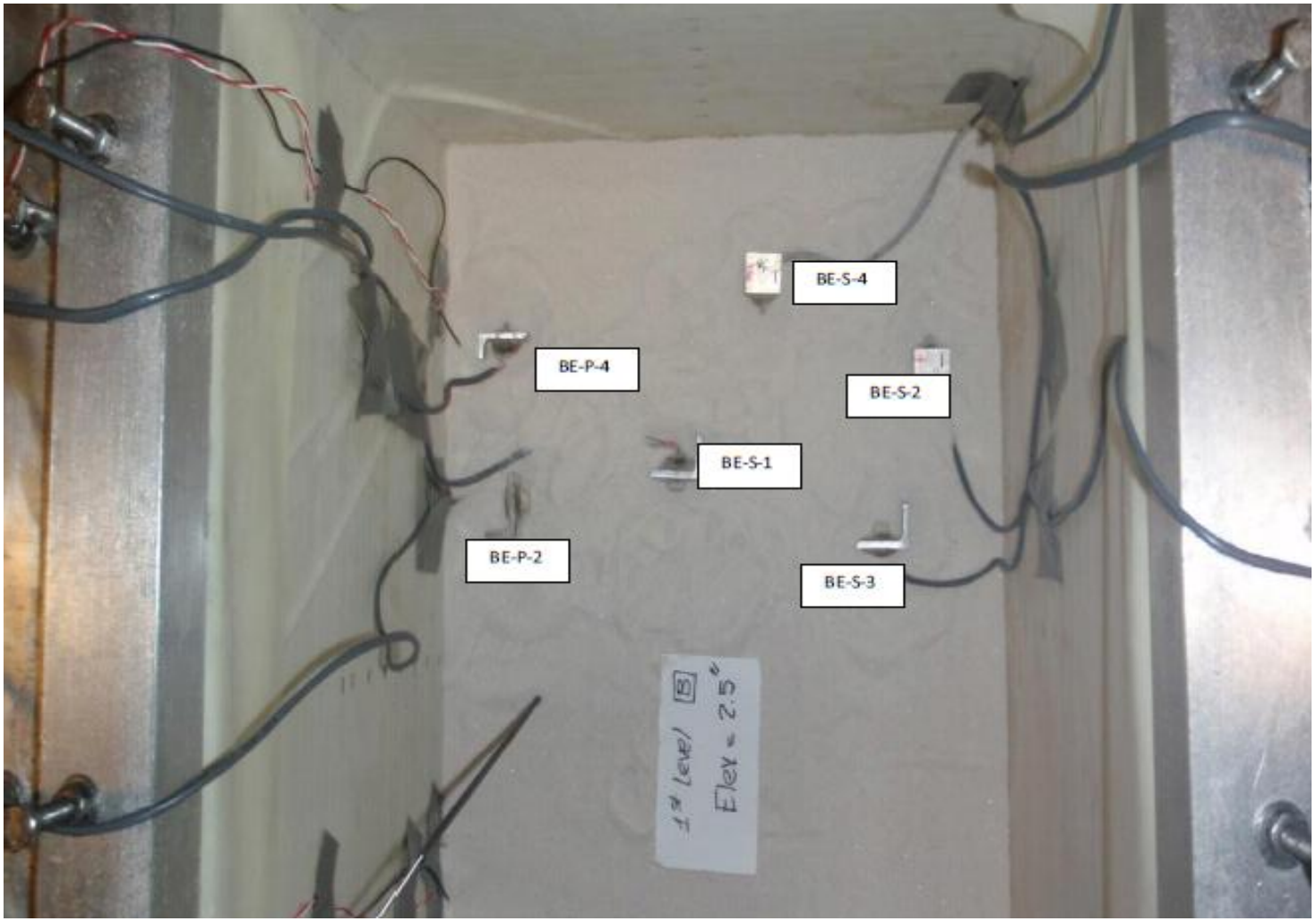


Figure 5.8: Position and orientation of the bender elements at elevation 2.5” from the base for saturated Ottawa sand e=0.625 (Test 4)

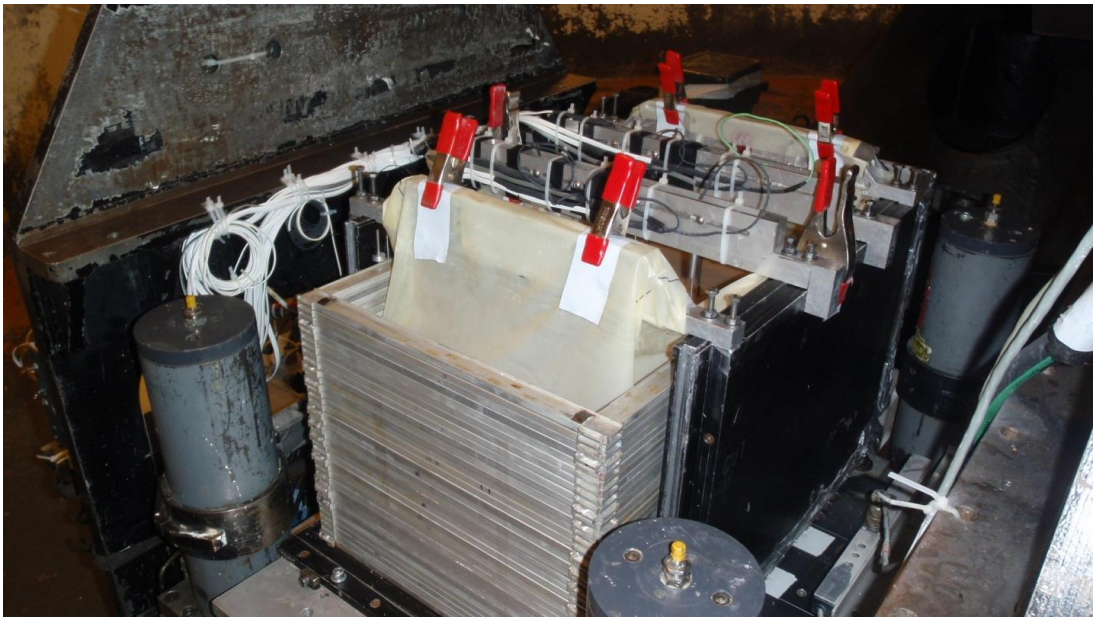

Figure 5.9: Placement of the model in the centrifuge basket over the 1-D shaker

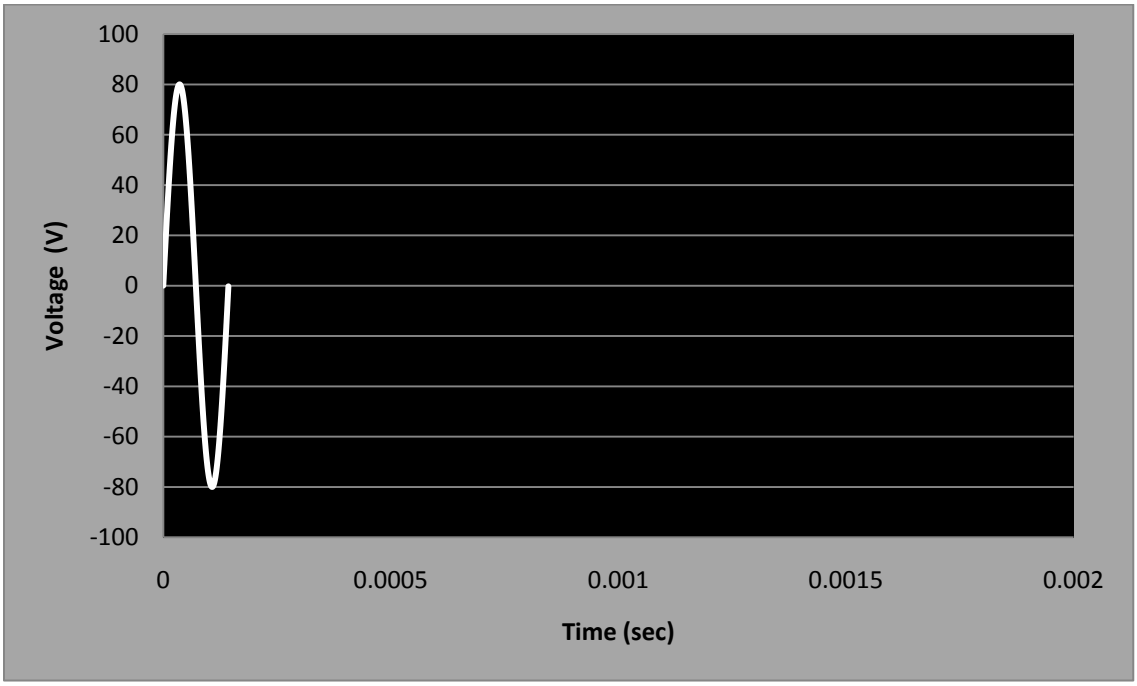


Figure 5.10: Output signal to the sender Bender Elements (f=7000Hz, Amplitude=80 V)

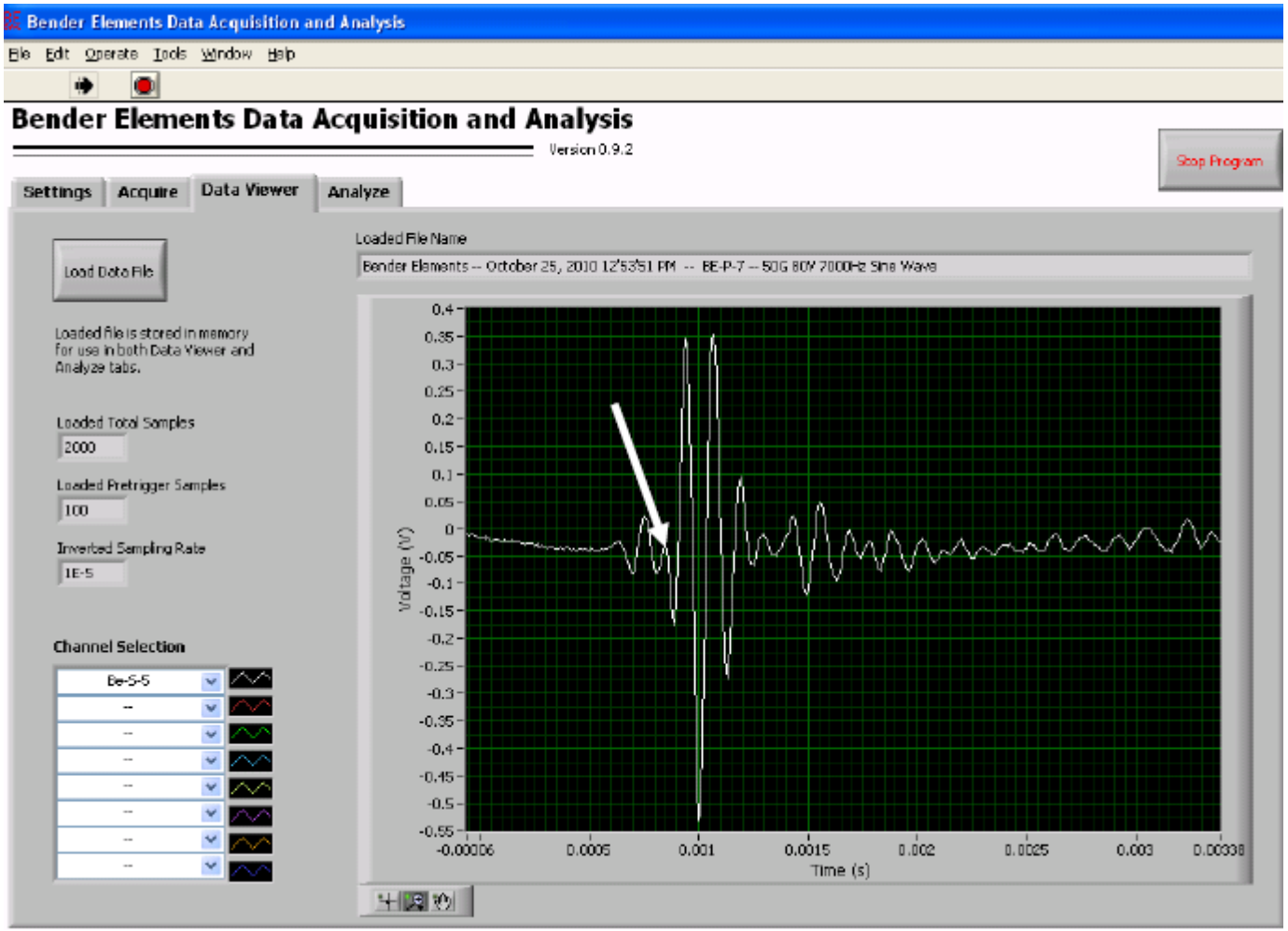


Figure 5.11: Screenshot of the S-wave signal received by [BE-S-5] for dry Ottawa sand e=0.723 at 50G (Test 1)

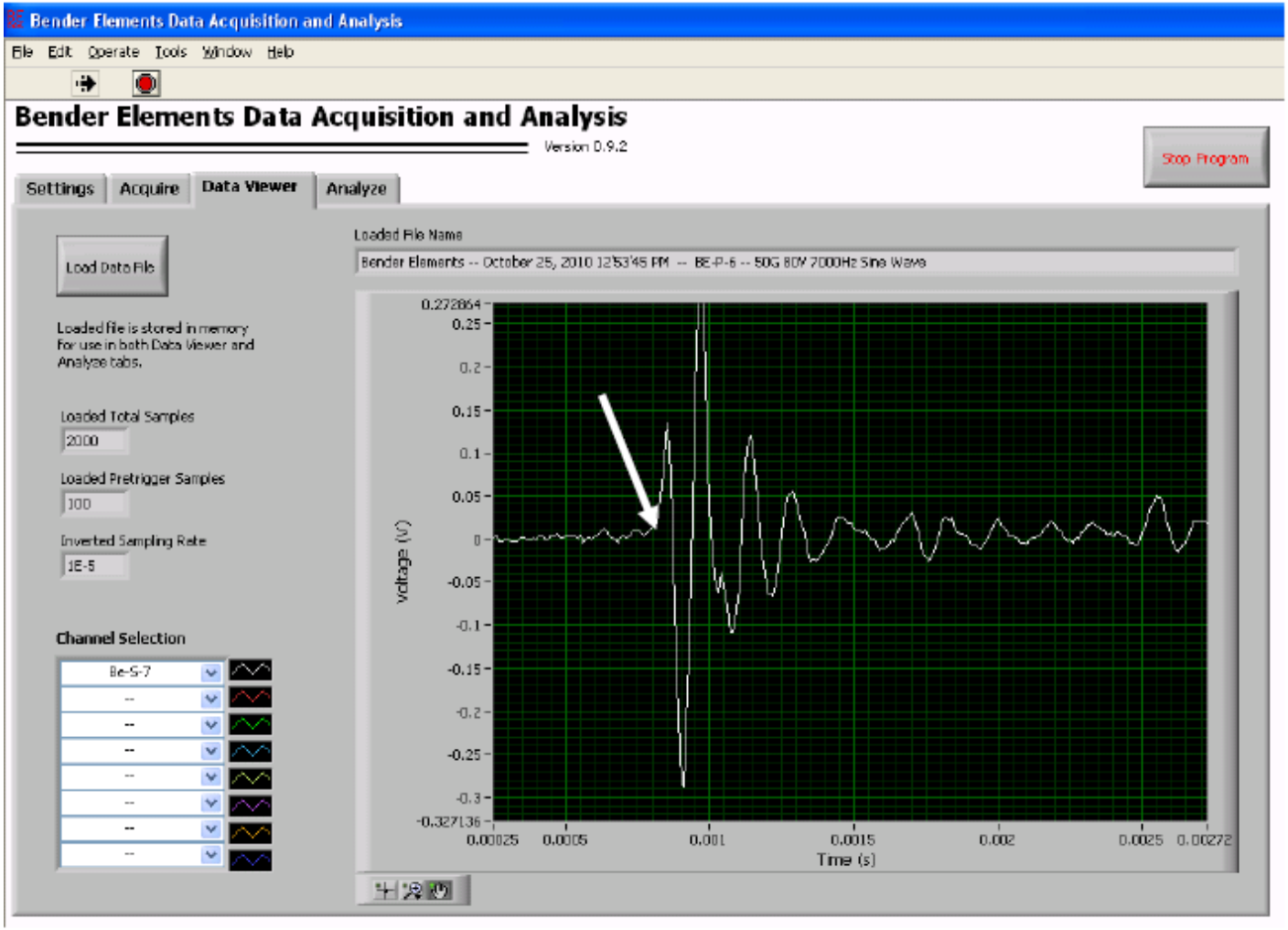


Figure 5.12: Screenshot of the S-wave signal received by [BE-S-7] for dry Ottawa sand e=0.723 at 50G (Test 1)

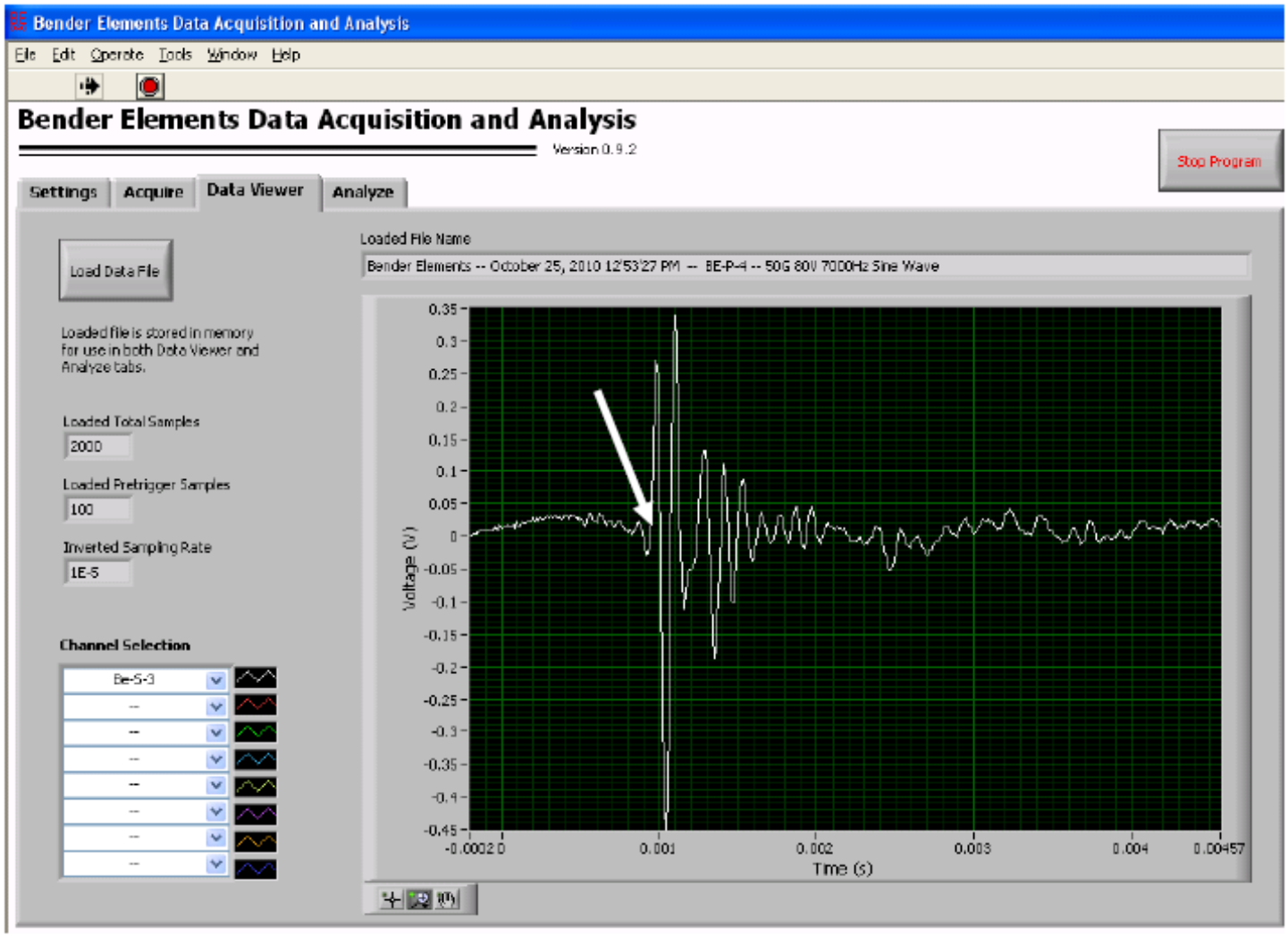


Figure 5.13: Screenshot of the S-wave signal received by [BE-S-3] for dry Ottawa sand e=0.723 at 50G (Test 1)

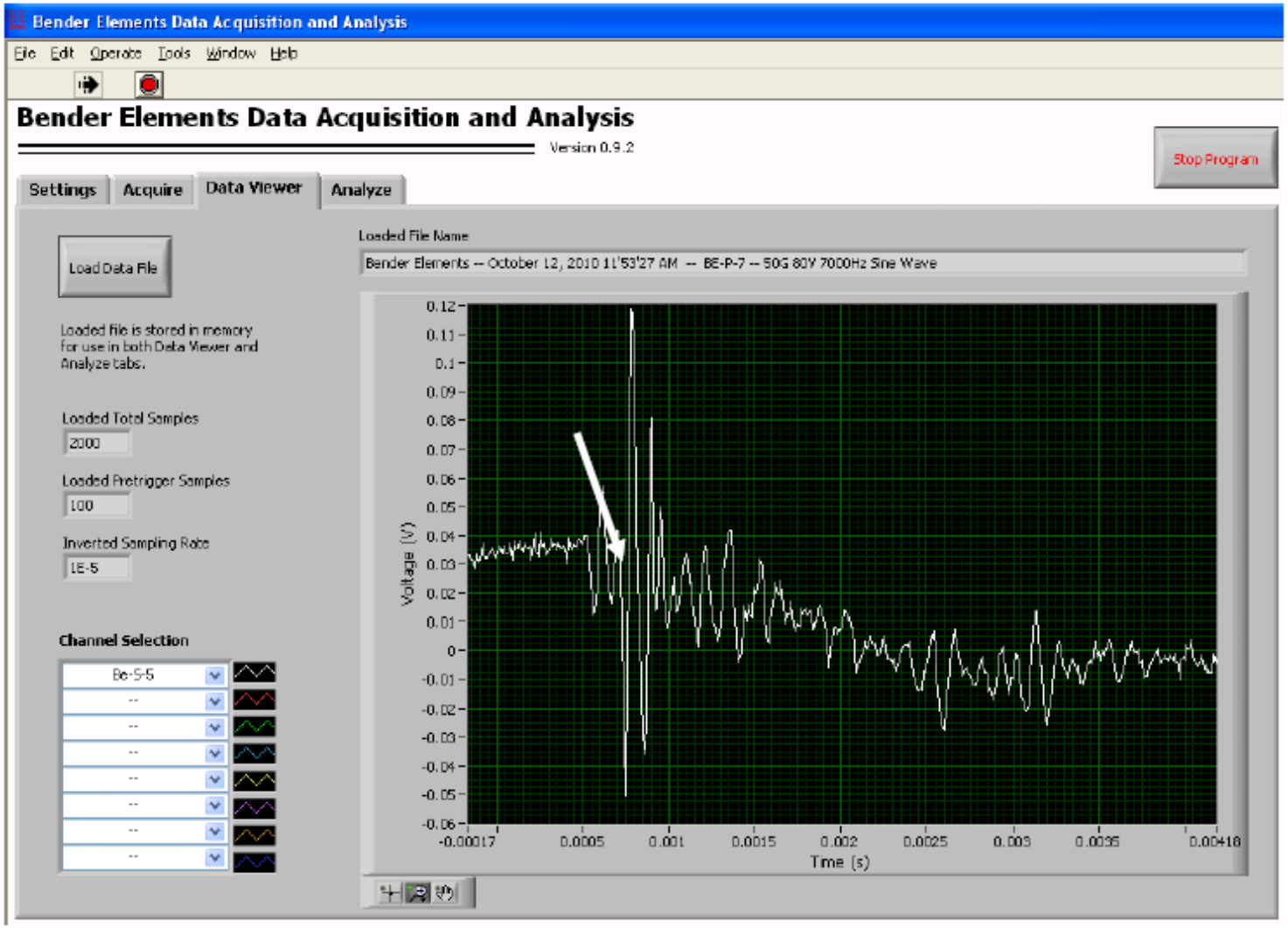


Figure 5.14: Screenshot of the S-wave signal received by [BE-S-5] for dry Ottawa sand e=0.595 at 50G (Test 2)

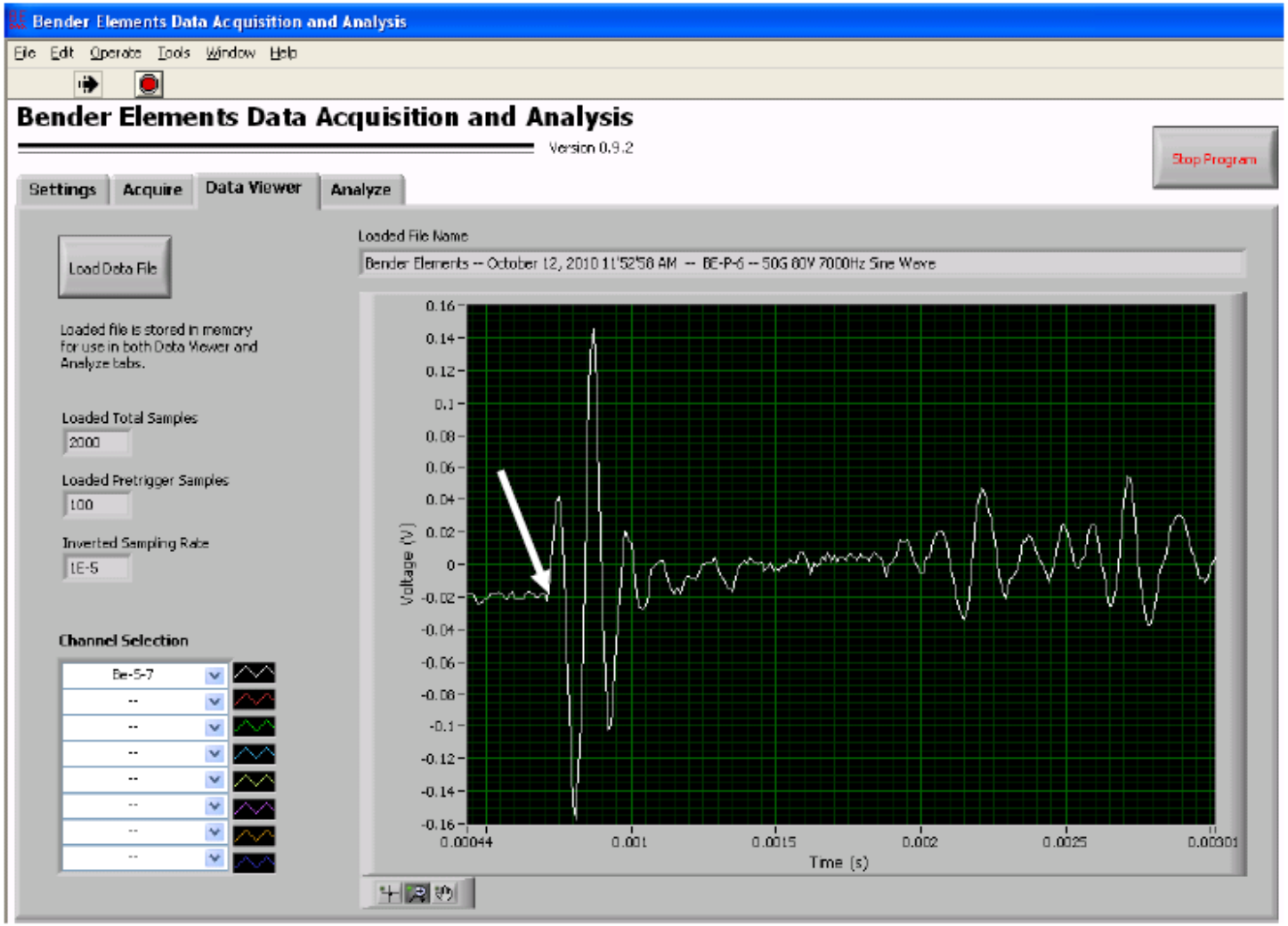


Figure 5.15: Screenshot of the S-wave signal received by [BE-S-7] for dry Ottawa sand e=0.595 at 50G (Test 2)

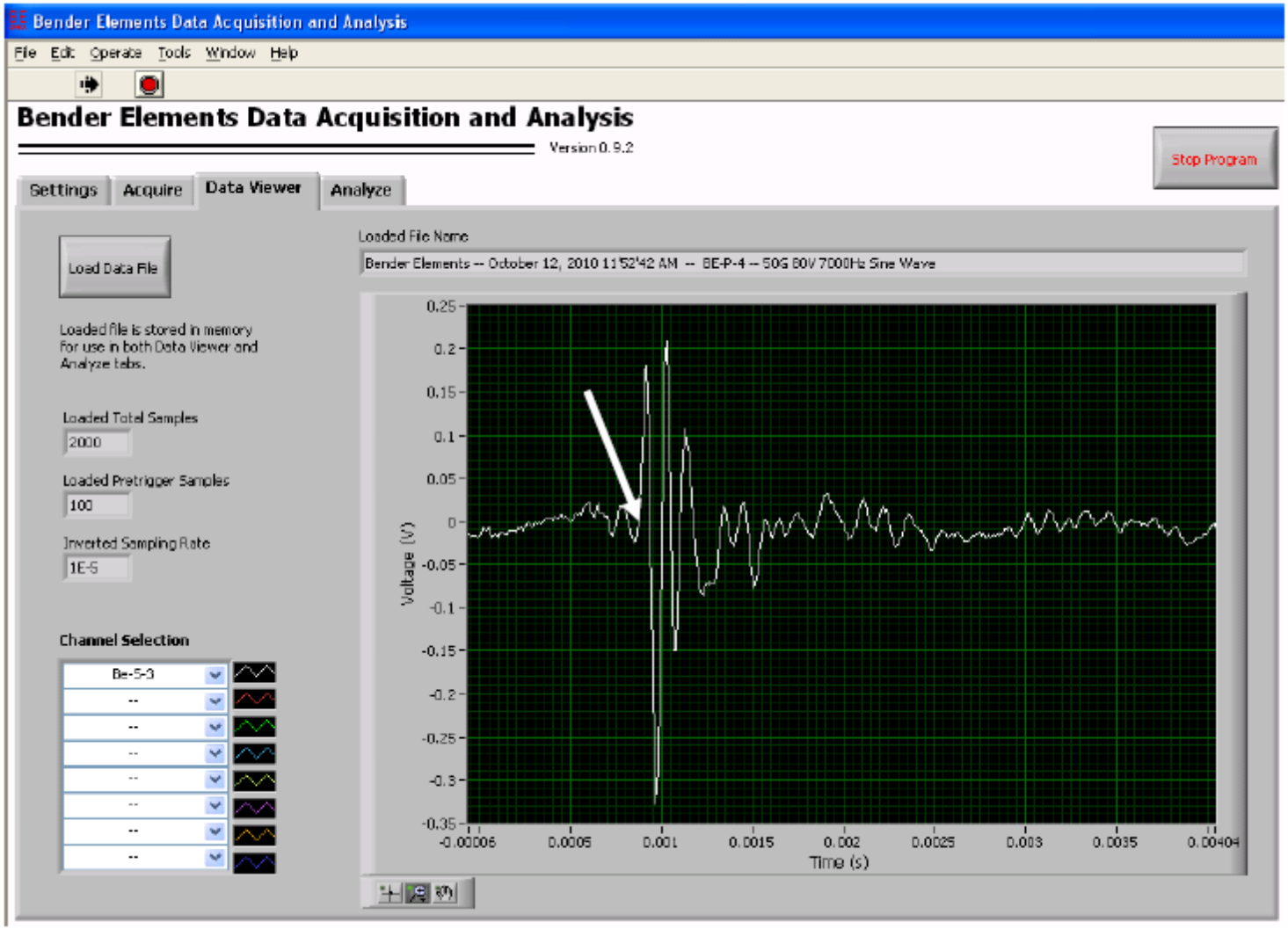


Figure 5.16: Screenshot of the S-wave signal received by [BE-S-3] for dry Ottawa sand e=0.595 at 50G (Test 2)

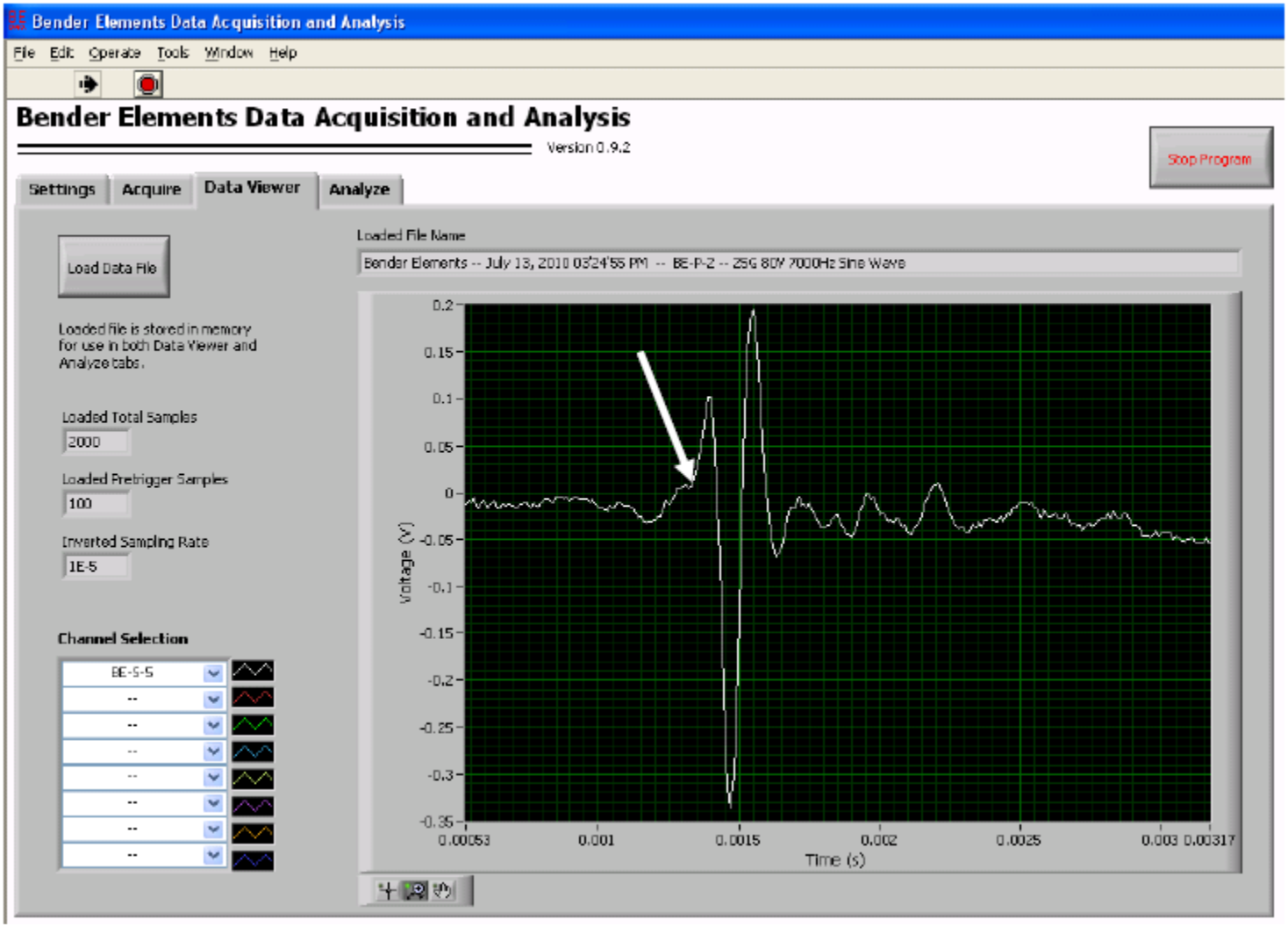


Figure 5.17: Screenshot of the S-wave signal received by [BE-S-5] for Saturated Ottawa sand e=0.723 at 25G (Test 3)

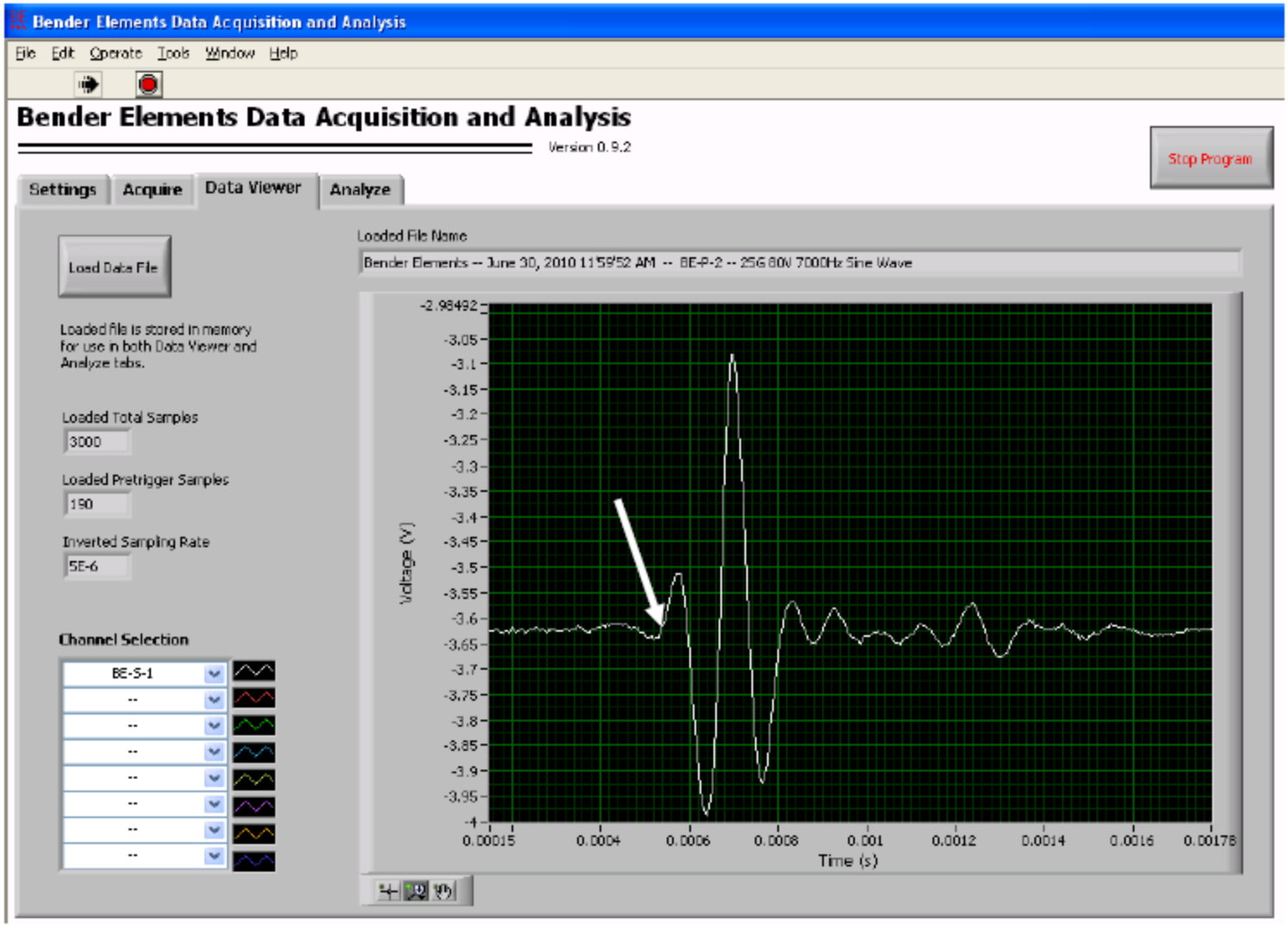


Figure 5.18: Screenshot of the S-wave signal received by [BE-S-5] for Saturated Ottawa sand e=0.625 at 25G (Test 4)

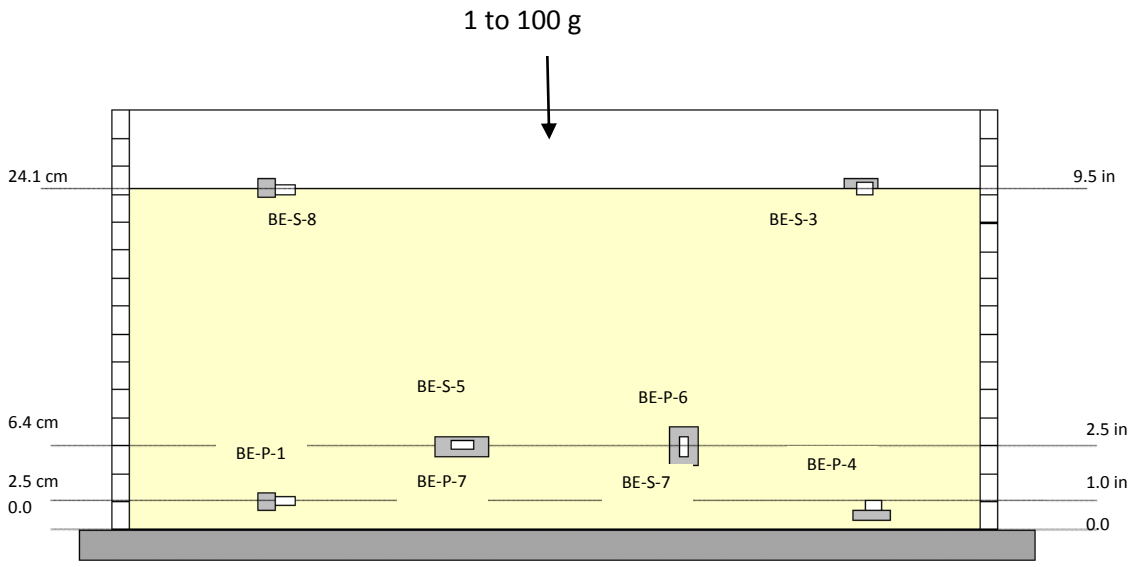


(a)

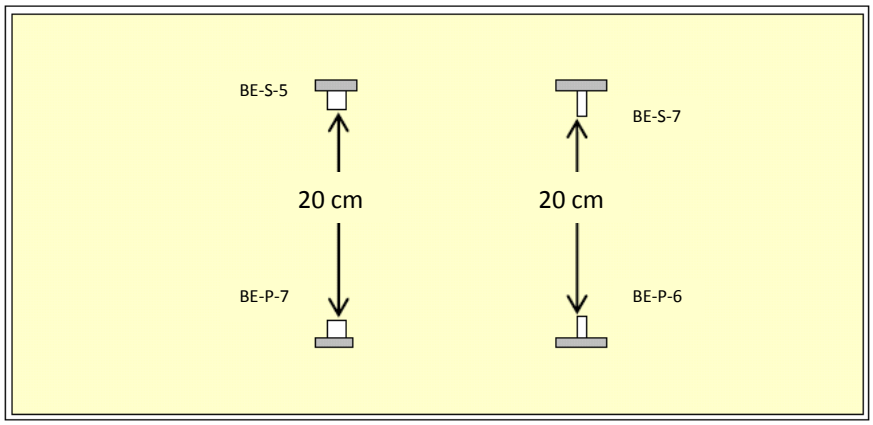


(b)

Figure 5.19: Setup and instrumentation of centrifuge model for Test 1 and 2 (model scale)

(a) Elevation

(b) Plan at elevation 2.5 inches from the base

(Not to scale. Bender Elements size is exaggerated for illustration)

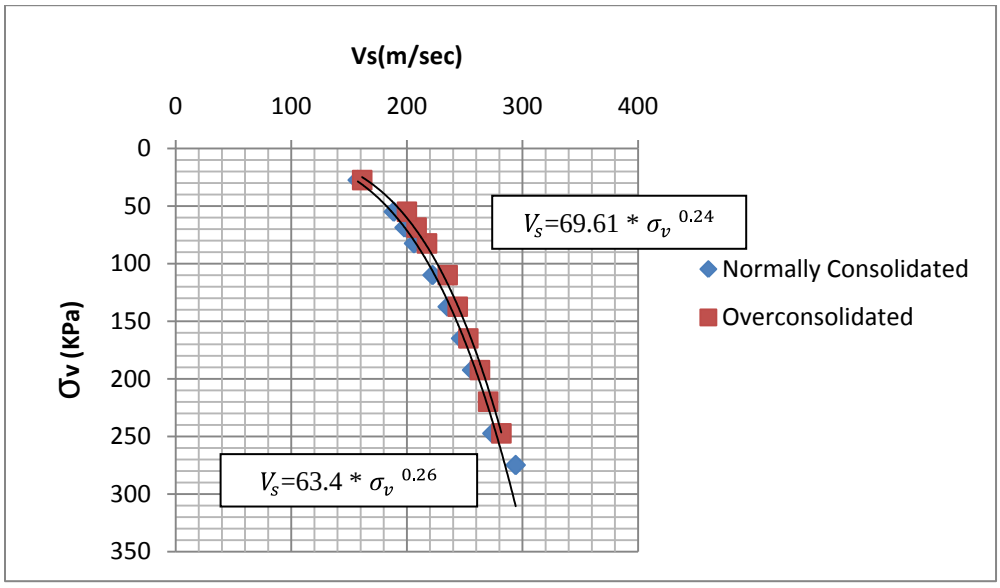


Figure 5.20: Shear wave velocity versus Vertical Stress calculated from [BE-P-7] to [BE-S-5] for dry Ottawa sand (Test 1, e=0.723) (the wave is horizontally propagating and vertically polarized)

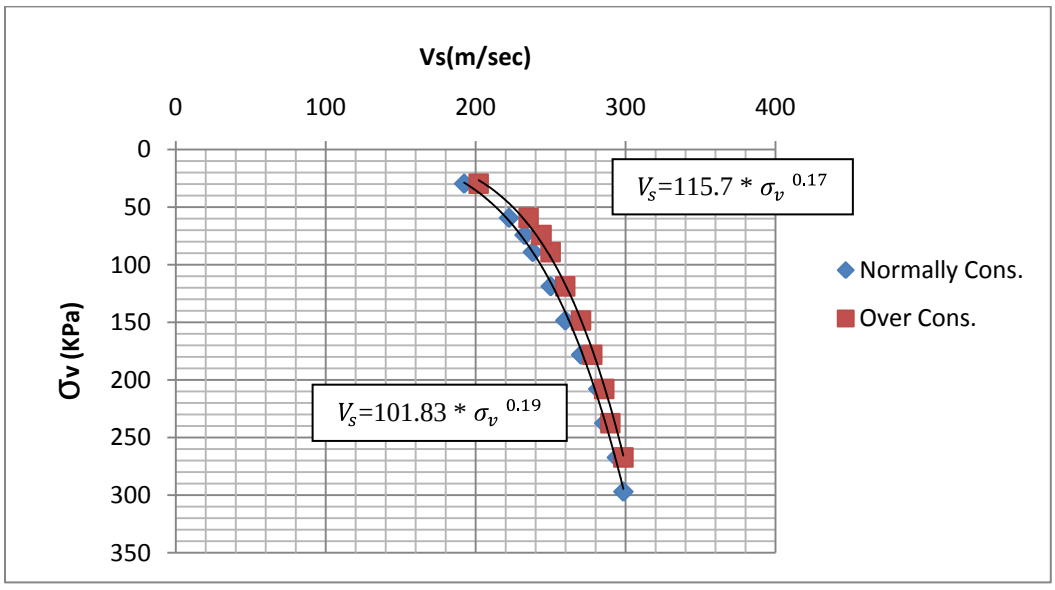


Figure 5.21: Shear wave velocity versus Vertical Stress calculated from [BE-P-7] to [BE-S-5] for dry Ottawa sand (Test 2, e=0.595) (The wave is horizontally propagating and vertically polarized)

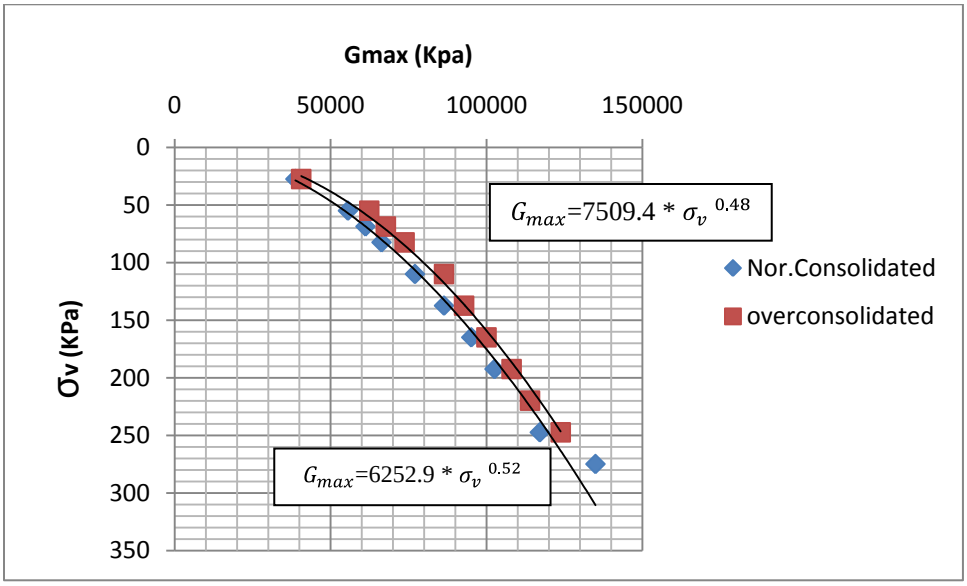


Figure 5.22: $G_{max}$ versus Vertical Stress calculated from [BE-P-7] to [BE-S-5] for dry Ottawa sand (Test 1, e=0.723) (The wave is horizontally propagating and vertically polarized)

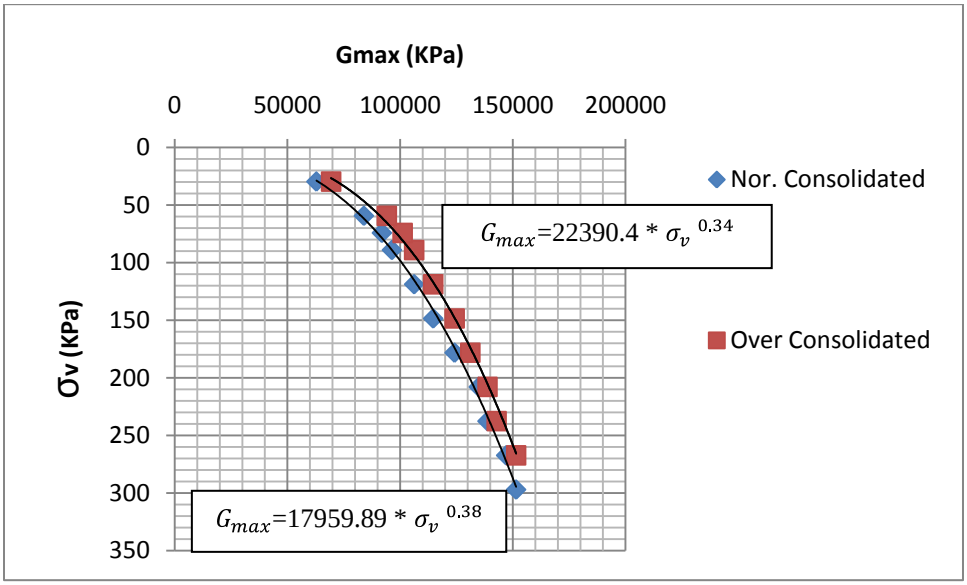


Figure 5.23: $G_{max}$ versus Vertical Stress calculated from [BE-P-7] to [BE-S-5] for dry Ottawa sand (Test 2, e=0.595) (The wave is horizontally propagating and vertically polarized

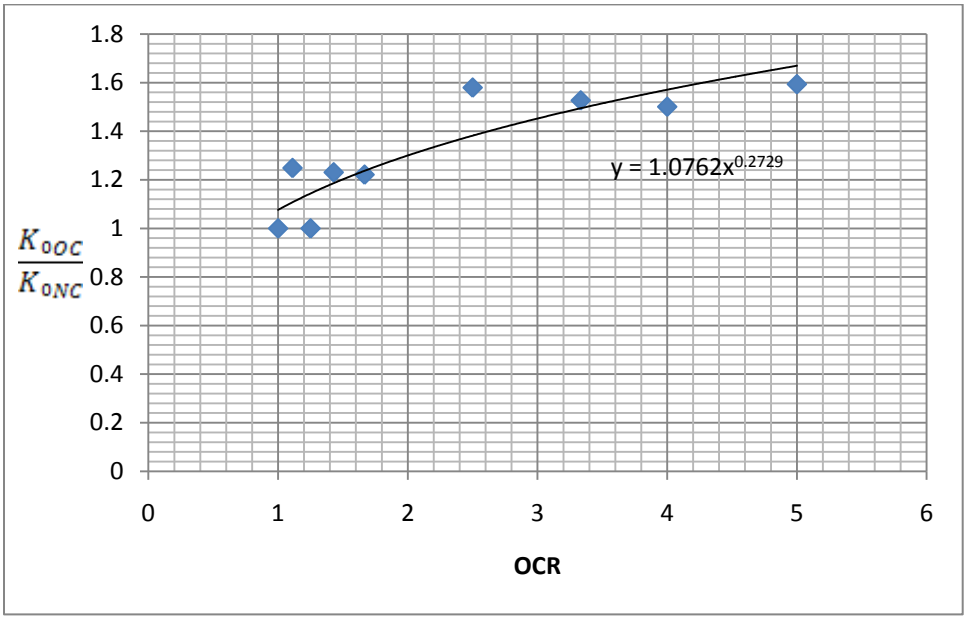


Figure 5.24: The ratio $K_0$oc/$K_0$nc versus OCR calculated from [BE-P-7] to [BE-S-5] for dry Ottawa sand (Test 1, e=0.723)

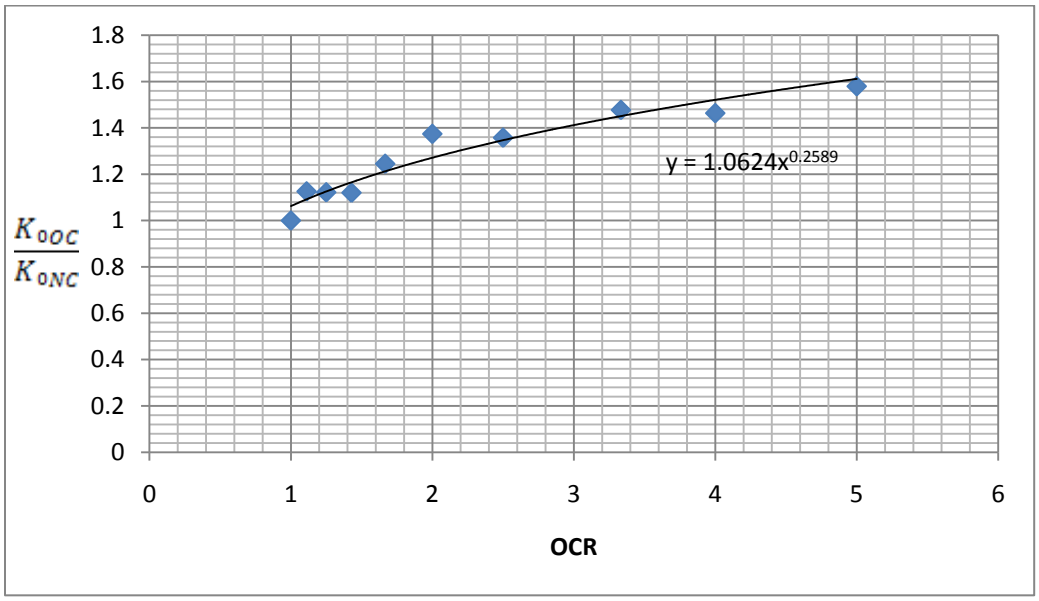


Figure 5.25: The ratio $K_0$oc/$K_0$nc versus OCR calculated from [BE-P-7] to [BE-S-5] for dry Ottawa sand (Test 2, e=0.595)

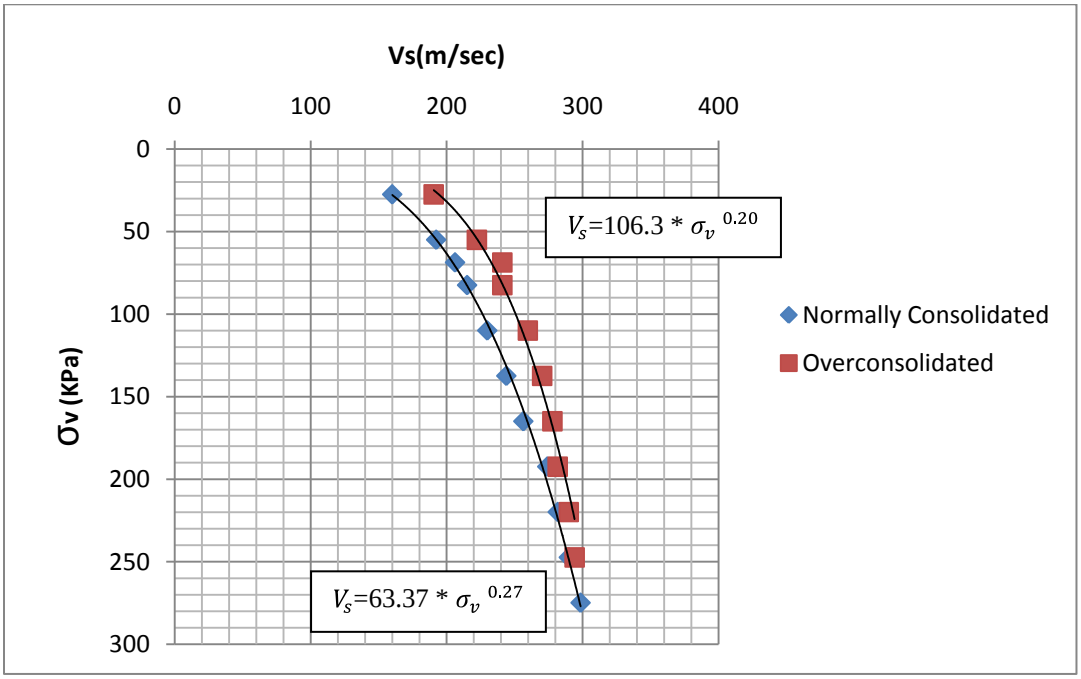


Figure 5.26: Shear wave velocity versus Vertical Stress calculated from [BE-P-6] to [BE-S-7] for dry Ottawa sand (Test 1, e=0.723) (The wave is horizontally propagating and horizontally polarized)

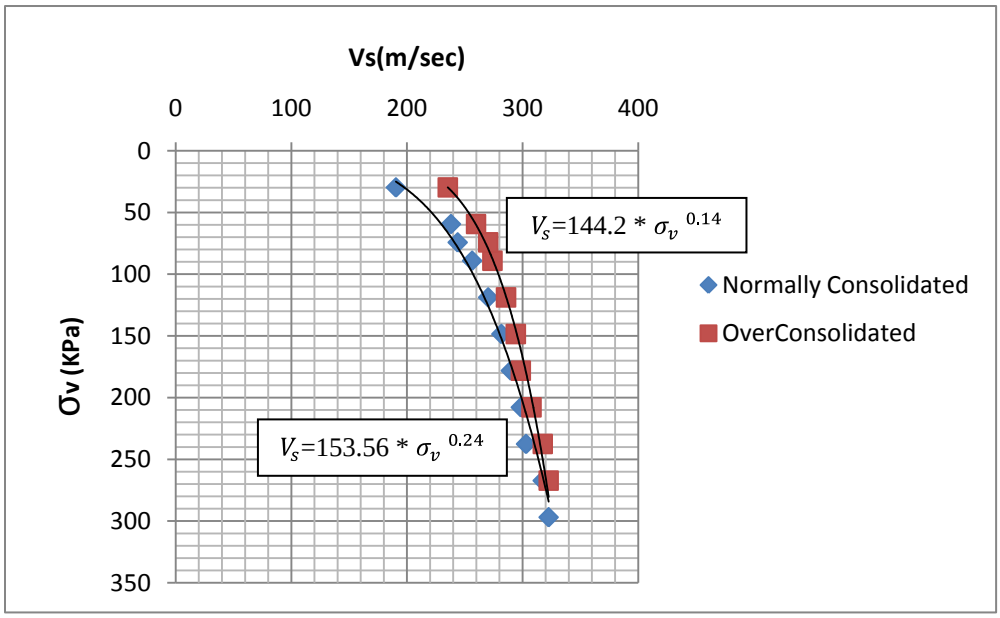


Figure 5.27: Shear wave velocity versus Vertical Stress calculated from [BE-P-6] to [BE-S-7] for dry Ottawa sand (Test 2, e=0.595) (The wave is horizontally propagating and horizontally polarized)

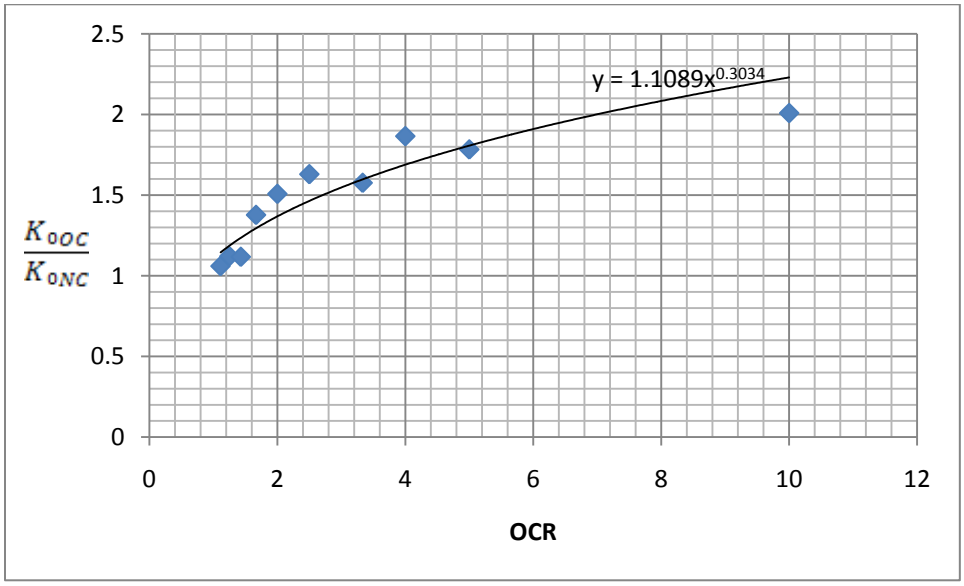


Figure 5.28: The ratio $K_0$oc/$K_0$nc versus OCR calculated from [BE-P-6] to [BE-S-7] for dry Ottawa sand (Test 1, e=0.723)

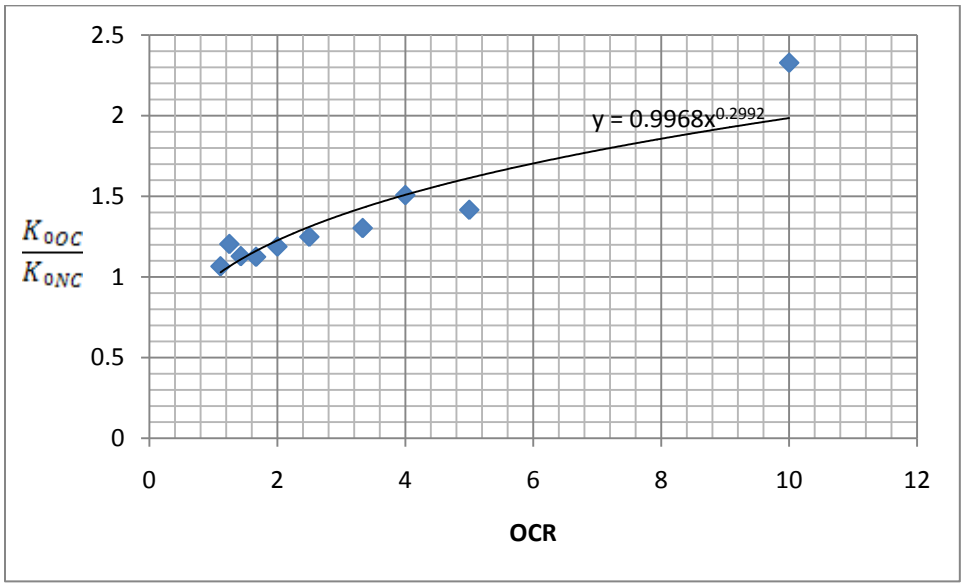


Figure 5.29: The ratio $K_0$oc/$K_0$nc versus OCR calculated from [BE-P-6] to [BE-S-7] for dry Ottawa sand (Test 2, e=0.595)

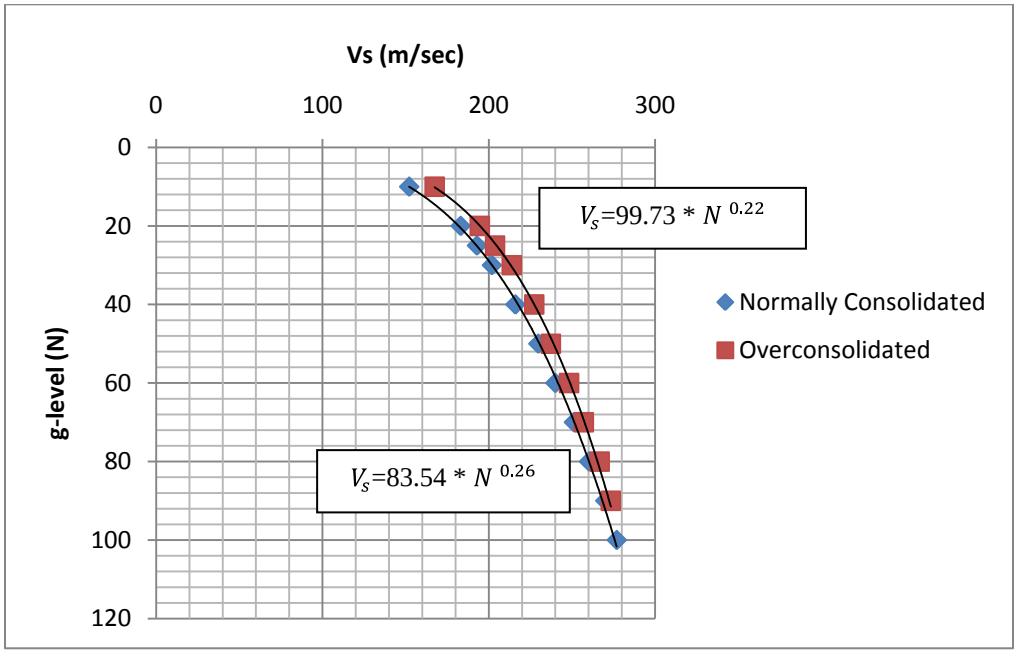


Figure 5.30: Average Shear wave velocity versus g-Level calculated from [BE-P-4] to [BE-S-3] for dry Ottawa sand (Test 1, e=0.723 ) (The wave is vertically propagating and horizontally polarized)

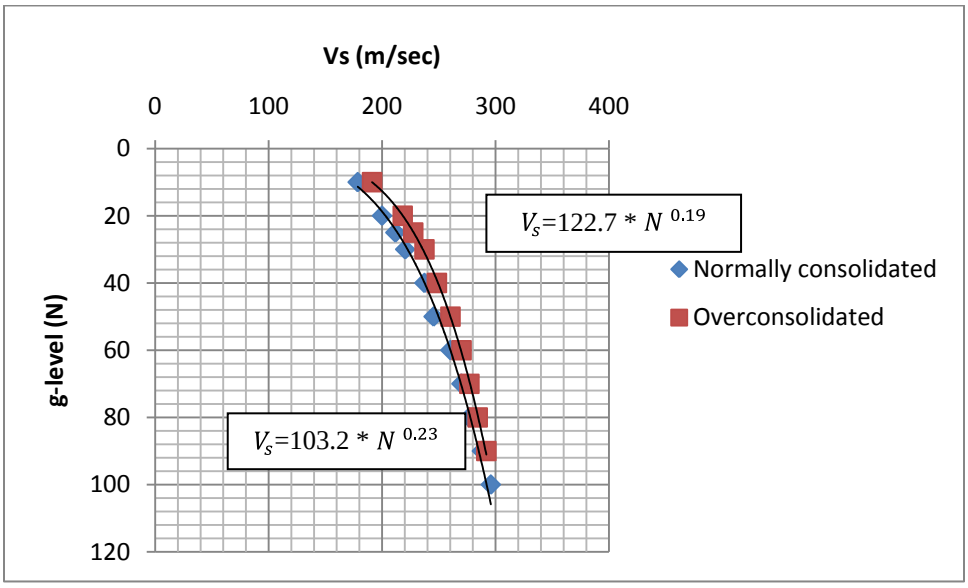


Figure 5.31: Average Shear wave velocity versus g-Level calculated from [BE-P-4] to [BE-S-3] for dry Ottawa sand (Test 2, e=0.595 ) (The wave is vertically propagating and horizontally polarized)

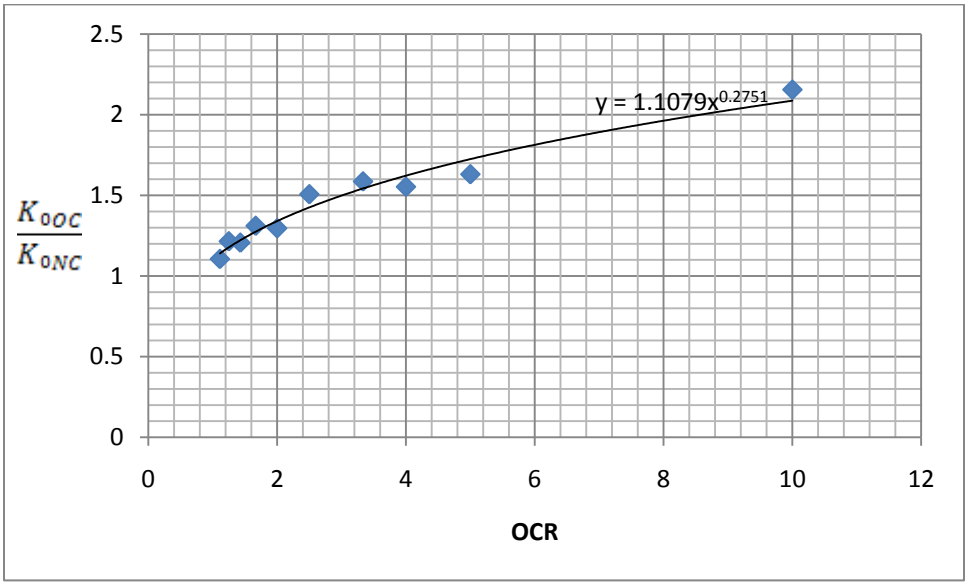


Figure 5.32: The ratio $K_0$oc/$K_0$nc versus OCR calculated from [BE-P-4] to [BE-S-3] for dry Ottawa sand (Test1, e=0.723)

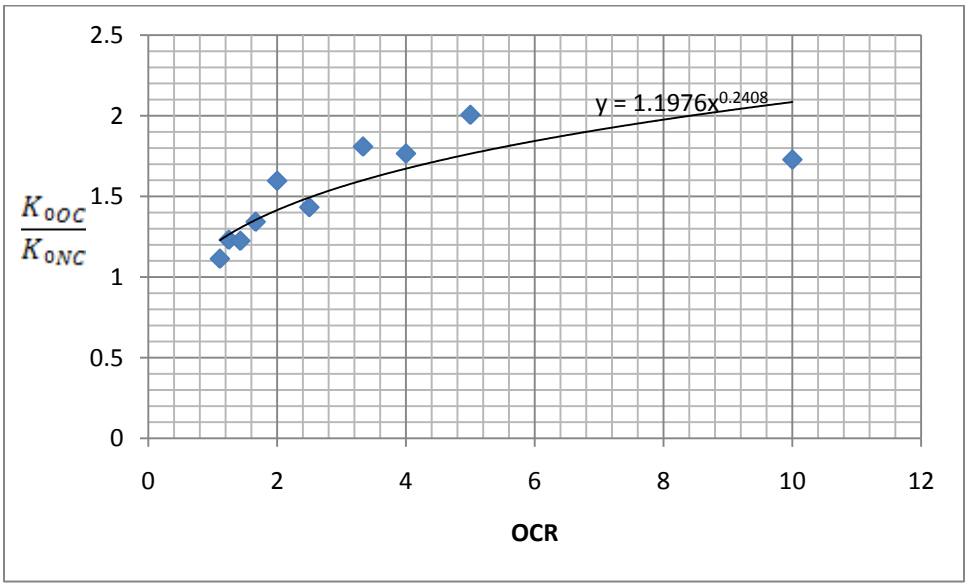


Figure 5.33: The ratio $K_0$oc/$K_0$nc versus OCR calculated from [BE-P-4] to [BE-S-3] for dry Ottawa sand (Test2, e=0.595)

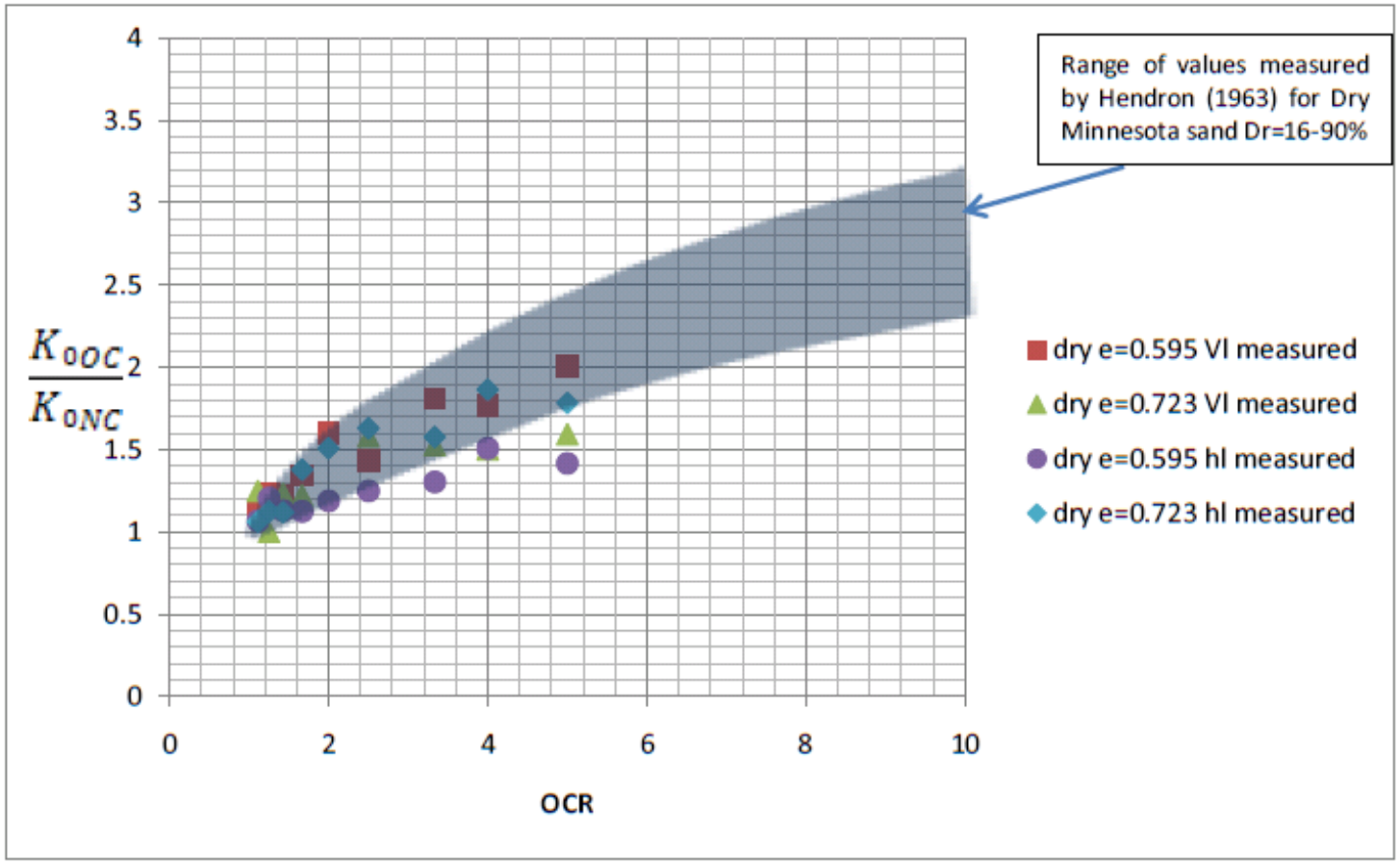


Figure 5.34: Summary of the ratio $K_0$ oc/$K_0$ nc versus OCR for different cases mentioned in this research and its comparison with the values from Hendron

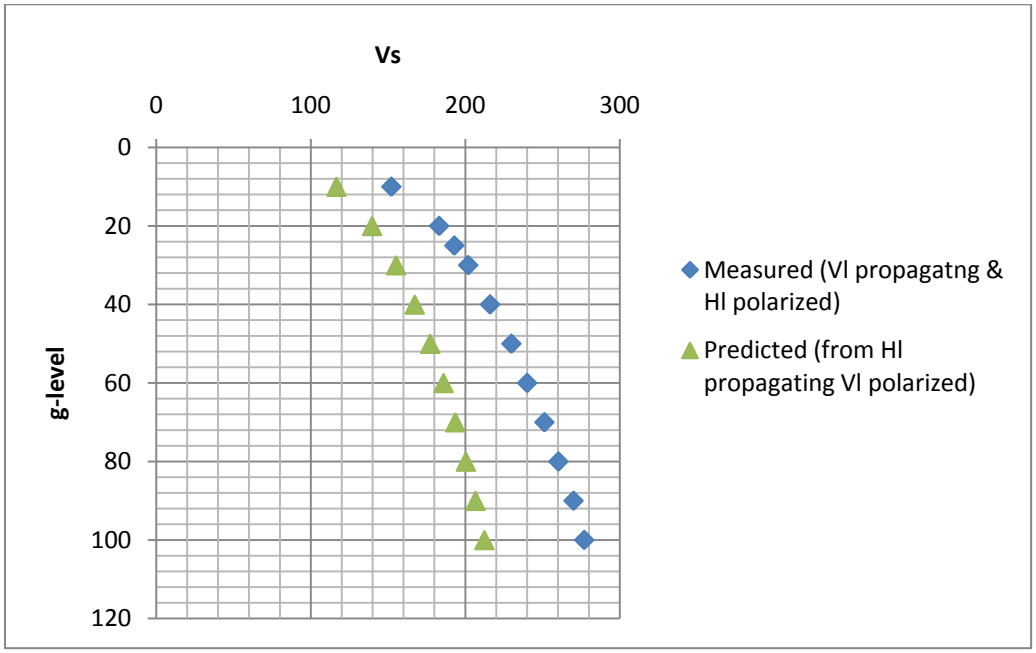


Figure 5.35: Measured and Predicted $V_s$ vertically Propagating (Dry Ottawa Sand e=0.723)

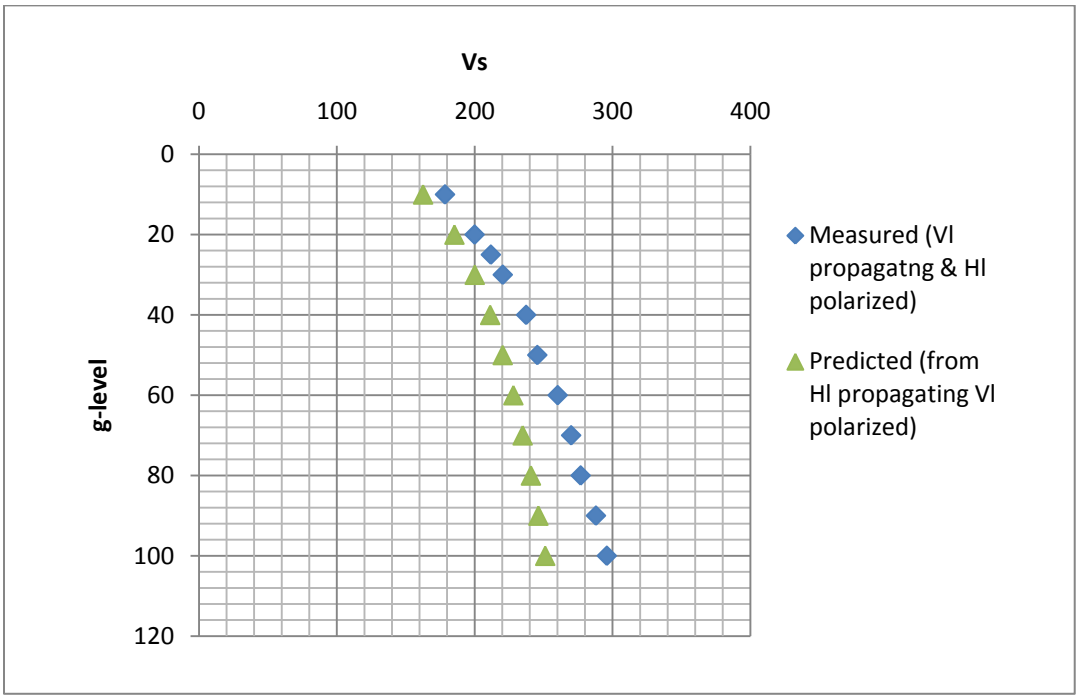


Figure 5.36: Measured and Predicted $V_s$ vertically Propagating (Dry Ottawa Sand e=0.595)

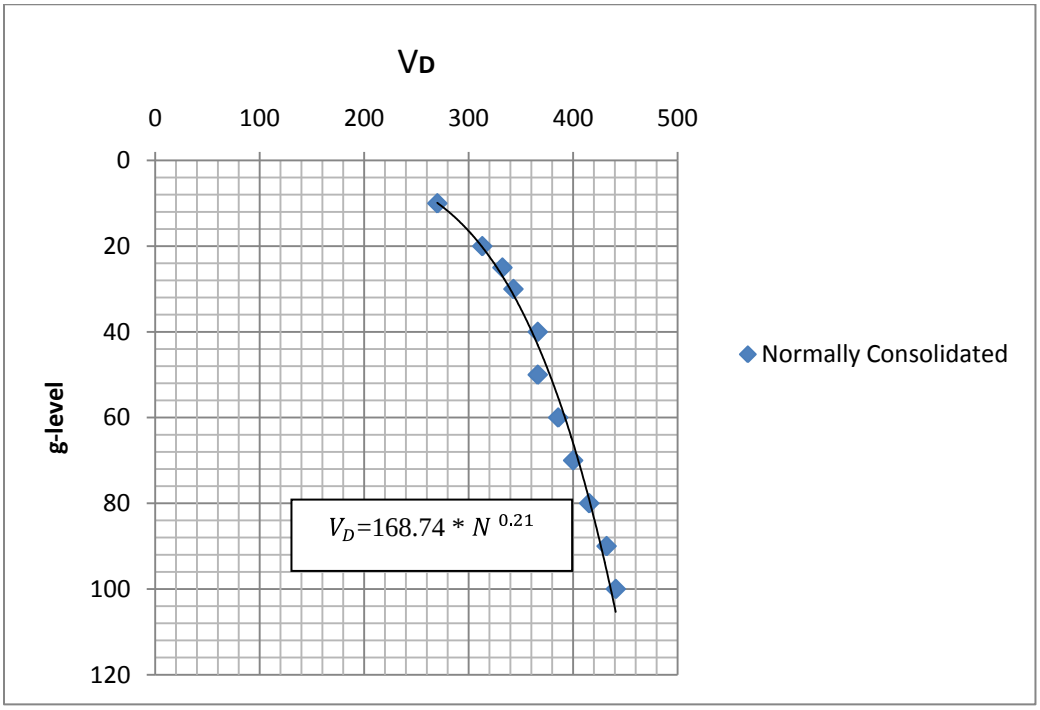


Figure 5.37: Average P-wave velocity versus g-Level calculated from [BE-P-1] to [BE-S-8] for dry Ottawa sand e=0.723 (The wave is vertically propagating and polarized)

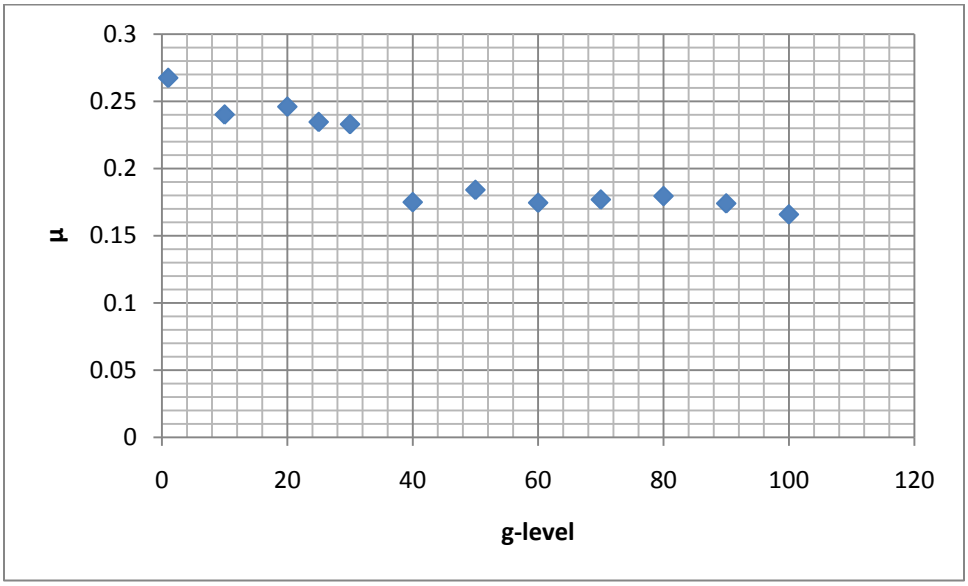


Figure 5.38: Average Poisson's ratio versus g-level for dry Ottawa sand e=0.723

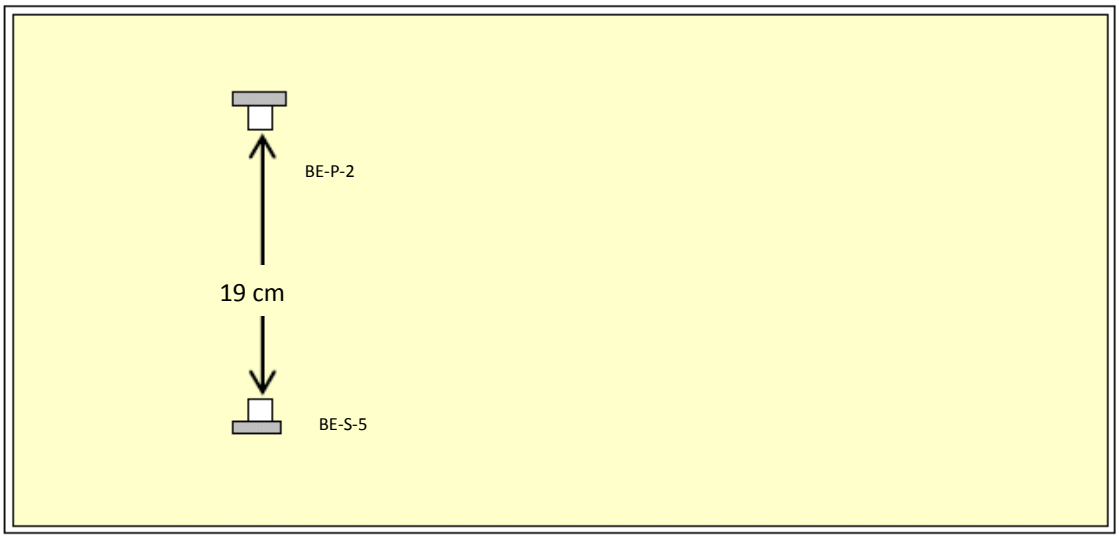


Figure 5.39: Setup and instrumentation of centrifuge model for Test 3 (Plan at elevation 2.5 inches from the base)

(Not to scale. Bender Elements size is exaggerated for illustration)

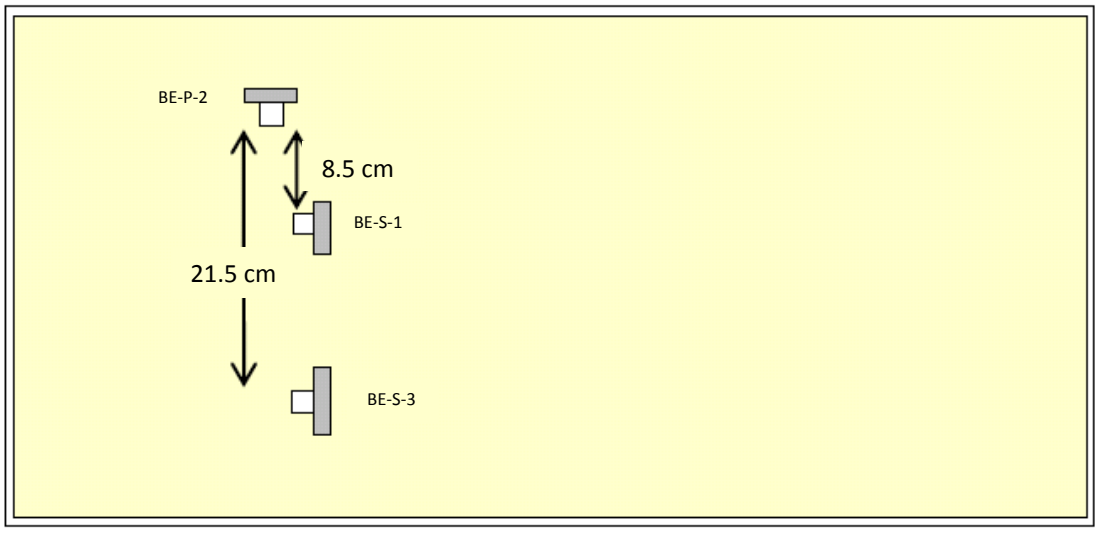


Figure 5.40: Setup and instrumentation of centrifuge model for Test 4 (Plan at elevation 2.5 inches from the base)

(Not to scale. Bender Elements size is exaggerated for illustration)

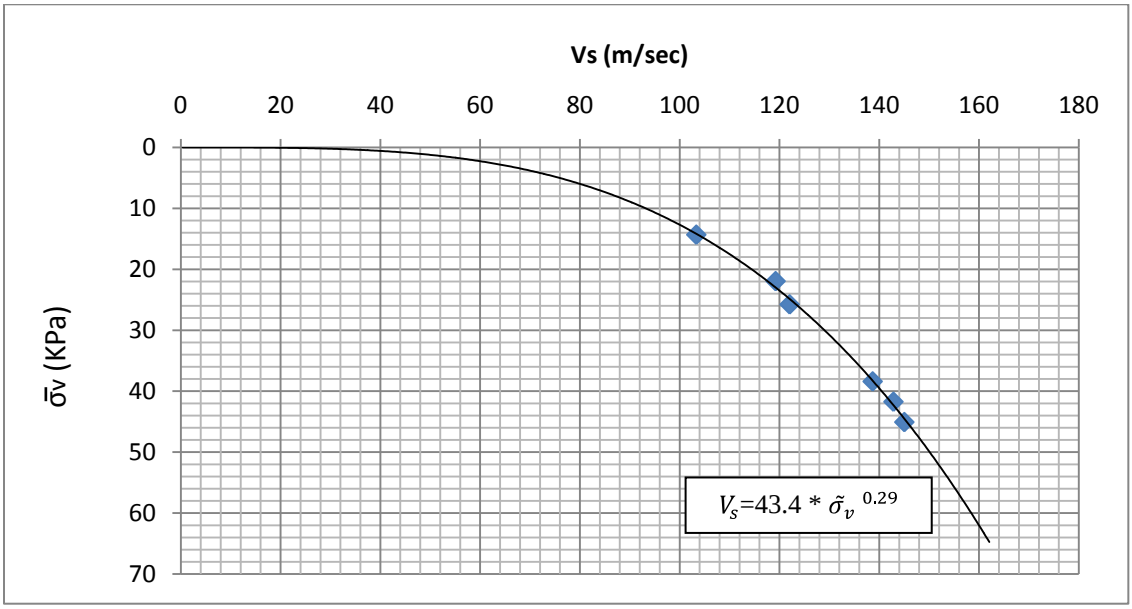


Figure 5.41: Shear wave velocity versus effective Vertical Stress calculated from [BE-P-2] to [BE-S-5] for saturated Ottawa sand e=0.723 (The wave is horizontally propagating and vertically polarized)

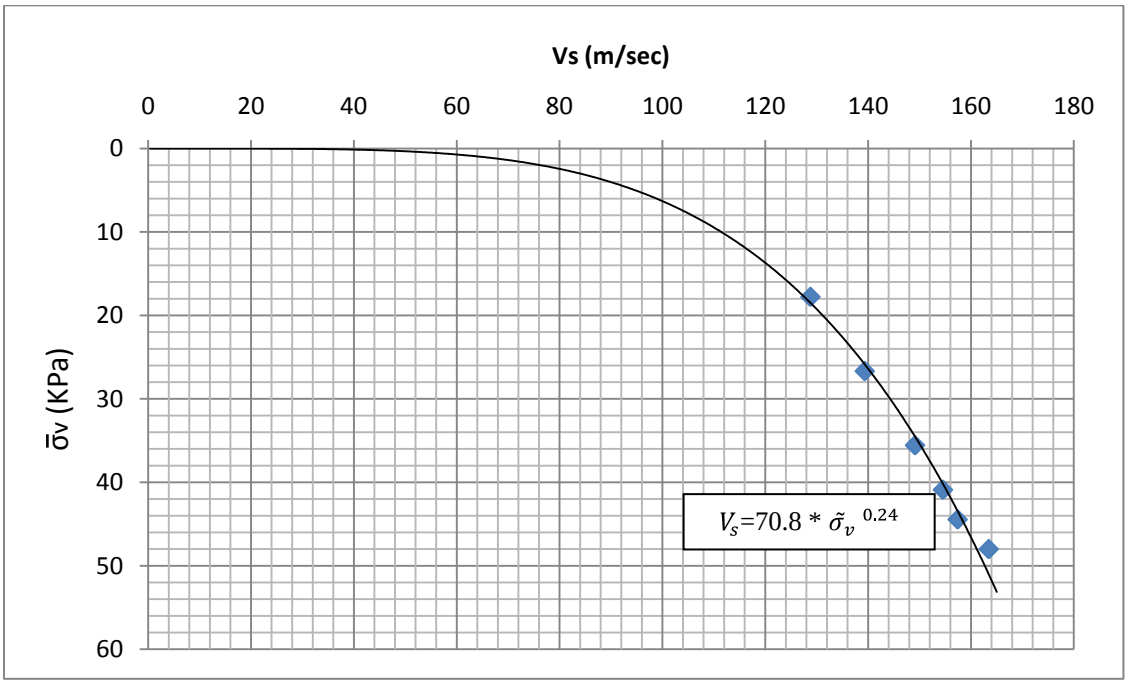


Figure 5.42: Shear wave velocity versus effective Vertical Stress calculated from [BE-P-2] to [BE-S-1] for saturated Ottawa sand e=0.625 (The wave is horizontally propagating and vertically polarized)

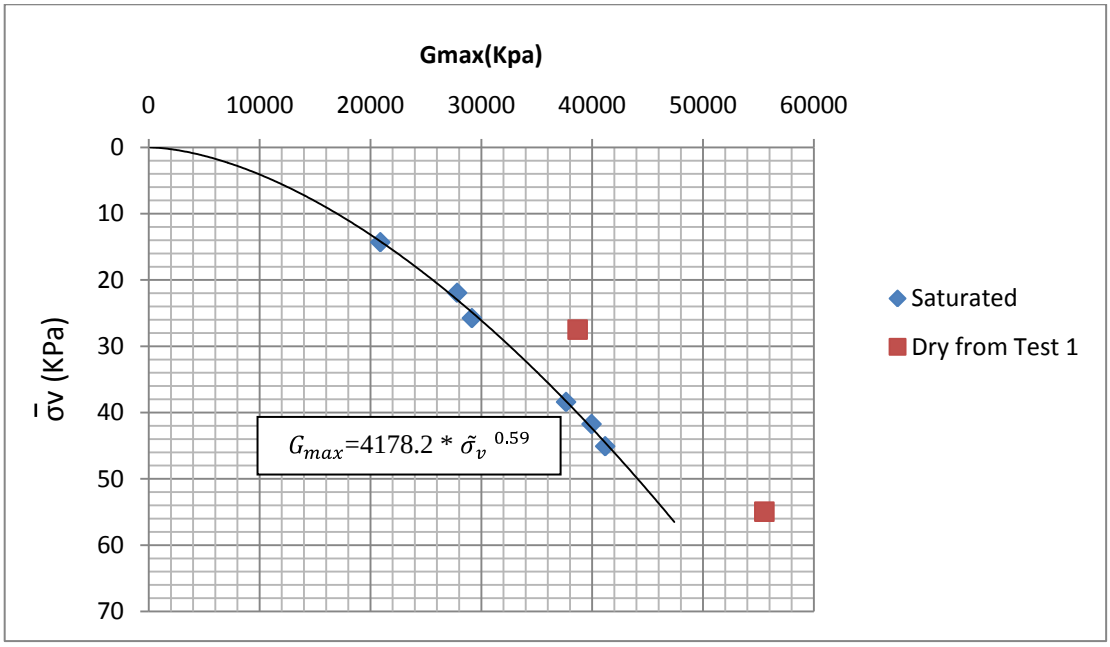


Figure 5.43: $G_{max}$ versus effective Vertical Stress calculated from [BE-P-2] to [BE-S-5] for saturated Ottawa sand e=0.723 (The wave is horizontally propagating and vertically polarized)

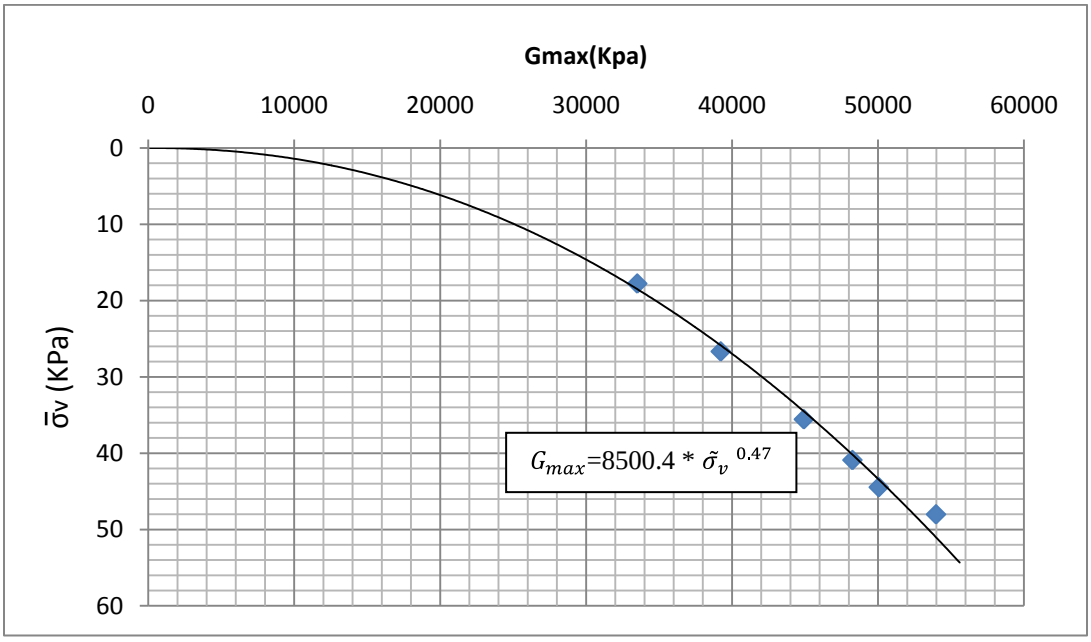


Figure 5.44: $G_{max}$ versus effective Vertical Stress calculated from [BE-P-2] to [BE-S-1] for saturated Ottawa sand e=0.625 (The wave is horizontally propagating and vertically polarized)

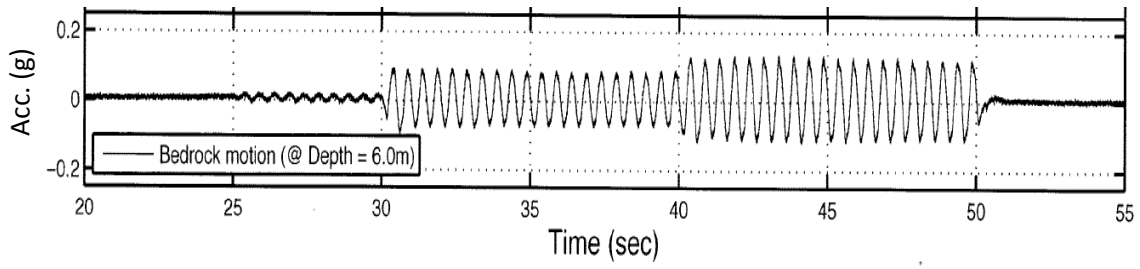


Figure 5.45: Prototype acceleration profile at the base of the box for saturated Ottawa sand e=0.723 (El-Ganainy, 2011)

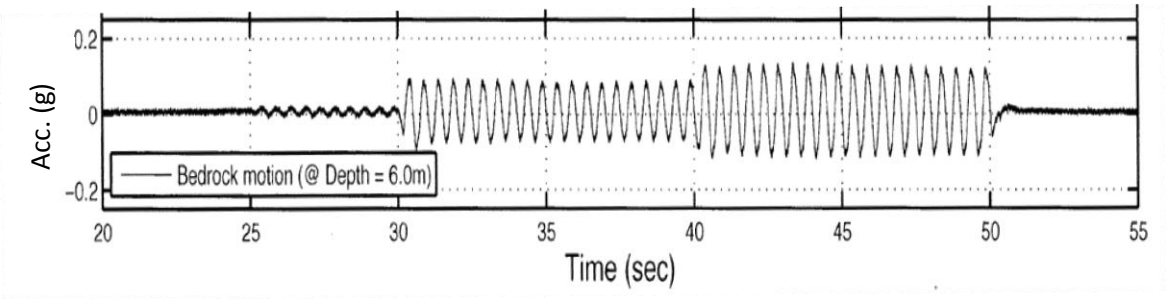


Figure 5.46: Prototype acceleration profile at the base of the box for saturated Ottawa sand e=0.625 (El-Ganainy, 2011)

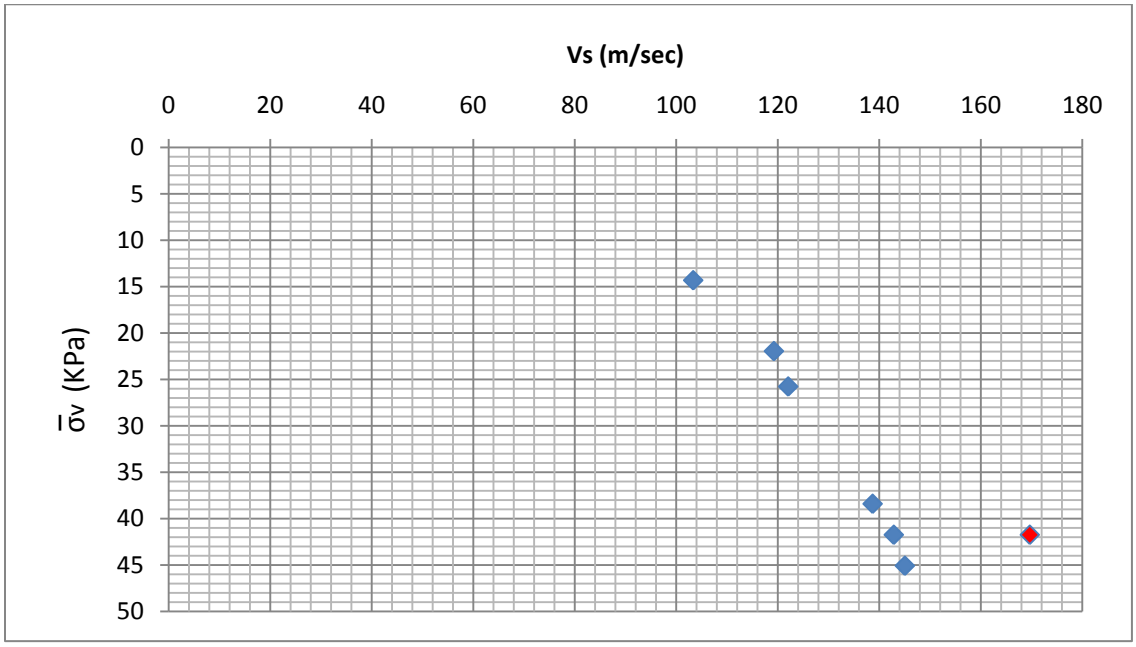


Figure 5.47: Change in Shear wave velocity due to bed rock acceleration in Figure 5.42 for saturated Ottawa sand e=0.723

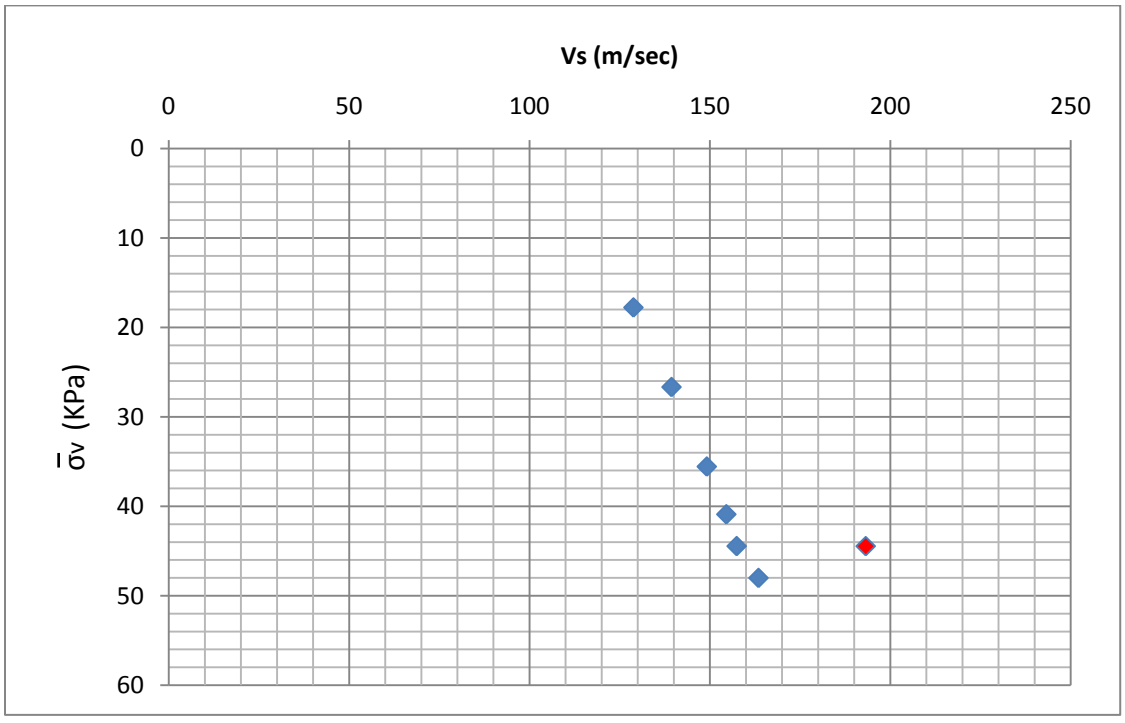


Figure 5.48: Change in Shear wave velocity due to bed rock acceleration in Figure 5.43 for saturated Ottawa sand e=0.625

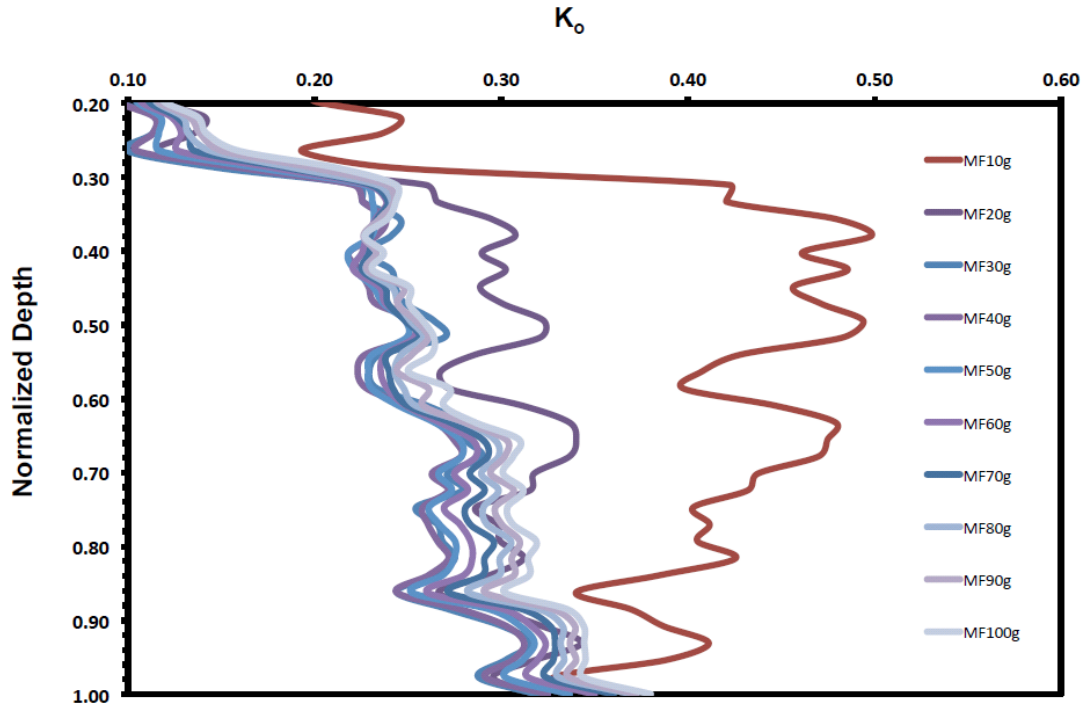


Figure 5.49: a plot showing the change of coefficient of earth pressure $K_0$ at different g-level along the depth of the laminar container for Dry Nevada Sand (Adapted from El-Ganainy, 2011)

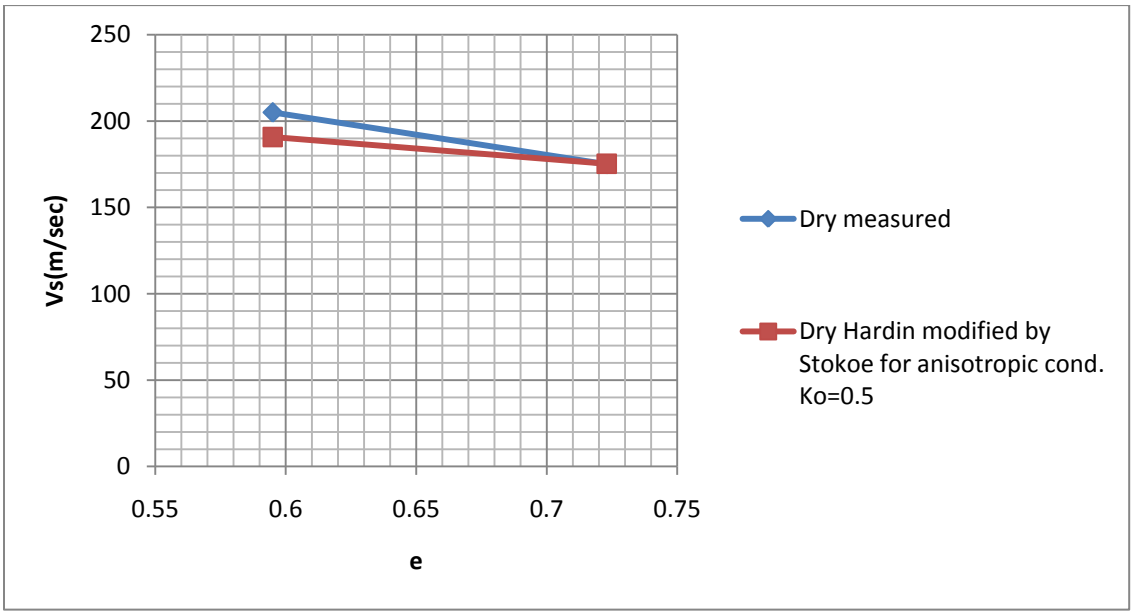


Figure 5.50: Comparison of the predicted and measured $V_s$ at $\sigma_v = 45$ kpa for dry Ottawa sand (The predicted data comes from Hardin equation modified to take the effect of anisotropy using Stokoe technique assuming $K_0$=0.5. The measured $V_s$ is taken at g-level about 15)

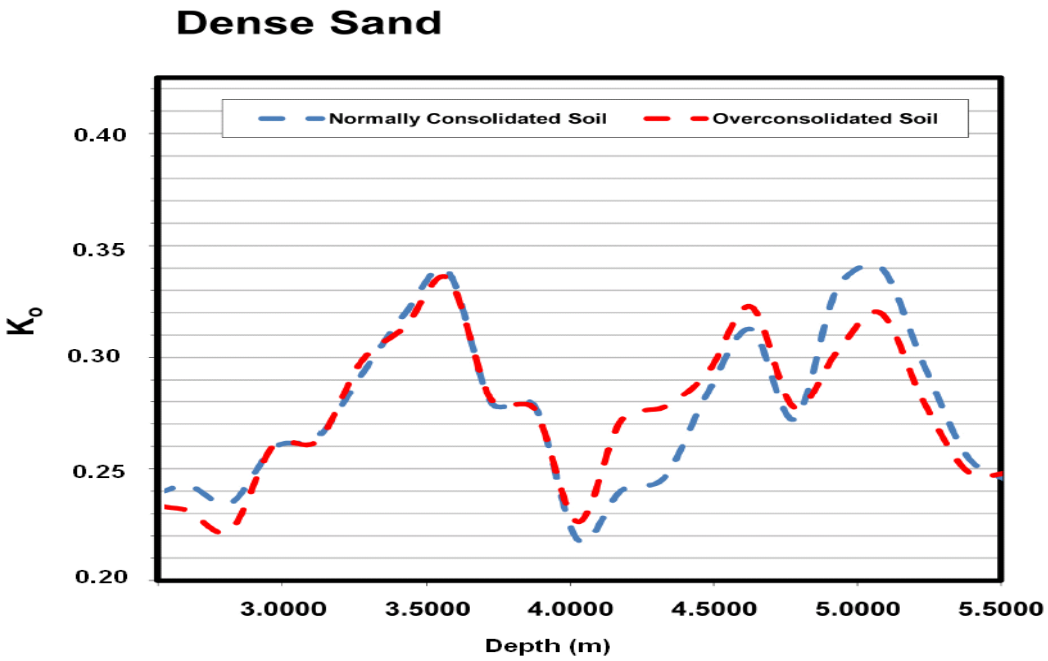


(a)

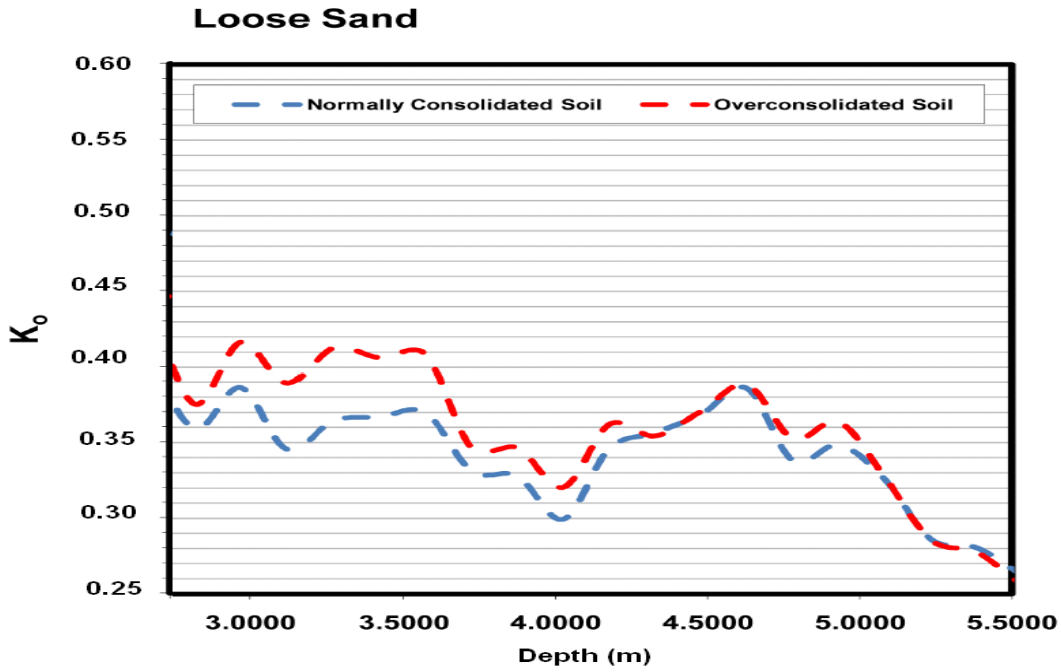


(b)

Figure 5.51: Measured Coefficient of Earth Pressure for a) Loose and b) Dense Saturated Ottawa Sand in the Laminar Container using the Tactile Sensor (El-Ganainy, 2011)

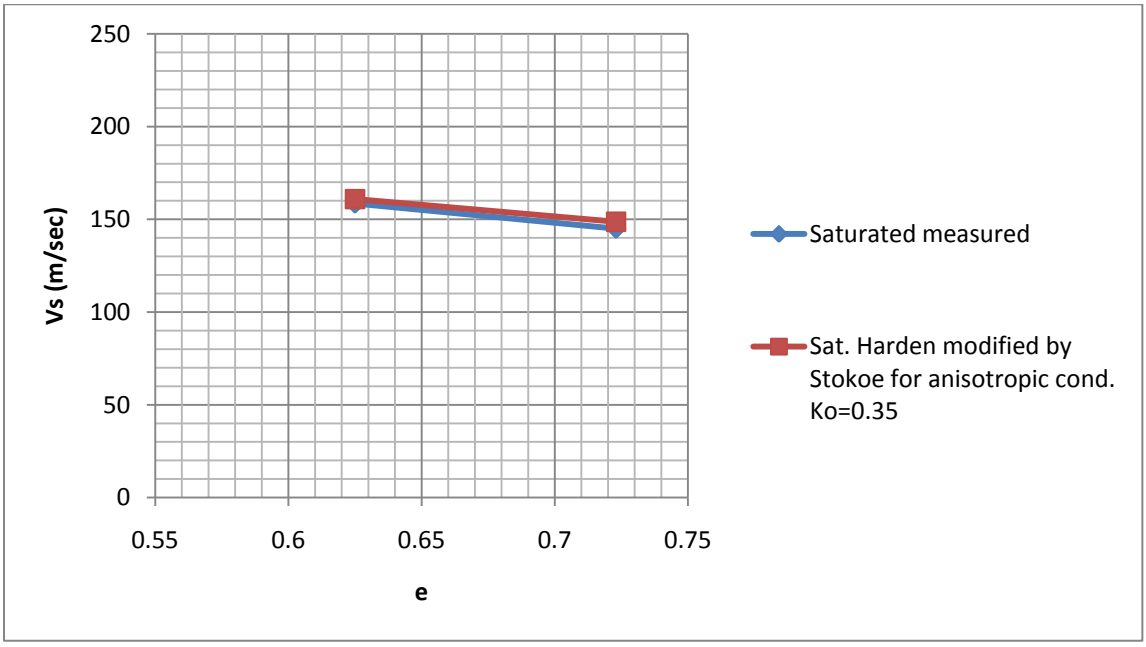


Figure 5.52: Comparison of the predicted and measured $V_s$ at $\tilde{\sigma}_v = 45$ kpa for saturated Ottawa sand (The predicted data comes from Hardin equation modified to take the effect of anisotropy using Stokoe technique assuming $K_0$=0.35. The measured $V_s$ is taken at g-level about 25)

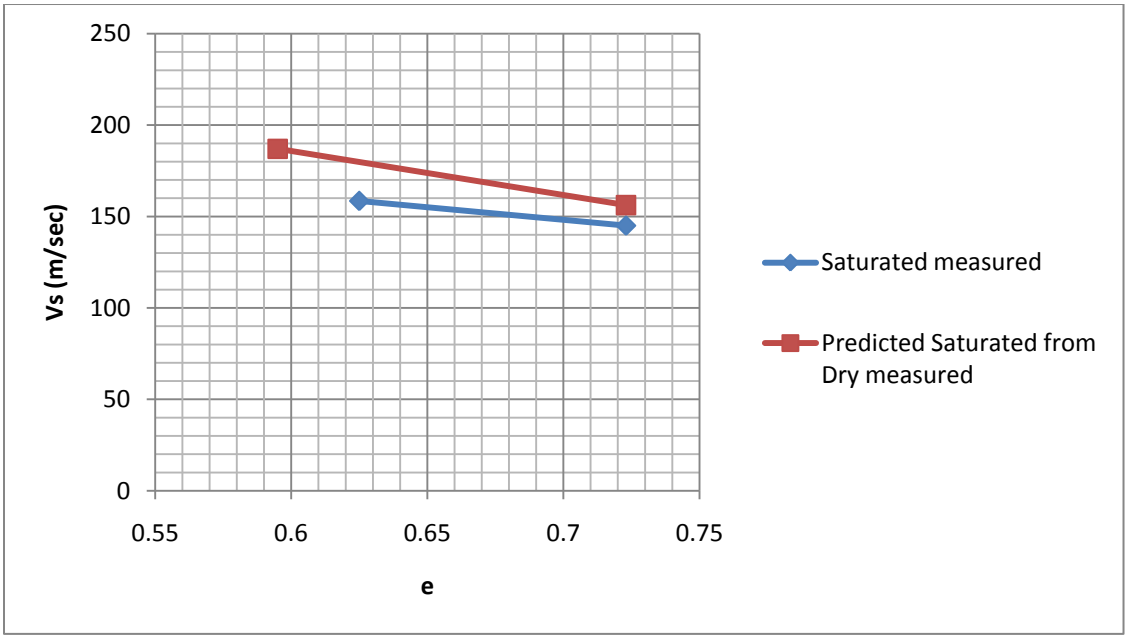


Figure 5.53: Comparison of the predicted and measured $V_s$ at $\tilde{\sigma}_v = 45$ kpa for saturated Ottawa sand (The predicted data comes from the dry measurements assuming $G_{max}$ is the same for dry and saturated soil as stated by Hardin. The measured $V_s$ is taken at g-level about 25)

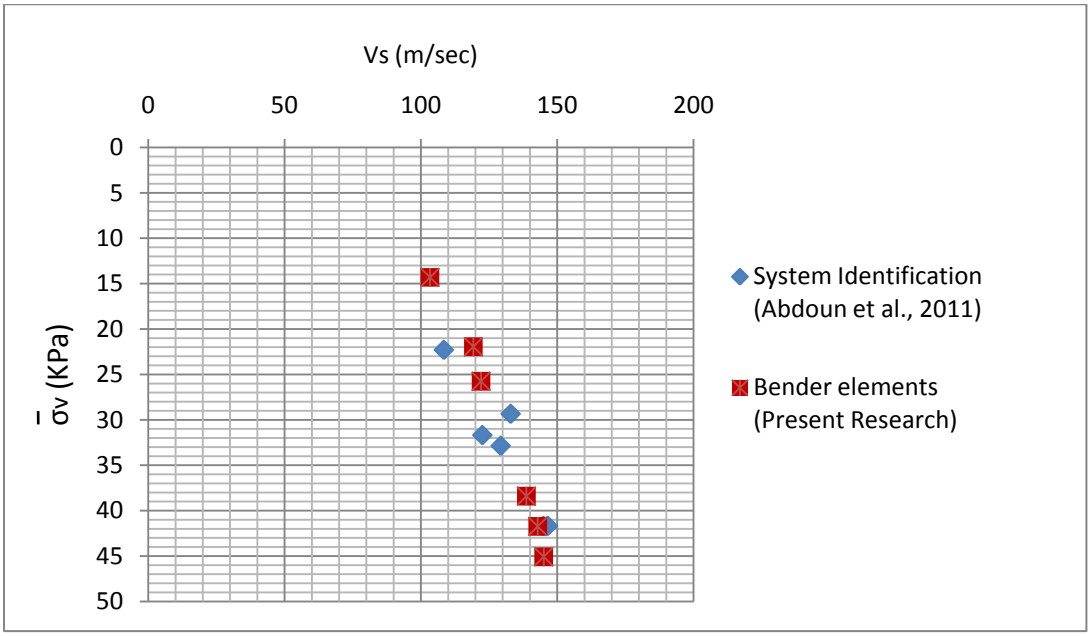


Figure 5.54: Comparison of the Shear Wave velocity measured by Bender Elements in this research and the value estimated by the system identification technique (Saturated Ottawa Sand, dry pluviation e=0.723)

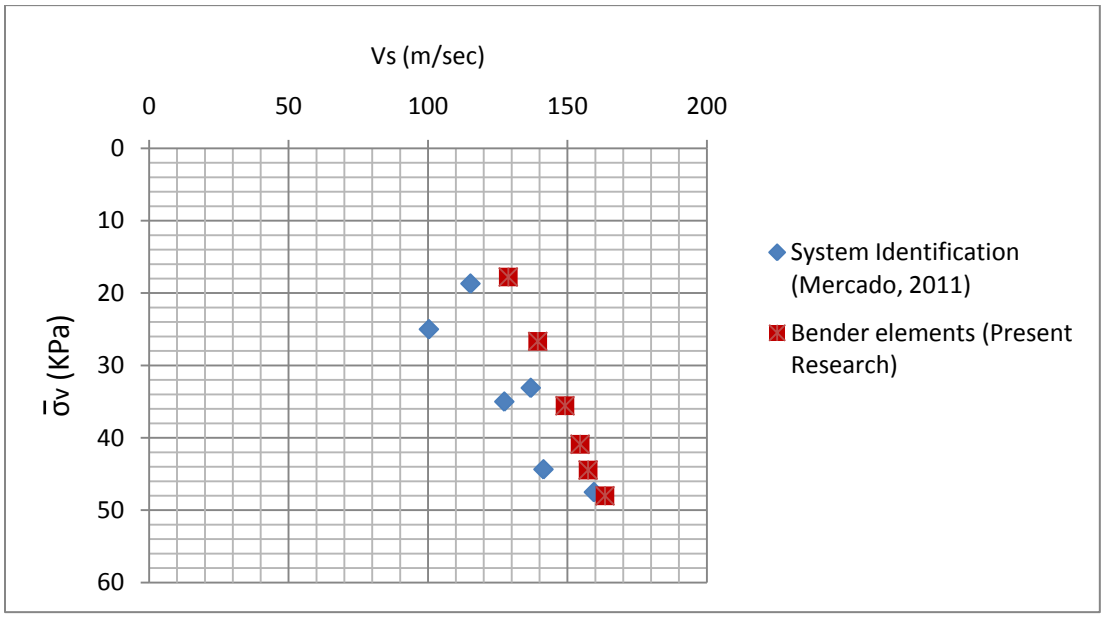


Figure 5.55: Comparison of the Shear Wave velocity measured by Bender Elements in this research and the value estimated by the system identification technique (Saturated Ottawa Sand, dry pluviation e=0.625)

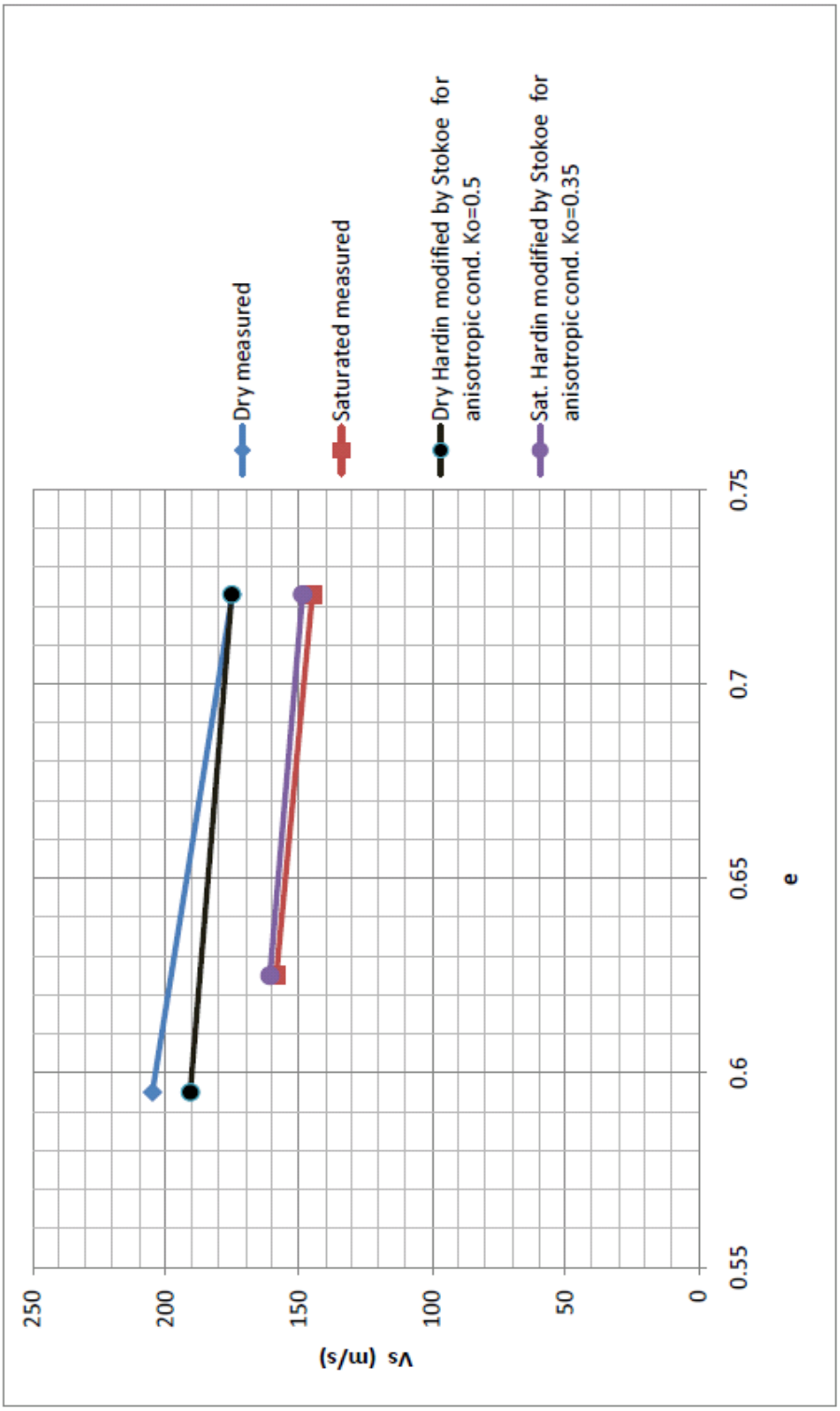


Figure 5.56: Shear wave velocity versus Voids ratio for both dry and saturated cases $(\tilde{\sigma}_v = 45\ kpa)$ (A summary plot)

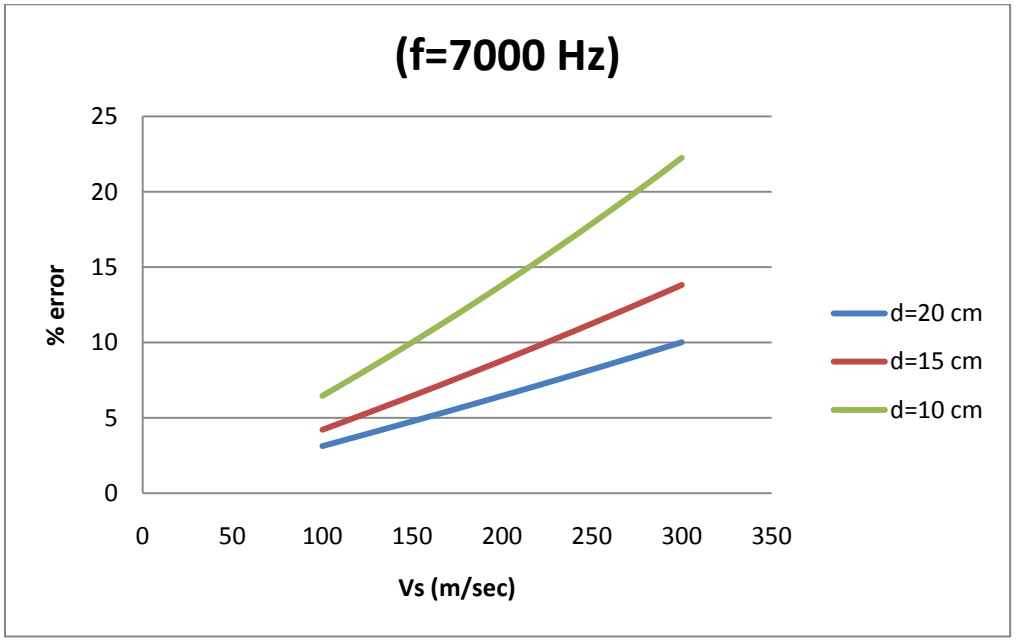


Figure 5.57: Parametric study for the expected error in first arrival determination due to near field effect (f=7000Hz)

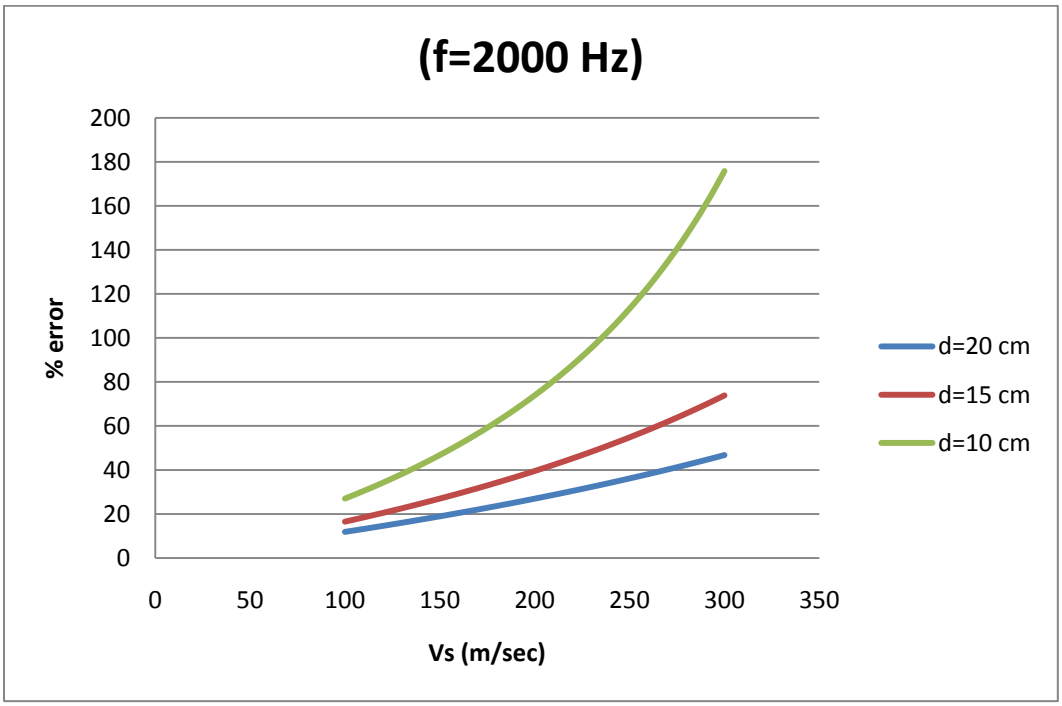


Figure 5.58: Parametric study for the expected error in first arrival determination due to near field effect (f=2000Hz)

# 6. SUMMARY, CONCLUSION AND RECOMMENDATIONS

The purpose of this research is to accurately measure seismic body wave velocities ($V_s$ & $V_D$) in the centrifuge soil models. The research focus on the shear wave velocity measurements, as the P-wave velocity becomes dependent on the fluid in the case of saturated soil.

Bender elements are used for measuring the seismic body wave velocity in this research. The bender elements are piezoelectric transducers. They are very sensitive to the surrounding environment. The use of bender elements in the centrifuge models was found to be challenging due to the noisy environment during the centrifuge operation. The research starts with solving the problems encountered in using bender elements in centrifuge models. After several trials, most of the challenges were overcome, as discussed in Chapter 4.

The next step was to use the enhanced bender elements system to characterize the dry and saturated Ottawa sand as discussed in Chapter 5. The analysis of the experimental data on dry and saturated Ottawa sand revealed some conclusions and recommendations. They can be summarized in the following points:

- The value of shear wave velocity seems to be relatively independent on OCR. This issue needs to be addressed in the liquefaction charts which are totally dependent on the shear wave velocity and neglect the effect of overconsolidation in liquefaction potential of saturated sand.

- The horizontally propagating shear wave velocity measurement for both vertically and horizontally polarized shear waves can be used to estimate $K_0$. This was not achieved in this research due to the deformation of the laminar container as discussed in Chapter 5. However, it can be theoretically achieved in case of using a more rigid container.
- The value of the coefficient of earth pressure tends to increase with OCR. The rate of increase tends to follow Hendron's results as discussed in Chapter 5.
- The Shear wave velocity horizontally propagating & vertically polarized tends to be less than that vertically propagating & horizontally polarized for the same effective stress. The difference can be very significant at high stress values. This issue needs to be considered, especially in the field measurements, where some techniques measure vertically propagating and others measure horizontally propagating shear waves.
- The results of the shear wave velocity vertically propagating & horizontally polarized compare very well with Hardin's equation after modifying it to take into account the stress anisotropy (after Stokoe). This was found to be the case for both dry and saturated Ottawa sand, which happens to be the same type of sand used to develop Hardin's equation.
- The results of the shear wave velocity in saturated Ottawa sand compare very well with the values obtained by the system identification technique.
- The effect of the previously defined preshaking on the saturated Ottawa sand is to increase the shear wave velocity of the sand by about 20%.

- Exciting the sender bender element with Sine wave having frequency of 7000 Hz and amplitude of 80 V was found to give the clearest results. The distance between the sender and the receiver is recommended to be around 20 cm in order to reduce the potential error in the measurements.
- It is recommended to use bending desks for measuring the P-wave velocity, as the bender elements seem to give weak P-wave signal. The bending desks tend to have higher amplitude. Moreover, they only produce P-waves as they are constrained from all directions. This might help in eliminating the misleading reflected S-waves in the output.
- To reduce the effect of the container deformation in changing the lateral stresses in soil models, it is recommended to use a more rigid box. If a laminar container needs to be used, it is recommended to use the circular laminar container. The circular symmetric shape of the container is expected to convert the lateral stresses into axial stresses in the rings resulting in minimal bending. This is expected to have the effect of significantly reducing the deformations in the box.

## REFERENCES


Abdoun et al. (2010), "Physical Modeling of Field Sand Liquefaction and Lateral Spreading Using Centrifuge and Large Scale Tests," (in review)

Akin, M., Steven L. Kramer and Tamer Topal. COMPARISON OF MEASURED AND ESTIMATED SHEAR WAVE VELOCITIES IN A SEISMICALLY ACTIVE AREA (ERBAA, TURKEY) 5th International Conference on Recent Advances in Geotechnical Earthquake Engineering and Soil Dynamics, 2010 SanDiego California

Andrus, R. D. and K. H. Stokoe, [1997]. "Liquefaction resistance based on shear wave velocity." Proceedings from Workshop on Evaluation of Liquefaction Resistance, NCEER-97-0022, Multidisciplinary Center for Earthquake Engineering Research, Buffalo, NY, 89-128.

Bellotti, R., M. Jamiolkowski, D. C. F. Lo Presti, and D. A. O'Neill, 1996, Anisotropy of Small Strain Stiffness in Ticino Sand, Geotechnique 46(1):115-131.

Brandenberg, S.J. ,S. Choi, B.L. Kutter, D.W. Wilson and J.C. Santamarina. A bender elements system for measuring shear wave velocities in Centrifuge models. Physical Modelling in Geotechnics-6th ICPMG '06-Ng, Zhang & Wang (eds)

Brandenberg, Scott J., Bruce L. Kutter and Daniel W. Wilson. Fast Stacking and Phase Corrections of Shear Wave Signals in a Noisy Environmen.t Journal of Geotechnical and Geoenvironmental Engineering, Vol. 134, No. 8, August 2008,

Brignoli, E.G.M., Gotti, M., Stokoe, K.H.,II, Measurement of Shear Waves in Laboratory Specimens by Means of Piezoelectric Transducers" Geotechnical Tesitng Journal, Vol. 19, No. 4, December 1996, pp. 384-397

Burland, J. B. [1989]. "Ninth Laurits Bjerrum Memorial Lecture: "Small is beautiful" - the stiffness of soils at small strains." Canadian Geotechnical Journal, 26(4), 499-516

Cai, G., Liu, S., Puppala, A., Assessment of the Coefficient of lateral Earth Pressure at Rest ($K_0$) from Seismic Piezocone Tests (SCPTU) Geo-Frontiers 2011

Deniz, Remzi Oguz, Bender elements and bending disks for measurement of shear and compressional wave velocities in large sand specimens. (2008). Civil Engineering Master's Thesis

Dobry, R., R. Borcherdt, C.B. Crouse, I.M. Idriss, W.B. Joyner, G.R. Martin, M.S. Power, E.E. Rinne, R.B. Seed [2000]. "New Site coefficients and site

classifications system used in recent building seismic code provisions", Earthquake Spectra, Vol. 16 (1), pp. 41-67.

El-Ganainy, 2011, PhD thesis (Unpublished). Personal communication

Fu, Lei, Xiangwu Zeng and J. Ludwig Figueroa.SHEAR WAVE VELOCITY MEASUREMENT IN CENTRIFUGE USING BENDER ELEMENTS IJPMG-Intemational Journal of Physical Modelling in Geotechnics

Hendron, 1963, The Behavior of Sand in One Dimentional Compression, PhD thesis

Holzer, T. L., M. J. Bennett, T. E. Noce, and J. C. Tinsley III [2005]. "Shearwave velocity of surficial geologic sediments in northern California: statistical distributions and depth dependence", Earthquake Spectra, Vol. 21, pp. 161–177.

Knox, D. P., K. H. Stokoe, II, and S. E. Kopperman, 1982, Effect of state of stress on velocity of low-amplitude shear waves propagating along principal stress directions in dry sand, Tech. Rept. GR82-23, Univ. of Texas-Austin, Austin, TX, 420 pp.

Kramer, S.L. [1996]."Geotechnical Earthquake Engineering", Prentice Hall, Englewood Cliffs, N.J., 653.

Lee, Jong-Sub and J. Carlos Santamarina. Bender Elements: Performance and Signal Interpretation JOURNAL OF GEOTECHNICAL AND GEOENVIRONMENTAL ENGINEERING © ASCE / SEPTEMBER 2005

Lee, N.-K. J., 1993, Experimental study of body wave velocities in sand under anisotropic conditions, Ph.D. Dissertation, Univ. of Texas-Austin, Austin, TX, 503 pp.

Lehane. B. and M. Fahey. [2002]. "A simplified nonlinear settlement prediction model for foundations on sand" Canadian Geotechnical Journal, Vol. 39-2, pp. 293-303.

Mayne, P. W., J. A. Schneider, and G. K. Martin, [1999]. "Small and large strain properties from seismic flat dilatometer tests.", Prefailure Deformation Characteristics of Geomaterials, Torina, Italy, Balkema, Rotterdam, 1, 419-426.

McGillivray, A. and P. W. Mayne. (2004). "Seismic piezocone and seismic flat dilatometer tests at Treporti." Geotechnical and Geophysical Site Characterization, ISC-2, Porto, Portugal, Millpress, Rotterdam, 2, 1623-1628.

McGillivray, A.V. [2007], "Enhanced integration of Shear wave velocity profiling in Direct-push site characterization system", Georgia Institute of Technology, PhD. Thesis.

Mercado, V., 2011. Personal communication

National Instruments Corporation, Technical Support.
http://www.ni.com/support/ (Date last accessed 04/18/2011)

PIEZO SYSTEMS, INC. Product catalog.
http://www.piezo.com/catalog.html (Date last accessed 04/18/2011)

R.N. (ed) Taylor, editor. Geotechnical Centrifuge Technology. Chapman and Hall, 1995

Rensselaer Geotechnical Centrifuge Center.
http://nees.rpi.edu/ (Date last accessed 04/18/2011)

Richart, F. E., Hall, J. R. and Woods, R. D. [1970]. "Vibrations of Soils and Foundations", Prentice-Hall, Englewood Cliffs, N.J., 414 p.

Roesler, S. K., 1979, Anisotropic shear modulus due to stress anisotropy, ASCE J. Geotechnical Eng. Div. 105(GT5):871-880, July.

Sasitharan, S., Robertson, P. K. and Sego. D. C. [1994]. "Sample disturbance from shear wave velocity measurements." Canadian Geotechnical Journal, Vol. 31(1), pp. 119-124.

Schnabel, P.B., Lysmer, J. and Seed, H. B. [1972]. "SHAKE: A Computer Program for Earthquake Response Analysis of Horizontally Layered Sites", Earthquake Engineering Research Center, University of California, Berkeley, Berkeley, CA. Report No. EERC 72-12.

Seed. H. B. and Idriss. I. M. [1970]. "Soil moduli and damping factors for dynamic response analyses", Rep. No. EERC-70/10, Earthquake Engg. Research Center, Univ. of California at Berkeley, Berkeley, California.

Seed, R. B., Cetin, K. O., Moss, R. E. S., Kammerer, A. M., Wu, J., Pestana, J. M., Riemer, M. F., Sancio, R. B., Bray, J. D., Kayen, R. E. and Faris, A. [2003]. "Recent advances in soil liquefaction engineering: A unified and consistent framework." 26th Annual ASCE Los Angeles Geotechnical Spring Seminar, Long Beach, CA, ASCE, Reston, VA, 71.

Shibuya, S., Yamashita, S., Mitachi, T. and Tanaka, H. [1995]. "Effects of sample disturbance on Gmax of soils - a case study." 1st International Conference on Earthquake Geotechnical Engineering, Tokyo, Japan, 1, 77.

Stewart. J.P., A.H. Liu and Y. Choi, [2003]. "Amplification factors for spectral acceleration in tectonically active regions" Bulletin of the Seismological Society of America, Vol. 93, No. 1, pp. 332-352.

Stokoe, K. H., II, S. H. H. Lee, and D. P. Knox, 1985, Shear moduli measurements under true triaxial stresses, pp. 166-185, In: Advances in the Art of Testing Soils Under Cyclic Conditions, V. Khosla (ed.), American Society of Civil Engineers, New York, NY.

Stokoe, K. H., II, S.-K. Hwang, J. N.-K. Lee, and R. D. Andrus, 1995, Effects of various parameters on the stiffness and damping of soils at small to medium strains, pp. 785-816, In: Pre-Failure Deformation of Geomaterials, Vol. 2, S. Shibuya, T. Mitachi, and S. Miura (eds.), A. A. Balkema, Rotterdam, The Netherlands, Proc., 1st Intl. Conf. on Pre-Failure Deformation Characteristics of Geomaterials, Sapporo, Japan, Sept. 12-14, 1994.

Sykora. D. E. and K. H. Stokoe [1983]. "Correlations of in-situ measurements in sands of shear wave velocity" Soil Dynamics and Earthquake Engineering, Vol. 20, pp. 125–136.

Tessari, A. F., Measuring Primary and Secondary Wave Velocities on a Geotechnical Centrifuge Using Bender Elements (2007) Civil Engineering Master's Thesis

Ubilla, J. O. , Physical Modeling of the Effects of Natural Hazards on Soil-Structure Interaction (2007) Civil Engineering PhD Thesis

Wang, Y.H., Lo, K.F., Yan, W.M., (2007). Measurement Biases in the Bender Element Test. Journal of Geotechnical and Geoenvironmental Engineering, ASCE, May 2007

Whitman, R.V., Dobry, R. and M. Vucetic, (Unpublished) "Soil Dynamics," Dynamic Response of Soil and Soil Foundation Systems Course, Rensselaer Polytechnic Institute, Spring 2010.

Wills. C. J. and W. J. Silva. [1998]. "Shear-wave velocity characteristics of geologic units in California", Earthquake Spectra, Vol. 14-3, pp. 533-556.

Yan-Guo Zhou and Yun-Min Chen. Laboratory Investigation on Assessing Liquefaction Resistance of Sandy Soils by Shear Wave Velocity. J. Geotech. and Geoenvir. Engrg. Volume 133, Issue 8, pp. 959-972 (August 2007)

Yu, P., and F. E. Richart, Jr., 1984, Stress ratio effects on shear modulus of dry sands, ASCE J. Geotechnical Eng. 110(3):331-345, March.

Zeghal, M., Elgamal, A.-W., Tang, H. T., and Stepp, J. C. (1995). "Lotung Downhole Seismic Array: Evaluation of Soil Nonlinear Properties," Journal of Geotechnical Engineering, ASCE, Vol. 121, No. 4, pp. 363-378.

## APPENDICIES

## A. OTTAWA SAND SPECIFICATIONS

U.S. SILICA®
Sands of Time

# PRODUCT DATA

## ASTM (1) GRADED SAND

UNGROUND SILICA

PLANT: OTTAWA, ILLINOIS

(1) AMERICAN SOCIETY FOR TESTING AND MATERIALS

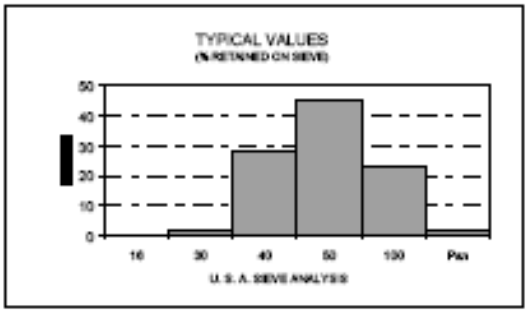


| USA STD SIEVE SIZE | | TYPICAL VALUES | | |
|---|---|---|---|---|
| | | % RETAINED | | % PASSING |
| MESH | MILLIMETERS | INDIVIDUAL | CUMULATIVE | CUMULATIVE |
| 16 | 1.180 | 0.0 | 0.0 | 100.0 |
| 30 | 0.600 | 2.0 | 2.0 | 98.0 |
| 40 | 0.425 | 28.0 | 30.0 | 70.0 |
| 50 | 0.300 | 45.0 | 75.0 | 25.0 |
| 100 | 0.150 | 23.0 | 98.0 | 2.0 |
| PAN | | 2.0 | 100.0 | 0.0 |

## TYPICAL PROPERTIES

| | | | |
|---|---|---|---|
| COLOR | WHITE | MINERAL | QUARTZ |
| GRAIN SHAPE | ROUND | pH | 7 |
| HARDNESS (Mohs) | 7 | SPECIFIC GRAVITY | 2.65 |
| MELTING POINT (Degrees F) | 3100 | | |

## TYPICAL CHEMICAL ANALYSIS, %

| | | | |
|---|---|---|---|
| $SiO_2$ (Silicon Dioxide) | 99.7 | MgO (Magnesium Oxide) | <0.01 |
| $Fe_2O_3$ (Iron Oxide) | 0.020 | $Na_2O$ (Sodium Oxide) | <0.01 |
| $Al_2O_3$ (Aluminum Oxide) | 0.06 | $K_2O$ (Potassium Oxide) | <0.01 |
| $TiO_2$ (Titanium Dioxide) | 0.01 | LOI (Loss On Ignition) | 0.1 |
| CaO (Calcium Oxide) | <0.01 | | |

## CONFORMS TO ASTM C778

December 15, 1997

DISCLAIMER: The information set forth in this Product Data Sheet represents typical properties of the product described; the information and the typical values are not specifications. U.S. Silica Company makes no representation or warranty concerning the Products, expressed or implied, by this Product Data Sheet.

WARNING: The product contains crystalline silica - quartz, which can cause silicosis (an occupational lung disease) and lung cancer. For detailed information on the potential health effect of crystalline silica - quartz, see the U.S. Silica Company Material Safety Data Sheet.

U.S. Silica Company P.O. Box 187, Berkeley Springs, WV 25411-0187 (304) 258-2500